MASTER'S THESIS

The Role of Lipin-2 and Lipin-3 in Lipid Homeostasis in the Small Intestine

Studies in the Mouse and CRISPR/Cas9 engineered Human Intestinal Cells

by

Lynn Johanna BAUFELD, MSc

Submitted in conformity with the requirements for the degree of

MASTER OF SCIENCE
(MSc)

Institute of Molecular Biosciences, University of Graz, AUSTRIA

In cooperation with

Department of Human Genetics, David Geffen School of Medicine, University of California Los Angeles, USA

Graz, 2016

Supervised by

Karen Reue, PhD
Frank Madeo, Univ.-Prof. Dr.rer.nat.

STATUTORY DECLARATION

I hereby declare that I have authored this thesis independently, that I have not used other than the declared sources/resources, and that I have explicitly marked all material which has been quoted either literally or by content from the used sources.

Graz, June 2016 Lynn Johanna Baufeld

ABSTRACT

Despite the general dogma of the monoacylglycerol acyltransferase (MGAT) pathway being the main route of triacylglycerol synthesis in the small intestine, recent studies of Lipin proteins have revealed a previously unappreciated importance of the glycerol-3-phosphate (G3P) pathway for intestinal lipid homeostasis.

The purpose of this study was to investigate the role of Lipin-2 and Lipin-3 in the small intestine. *Lpin2*$^{-/-}$*/Lpin3*$^{-/-}$ double knockout mice were used to assess mRNA and protein levels of enzymes involved in lipid metabolism in the enterocytes. Immunofluorescence microscopy was conducted to study the cellular localization and interactions between proteins. With the use of CRISPR/Cas9, human intestinal cells were engineered to disable the *LPIN2* and *LPIN3* genes and were examined as a model to study the cellular function of Lipin-2/3.

We identified a critical role for Lipin-2/3 in intestinal processing of dietary lipids. Specific processes that are influenced by Lipin-2/3 include chylomicron synthesis/secretion, lipid uptake from a dietary bolus, enterocyte triacylglycerol and phospholipid homeostasis, apolipoprotein B48 processing and degradation, and release of fatty acids from lipid droplet stores in enterocytes.

ZUSAMMENFASSUNG

Es ist allgemein bekannt, dass der Monoacylglycerin Acyltransferase (MGAT) Weg vorrangig für die Triacylglycerin-Synthese im Dünndarm verantwortlich ist. Forschungsergebnisse von Studien der letzten Jahre, die sich mit der Funktion der Lipin Proteine beschäftigten, zeigen den Glycerin-3-phosphat (G3P) Weg in neuem Licht und schreiben ihm eine zuvor ungeahnte Bedeutung in der Darm-Lipidhomöostase zu.

Ziel dieser Studie war es, zu untersuchen welche Rolle die Phosphatidat-Phosphatasen Lipin-2 und Lipin-3 im Dünndarm spielen. *Lpin2*$^{-/-}$*/Lpin3*$^{-/-}$ Doppel-Knockout Mäuse wurden verwendet, um die mRNA- und Proteinlevel verschiedener Enzyme, die am Lipidmetabolismus in den Enterozyten beteiligt sind, zu bestimmen. Die zelluläre Lokalisation sowie die Wechselwirkungen zwischen Proteinen wurden mit Hilfe der Immunofluoreszenzmikroskopie untersucht. Das *Genome Editing* System CRISPR/Cas9 wurde herangezogen, um eine menschliche Darm-Zelllinie genetisch so zu verändern, dass die Gene *LPIN2* und *LPIN3* deaktiviert werden. Diese Zelllinie diente dann als Modell zur Untersuchung zellulärer Funktionen von Lipin-2/3.

Wir konnten zeigen, dass Lipin-2/3 eine entscheidende Rolle bei der Verarbeitung von Lipiden, die über die Nahrung aufgenommen werden, spielen. Lipin-2 und Lipin-3 beeinflussen eine Reihe an spezifischen Prozessen wie die Synthese und Sekretion von Chylomikronen, die Lipidaufnahme aus einem Nahrungsbolus, die Homöostase von Triacylglycerin und Phospholipiden in Enterozyten, die Verarbeitung und den Abbau von Apolipoprotein B48, sowie die Freisetzung von Fettsäuren aus den Lipidtröpfchen, die im Zytosol der Enterozyten gespeichert sind.

ACKNOWLEDGEMENTS

First of all, I would like to express my sincere gratitude to Karen Reue at UCLA for giving me the opportunity to join her lab. Her enthusiasm for the research she does is contagious and her knowledge and support has enabled me to learn and grow a lot while working on this thesis.

I would like to thank my fellow work colleagues (Laurent, Jenny, Albert, Emilio, Jessica, and Huan) for the stimulating discussions, the helpful troubleshooting, and the inspiring and fun times we had working together in the lab. Special thanks belong to Peixiang Zhang for his insight on the topic and his help and guidance with my work.

I would like to thank my supervisor Frank Madeo at the University of Graz for his advice, support and honest opinion throughout the course of my studies and for always encouraging me in my endeavors that reach far outside our campus' walls.

Furthermore, I want to thank Mike Gottschalk for his expertise in graphic design. He was very helpful in putting together some of the illustrations used in this thesis.

Last but not least, I would like to thank my family for their encouragement throughout my studies and their unceasing support no matter how far apart we are.

TABLE OF CONTENTS

LIST OF FIGURES

LIST OF TABLES

LIST OF ABBREVIATIONS

ABC transporter	ATP-binding cassette transporter
ACAD8	acyl-CoA dehydrogenase 8
ACOT8	acyl-CoA thioesterase 8
ACS	acyl-CoA synthetase
ACSL	acyl-CoA synthetase for long-chain FA
AGPAT	acyl-CoA:1-acylglycerol-3-phosphate acyltransferase
ANGPTL4	angiopoietin-like 4
AOX	acyl-CoA oxidase; also known as ACOX
AP2	adipocyte protein 2; also known as FABP4
ApoA-I/-IV	Apolipoprotein A-I/A-IV
ApoB48	Apolipoprotein B48
ATGL	adipose triglyceride lipase
CD36	Cluster of differentiation 36; also known as FAT
CDS	coding DNA sequence
CL	cardiolipin
CM	chylomicron
CMA	chaperone-mediated autophagy
CoA	Coenzyme A
COPII	cytosolic coat protein II
CPT1A	carnitine palmitoyltransferase 1A
DAG	diacylglycerol
DGAT	diacylglycerol acyltransferase
DKO	double knockout
EM	electron microscope
ER	endoplasmic reticulum
ERAD	ER-associated degradation pathway
FA	fatty acid
FABP	fatty acid binding protein
FAT	fatty acid translocase

FATP	fatty acid transport protein
FFA	free fatty acid
FST	follistatin
G3P	glycerol-3-phosphate
GPAT	glycerol-3-phosphate acyltransferase
gRNA	guide ribonucleic acid
GRP78	78 kDa glucose-regulated protein; also known as HSPA5
HFD	high-fat diet
HMGCL	hydroxymethylglutaryl-CoA lyase
HMGCS1/2	hydroxymethylglutaryl-CoA synthase 1/2
HRP	horseradish peroxidase
Hsc70	heat-shock cognate 70
HSL	hormone-sensitive lipase
I-FABP	intestinal-fatty acid binding protein; also known as FABP2
KO-mouse	knockout-mouse
LAMP-2A	lysosome-associated membrane protein type 2A
L-FABP	liver-fatty acid binding protein; also known as FABP1
LCFA	long-chain fatty acid
LD	lipid droplet
LPA	lysophosphatidic acid
LPCAT3	lysophospholipid acyltransferase 3
MAG	monoacylglycerol
MGAT	monoacylglycerol acyltransferase
MGL	monoacylglycerol lipase
MTP	microsomal triglyceride transfer protein
NLS	nuclear localization sequence
NPC1L1	Niemann-Pick C1 like 1
PA	phosphatidic acid
PAM	protospacer adjacent motif
PAP	phosphatidate phosphatase
PC	phosphatidylcholine
PCTV	prechylomicron transport vesicle

PDI	protein disulfide isomerase
PE	phosphatidylethanolamine
PG	phosphatidylglycerol
PGC-1α	peroxisome proliferator-activated receptor-gamma co-activator-1 alpha
PI	phosphatidylinositol
PI3P	phosphatidylinositol-3-phosphate
PKA	protein kinase A
PKCζ	protein kinase C-zeta
Plin	Perilipin
preCM	prechylomicron
PPARα/γ	peroxisome proliferator-activated receptor alpha/gamma
PS	phosphatidylserine
PUFA	polyunsaturated fatty acid
TAG	triacylglycerol
VAMP7	vesicle-associated membrane protein 7
WT	wild-type

1 INTRODUCTION

1.1 Dietary Fat Metabolism

Dietary fats serve as a key energy source and are critical for normal metabolism. Over 40% of the caloric content of the diet consumed in the western world are dietary fats. (1) They provide our bodies with energy for many metabolic functions in addition to essential fatty acids (FAs) and fat-soluble vitamins. The major component of dietary fat is triacylglycerol (TAG), which consists of a glycerol molecule esterified to three FA. Other types of lipid such as phospholipids, cholesterol or long-chain fatty acids (LCFA) are also a part of the Western daily diet.

After ingestion several lipolytic enzymes begin digesting the fats. The released FAs are very efficiently taken up by the small intestine, leaving <5% of the ingested lipids to escape with feces. (2) The FAs are absorbed by the epithelial cells lining the villi, the so-called enterocytes. Once within the cells they are re-esterified into triglycerides, which are then either packed into lipid droplets for storage or incorporated into chylomicron particles. On the basolateral side of the cell chylomicrons are released through exocytosis into the lymphatic system. When they reach the thoracic duct they enter the blood circulation and distribute throughout the body to transport lipids to peripheral tissues. (3,4) Some of the absorbed dietary lipids are used as building blocks for phospholipid membranes, others play a role as intracellular lipid signaling molecules. Excess lipids, with TAGs as the primary unit of storage, are packed into cytosolic lipid droplets until they are needed. More than 90% of the content of white adipocytes is comprised of TAGs which makes them the main fat storage compartment. (5)

Despite decades of studies and research, knowledge remains incomplete regarding the metabolism of dietary fats. It has long been thought that the monoacylglycerol acyltransferase (MGAT) enzyme family is the main pathway determining the fate of dietary fatty acids and their assembly into chylomicrons in enterocytes. Things were shaken up when the Lipin family of enzymes was discovered in 2001. (6) Studies with

these phosphatidate phosphatase (PAP) proteins, which catalyze the dephosphorylation of phosphatidic acid to diacylglycerol, indicate that a distinct pathway controlled by Lipin proteins is also necessary for the proper utilization of dietary fatty acids. With their additional function as co-regulators of gene expression promoting fatty acid oxidation, Lipins take a unique place among glycerolipid synthesis enzymes. (7) The physiological roles of Lipins are complex because their function and activity depend on the member of the Lipin family (three members) involved, as well as on the specific tissue and subcellular localization.

Deficiency of Lipins results in serious metabolic diseases in humans as well as in mice. After observing a dramatic phenotype of abnormal intestinal lipid homeostasis in a mouse model lacking Lipin-2 and Lipin-3, the goal of this study was to investigate and understand the underlying effects and changes taking place in enterocytes. We utilized mutant mouse models for physiological studies, and created a genetically modified human intestinal cell line deficient in both Lipin-2 and Lipin-3 with CRISPR/Cas9 to study the mechanism of Lipin-2/3 action in intestinal dietary lipid assimilation and utilization.

1.1.1 Digestion of Dietary Fats

In humans, the digestion of dietary lipids begins with two enzymes that start hydrolyzing long-chain triglycerides into diacylglycerol (DAG) and free fatty acids (FFAs). Both the lingual lipase secreted by Von Ebner's glands in the mouth and the gastric lipase released by the gastric chief cells in the stomach's mucosa have their pH optimum in an acidic environment. (8,9) The major part of digestion takes place in the small intestine where bile acids produced by the liver act as detergents and facilitate the formation of micelles to increase the surface area for better digestion of the fats. Micelles in the intestinal lumen are acted upon by pancreatic lipase, which binds directly at the oil/water interface, and it's co-factor, colipase, which prevents expulsion of the lipase into the water phase and the inhibitory effects from bile salts. (10,11) The rate of hydrolysis in the intestinal lumen becomes more efficient with a better emulsification of dietary fats. (12,13) To digest dietary fats before entering the enterocyte, the pancreatic lipase acts mainly on the *sn*-1 and *sn*-3 positions of the TAG molecule to release *sn*-2-

monoacylglycerol (*sn*-2-MAG) and two FFAs. A fraction of those molecules undergoes isomerization of *sn*-2-MAG into *sn*-1,3-MAG; the latter can then be further hydrolyzed into glycerol and a FA. (14) This isomerization in an aqueous medium occurs more slowly than the uptake of *sn*-2-MAG from the enterocytes, which therefore is the main form of MAG absorbed by the cells. (15)

1.1.2 Intestinal Uptake of Dietary Fats

Absorption of dietary lipids takes place in the enterocytes, the epithelial cells lining the villi of the small intestine. Two models of how fatty acids generated from digestion cross from the intestinal lumen through the apical brush border membrane have been proposed in the past and most likely coexist: protein-independent diffusion and protein-facilitated mechanisms. (16,17) Studies in adipocytes have shown that the protein-independent flip-flop mechanism is capable of supplying FA to the esterification machinery fast and sufficiently enough so that the cross-membrane transport is not a rate limiting step. (18) On the contrary, several candidate proteins have been found that may play a role in the saturable and competitive long-chain fatty acid (LCFA) transport system. (19)

1.1.2.1 Cellular Uptake of LCFA

The fatty acid translocase (FAT/CD36) is a transmembrane protein with a broad ligand specificity. (20) It is highly expressed in enterocytes in the proximal small intestine (duodenum and jejunum) where it facilitates FA uptake. (21) Additionally CD36 plays an important role in directing the absorbed FA towards chylomicron production. (22) Besides this it is also involved in sensing LCFA and regulating fat absorption at various levels, including mediating the perception of FA in lingual taste bud cells and releasing two gut hormones, secretin and cholecystokinin, to initiate the cephalic phase of digestion. (17,23) Because CD36 might be rapidly saturated with FAs present in the lumen, its contribution to the net absorption is small. However, signaling through CD36-associated Src kinases and downstream via ERK 1/2 may be important for phosphorylating proteins required in processing of prechylomicron transport vesicles

(PCTV) such as apolipoprotein B48 (ApoB48) and microsomal triglyceride transfer protein (MTP). (24) CD36 has also been identified of being a part of the PCTV formation process in the endoplasmic reticulum (ER). (25) High concentrations of LCFA possibly downregulate CD36 via ubiquitination and lysosomal degradation, which might work as a feedback loop. The decrease in CD36 is associated with a reduced ERK 1/2 activation which may help upregulate MTP abundance. (26)

Calveolin-1 has recently been studied as a new player in intestinal fatty acid uptake. It is located in lipid rafts and dietary lipids are taken up by caveolae in the enterocyte brush border through endocytosis. The caveolin-1 containing endocytic vesicles then transport the FA through the cytosol. (27)

The fatty acid transport protein (FATP) family has 6 members. FATP2-4 are expressed in the small intestine with FATP4 as the predominant one. FATP4 is not classified as a brush border transporter since it is expressed intracellularly. It is located at the ER and subapical membranes where it facilitates FA uptake by trapping the acyl-CoA derivatives generated by its endogenous acyl-CoA synthetase (ACS) activity. (16,28) In contrast to native LCFA molecules, which are freely diffusible, these acyl-CoA products are hydrophilic and undergo rapid metabolic conversion into more complex lipid species such as di- and triacylglycerols or phospholipids. Studies with FATP4 knockout mice showed that the protein is crucial for proper functioning skin but there was no obvious effect on intestinal lipid absorption. This does not automatically imply that FATP4 is not involved in intestinal lipid transport, but it seems to be dispensable for the process. (29–31)

1.1.2.2 Cellular Uptake of MAG

The absorption of monoacylglycerol by enterocytes has been shown to happen through passive diffusion. (32) A protein transporter has also been proposed, as the MAG uptake is a saturable function of the MAG monomer concentration. The tentative transporter is shared by MAG and FAs because MAG can competitively suppress fatty acid uptake, which glycerol, DAG, and TAG cannot. (33,34) To date the identity of the transporter protein is still unknown.

1.1.2.3 Cholesterol Influx and Efflux in Enterocytes

The transfer of cholesterol from the intestinal lumen to the brush border membrane is facilitated by bile salt micelles as well. The uptake had long been considered a passive diffusion process. New studies suggest Niemann-Pick C1 like 1 (NPC1L1) as a cholesterol uptake transporter. (35) In the opposite direction two ATP-binding cassette (ABC) transporter proteins, ABCG5 and ABCG8, work together as cholesterol efflux transporter moving excess cholesterol back into the intestinal lumen. (36,37) The overall intestinal cholesterol homeostasis is regulated through a balance between sterol uptake, *de novo* synthesis, and its regulated export as a part of lipoproteins. An alternative pathway has been proposed involving high-density lipoprotein (HDL) formation, which is mediated through the ATP-binding cassette transporter ABCA1. (38) Membrane-free cholesterol along with phospholipids is mobilized through the export pump where it binds to extracellular lipid-poor apolipoprotein A-I (ApoA-I) forming a nascent HDL, which then enters the lymphatic circulation. (17)

1.1.3 Intracellular Transport of Dietary Fatty Acids

Once FAs are inside the enterocyte they are targeted by cytosolic fatty acid binding proteins (FABPs) which bind and deliver them to specific metabolic sites. Two proteins of the FABP family are highly expressed in the small intestine: liver-FABP (L-FABP or FABP1) and intestinal-FABP (I-FABP or FABP2). (39) These two FABPs were shown to deliver FAs by different mechanisms. For FABP1 a diffusion-mediated transfer process is suggested while the data for FABP2 supports the concept of a transient collisional interaction of FABP2 with the phospholipid membrane where it can directly extract fatty acids from membranes. (40) This supports the idea that FABP2 may increase the cytosolic flux of FAs via intermembrane transfer. FABPs bind a single LCFA with high affinity, with the exception of FABP1, which binds two fatty acids or a variety of other lipids including bile salts, lysophospholipids, cholesterol, acyl-CoA, and MAG. (41) An additional function of FABP1 is mediating the budding of PCTVs from the ER. (42)

Using knockout (KO) mice for either FABP1 or FABP2 it was demonstrated that each protein participates in specific pathways of intestinal lipid metabolism. FABP2 appears to target dietary FAs toward triacylglycerol synthesis, while FABP1 seems to target FAs toward oxidative pathways and dietary MAGs toward anabolic pathways. This is supported by different whole body responses when animals are fasted. FABP2 KO mice lose more fat mass and FABP1 KO mice lose less lean mass compared to wild-type mice. (43)

1.1.4 Intracellular Processing of FA and MAG

The first step of processing fatty acids by enterocytes is the activation of FA by thioesterification of the carboxyl group with Coenzyme A (CoA) mediated by acyl-CoA synthetase enzymes specific for long-chain FA (ACSL). (44) Thirteen ACSLs have been identified with ACSL3 and ACSL5 as the major ones in the small intestine. (45,46) There is evidence that these ACSLs contribute to the metabolic channeling of FA. Studies in hepatocytes suggest that ACSL3 delivers FA-CoA for phospholipid synthesis while ACSL5 catalyzes FA-CoA for TAG synthesis. (44) Additionally, some of the acyl-CoA fatty acids can also be used for energy production through mitochondrial β-oxidation. (47)

1.1.4.1 Enzymatic Pathways Mediating Intestinal TAG Synthesis

Intracellularly, MAG and fatty acid components are reconstituted to form TAG via two known pathways – the MAG pathway and the glycerol-3-phosphate (G3P) pathway. (48,49) The prevailing dogma has been that the G3P pathway is the primary route for TAG synthesis in nearly all tissues *except* intestine, which relies primarily upon the MAG pathway.

The enzymes involved in these TAG synthesis pathways have multiple homologues. Three homologous genes were identified for monoacylglycerol acyltransferases (MGATs) while two code for diacylglycerol acyltransferases (DGATs). In the G3P pathway four G3P acyltransferases (GPATs), three acyl-CoA-G3P acyltransferases (AGPATs) and three Lipin phosphatidate phosphatases are known. Individual isoforms of these

enzymes differ in their tissue expression patterns, subcellular localization, catalytic properties, and regulation. In many cases, isoforms of a specific enzyme class may be able to compensate for one another to some extent, but studies have shown that the multiple isoforms are not completely redundant and each may have essential roles in specific cellular processes. (50) The focus in this thesis lies on the enzymes involved in TAG synthesis in the enterocyte.

In most mammalian cells the G3P pathway is the major one for TAG synthesis. (5) In intestine however, the MAG pathway has been postulated as the main route generating up to 90% of newly synthesized TAG due to an abundance of MAG released from dietary lipids. (51,52) MAG is transformed into TAG by the consecutive action of MGAT and DGAT enzymes. (53) Of the three isoforms, MGAT (1-3), only MGAT2 and 3 are highly expressed in the proximal and distal intestine, respectively. (54,55) In the enterocytes they are located on the cytoplasmic side of the smooth ER. (56)

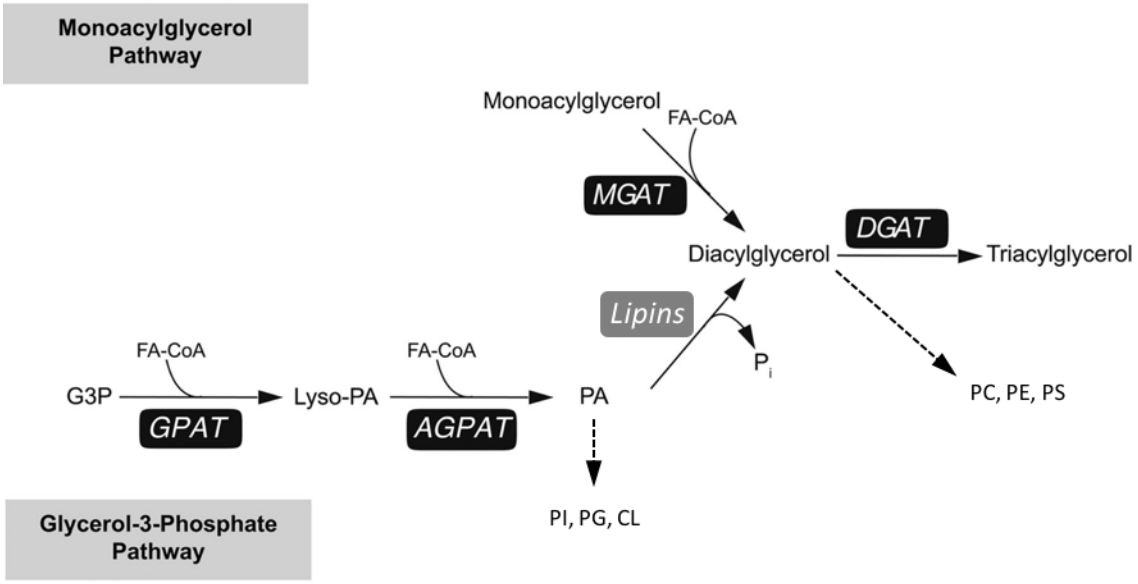

Figure 1.1. Two pathways of glycerolipid synthesis. The biosynthesis of TAG is managed by either acylation of MAG by Monoacylglycerol acyltransferase (MGAT) to DAG or the stepwise acylation of G3P to LPA by G3P acyltransferase (GPAT) and then the transformation into PA by acyl-CoA G3P acyltransferase (AGPAT). PA is a precursor for the phospholipids PI, PG and CL or is hydrolyzed by Lipin (PA phosphatase) to form DAG. While DAG is a precursor for the synthesis of PC, PE, and PS, a final esterification step performed by the diacylglycerol acyltransferase (DGAT) results in the formation of TAG. (adapted from (50))

The G3P pathway describes the stepwise acylation of G3P with two FA moieties to lysophosphatidic acid (LPA) and then phosphatidic acid (PA) which is catalyzed by two

consecutive enzymes – GPAT and AGPAT. This is followed by hydrolysis of the phosphate group by the Lipin enzyme (or phosphatidate phosphatase; PAP) resulting in DAG. (5,57) The two pathways converge where DGAT transforms DAG into a TAG molecule. Lipid intermediates produced by the G3P pathway serve as substrates for phospholipid biosynthesis.

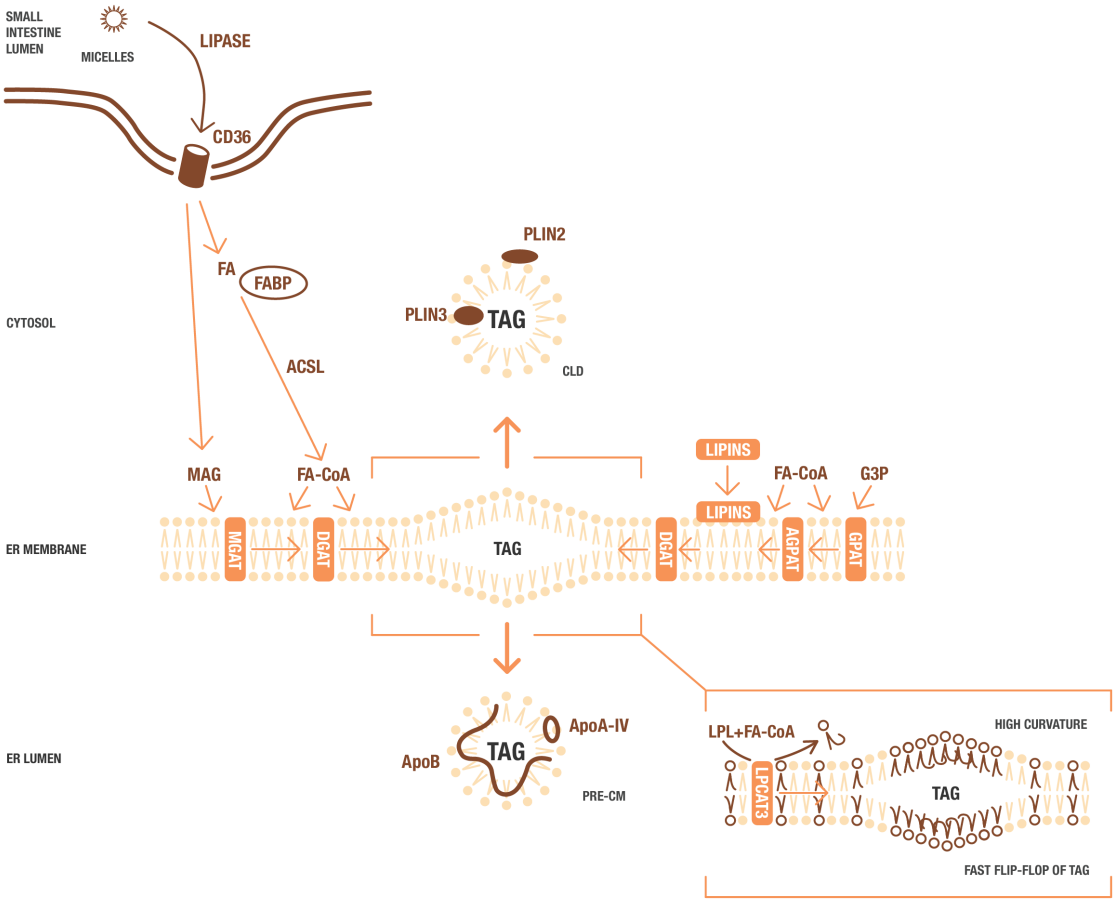

Figure 1.2. Model showcasing the two pathways of TAG synthesis in the ER membrane. Apart from Lipins, which translocate after activation by FAs, all acyltransferase enzymes are localized in the ER membrane. Upon uptake, FA is bound to fatty acid binding protein (FABP) in the cytosol and gets transformed into FA-CoA, which works as the building block for TAG synthesis. First a lens of newly synthesized TAG starts growing in the phospholipid bilayer, which then bulges into the ER lumen or the cytoplasm of the cell to either build TAG-rich prechylomicrons (pre-CM) for secretion or cytosolic lipid droplets (CLD) for storage, respectively. This is facilitated by LPCAT3 incorporating arachidonate-containing phospholipids that enable a more dynamic movement of the membrane as well as faster flip-flop movement of TAGs across the phospholipid layer. (adapted from (58,59))

When TAG is formed it must traverse the ER membrane to enter the cisternae. TAG has a membrane solubility of about ~3%. Once this is exceeded, the phospholipid bilayer is split and the TAGs from a small lens which keeps growing until it expands and bulges into either the cytoplasmic side to build lipid droplets as part of the TAG storage pool or

the luminal side as a precursor of lipoproteins. (60,61) Recent studies have proposed the involvement of lysophospholipid acyltransferase 3 (LPCAT3) in the process of enriching arachidonate-containing phospholipids in the ER membrane to create a more dynamic membrane environment that facilitates the flip-flop of TAGs. This enables a sufficient supply of TAGs to the luminal side to ensure efficient lipidation of ApoB-containing lipoproteins. (62,59,63)

1.1.5 Lipins

Multiple studies have shown that Lipin proteins are of importance in maintaining TAG homeostasis in several tissues such as muscle, liver, brain, and adipose tissue. (6,64–68) In the 1960s, several research groups detected significant levels of magnesium-dependent PAP activity in the intestinal mucosa from different animal species. (69–74) The hypothesis from these results was that PAP activity plays a critical role in mucosal cell proliferation, whereas MGAT activity is more critical in synthesizing TAGs that are used in the formation of chylomicrons. (75)

Lipins were first discovered through studies in spontaneously mutated fatty liver dystrophy (*fld*) mice that revealed a novel gene (*Lpin1*) encoding the underlying deficient protein Lipin-1. (6,76) Lipins are evolutionarily conserved in different species. Yeast has 1 homolog whereas mammals have three Lipin protein isoforms – Lipin-1, Lipin-2, and Lipin-3. All three exhibit similarities in their protein structures. They each consist of a nuclear localization sequence (NLS), a DIDGT motif for identification of the catalytic site, and an LXXIL motif that is necessary for the activity as a coactivator of transcription. (77,78) Lipin proteins reside in the cytosol and only when stimulated by fatty acids they translocate to the ER membrane. (79,80) This characteristic distinguishes Lipins from all the other acyltransferase enzymes in the G3P pathway, which are integral ER membrane proteins. (5,81) In addition, Lipins can localize to the nucleus. (82–85) There they act as transcriptional co-activators through interactions with peroxisome proliferator-activated receptor-γ co-activator-1α (PGC-1α) and peroxisome proliferator-activated receptor-α (PPARα) to regulate target genes, which encode proteins involved in fatty acid uptake, activation, and oxidation. (86,87)

The existence of three lipin proteins catalyzing the same biochemical reaction raises questions of whether they share or have distinct physiological roles and whether they are redundant or able to compensate for each other. Expression studies have shown that the mRNA levels of Lipins vary in their tissue distribution. Lipin-1 mRNA is highly expressed in adipose tissue, skeletal muscle, and testis but is undetectable in intestine. (72) In contrast, Lipin-3 is most prominently expressed in both mouse and human small intestine; Lipin-2 is also expressed in the small intestine, but at a lower level than its expression in liver and brain. (66,88) In certain contexts the Lipin isoforms can be compensatory for one another (see below), but further studies on their specific roles in different tissues are necessary to gain more insight into their interplay.

1.1.5.1 Lipin-2 and Lipin-3 Double Knockout Mice – *what we know so far*

Studies with mouse models deficient in Lipin-2, Lipin-3 or a combination of both (Lipin-2/3KO or double knockout, DKO) have shown that both Lipins play distinct roles in intestinal lipid homeostasis but are able to partially compensate for each other in the case of loss. The loss of both Lipins however, results in a dramatic defect in intestinal lipid metabolism. Lipin-2/3KO mice are born with reduced body weight due to a lower percent fat mass compared to wild-type mice (Figure 1.3). This stays as a significant phenotype throughout their life. On a high fat diet, the DKO mice undergo a rapid and very drastic weight loss, indicating an inability to utilize excess dietary lipids. Investigation of small intestine samples showed abnormal histologic morphology with an overall increased intestinal circumference, hyperplastic villi, and lipid accumulation in the enterocytes lining the villi. Compared to wild-type mice, significantly lower levels of serum TAGs were measured in the DKO mice after an oil gavage in the presence of agents to prevent lipoprotein uptake, which points to reduced secretion of intestinal lipoproteins following a meal. Acute feeding with BODIPY-stained fatty acids revealed a reduced incorporation of fatty acids into TAG droplets in enterocytes in DKO mice.

Through electron microscopy, abnormal prechylomicron transport vesicles (PCTV) were detected with distinct differences in DKO mice and slightly abnormal appearance in Lipin-2 and Lipin-3 single knockout mice. It is unlikely to be the cause for impaired chylomicron secretion alone, because this was only present in Lipin-2/3KO mice. When

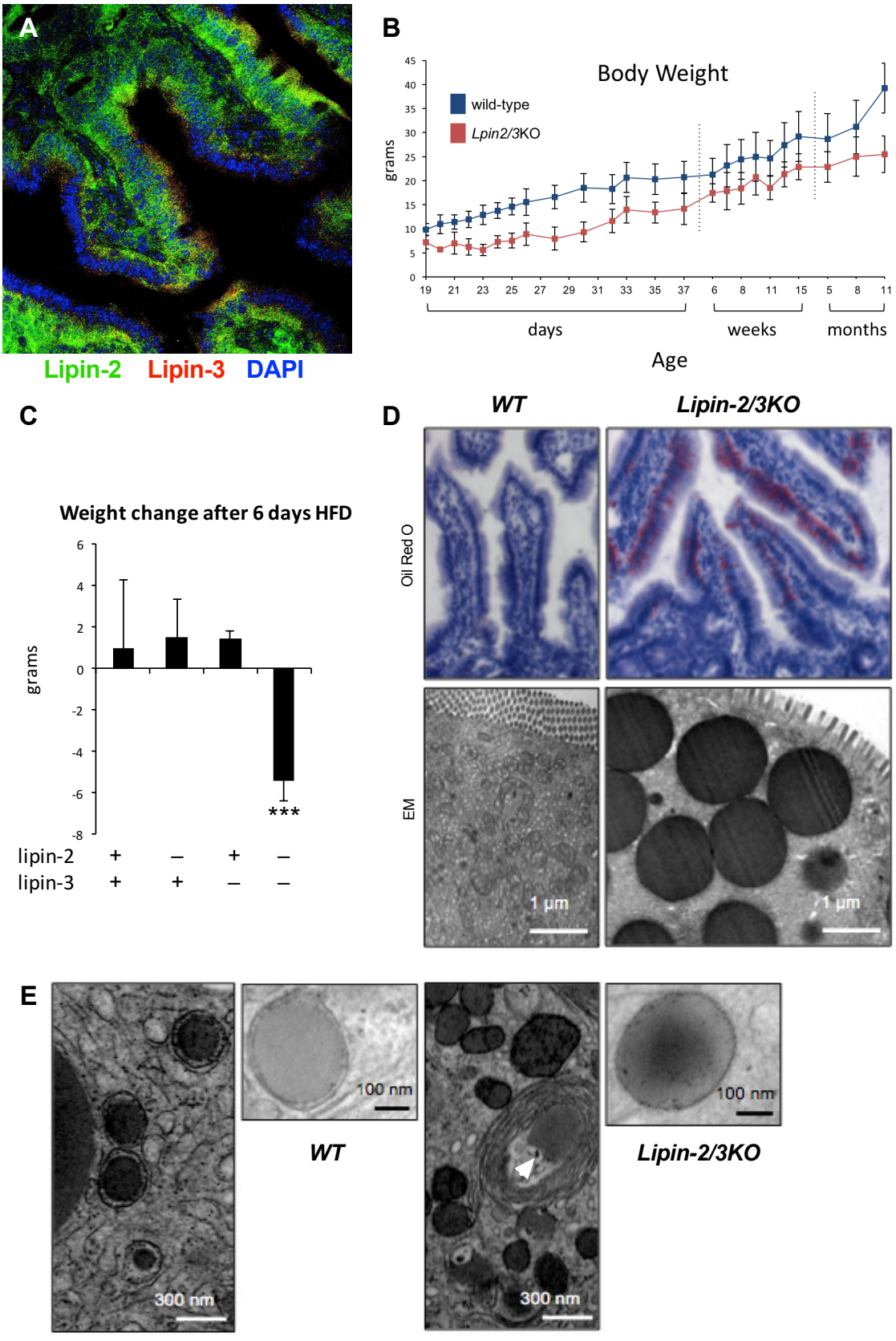

Figure 1.3. Unpublished data and results from previous studies with Lipin-2/3KO mice. (A) Immunofluorescence staining of Lipin-2 and Lipin-3 in the villus enterocytes of the small intestine. Lipin-2 is distributed throughout the cell, while Lipin-3 is concentrated mainly on the apical side. (B) DKO mice start off with and keep a lower body weight compared to wild-type mice. (C) Changing the diet from standard chow to a high-fat diet results in a rapid dramatic weight drop in percentage of whole-body fat mass in the Lipin-2/3KO mouse; mean ± standard deviation, *** p≤0.001. (D) Light microscopy analysis (200x magnification) of fasted intestinal sections stained with Oil Red O and electron microscope (EM)

analysis stained with osmium tetroxide (stains lipids black) depict cytosolic lipid droplet accumulation in enterocytes of DKO mice. (E) EM analysis of enterocytes, 2 hours after refeeding by oil gavage, shows abnormal phenotype of lipid droplets in Lipin-2/3KO mice with no surrounding membrane or one so tightly enclosing the LD that no electron-lucent space is visible in-between (see high-magnification image). "Whorled" membrane structures are found that sometimes surround LDs (white arrowhead).

assessing the levels of different phospholipids, Lipin-2 is the influencing factor. Mass spectrometry analysis of the phospholipid content in small intestine tissue showed lower levels of phosphatidylethanolamine (PE), phosphatidylserine (PS), cardiolipin (CL), and lysophosphatidylcholine (LYPC), while phosphatidylcholine (PC) levels were the same in the Lipin-2/3KO compared to the wild-type mice. It is more than clear that the role of Lipins in the G3P pathway is critical in intestinal lipid metabolism. All this data leaves the question to why and how lipid accumulates in the enterocytes and what the underlying mechanisms for a reduced lipid uptake and an impaired chylomicron secretion are. (all unpublished data)

1.1.6 Cytosolic Lipid Droplets

The current hypothesis on lipid droplets (LDs) sees them as a transient storage pool of lipids that helps optimize the absorption of fats during food consumption, mainly when the capacity for chylomicron formation and secretion is overwhelmed by the amount of digested MAG and FAs absorbed by the cell. (89) LDs also provide a sustained lipid supply to cells during times of fasting. Additionally, they smoothen the hypertriglyceridemia curve as a function of time after the consumption of a high fat meal through mobilization (hydrolysis and autophagy) of their lipids in the postprandial phase. (90) The amount of dietary fats consumed correlates with the level of TAG accumulated in CLD, especially in the proximal small intestine. Clearance of CLD takes place within 12 h. (91)

Structurally, LDs have a core consisting of neutral lipids (TAGs and cholesterol esters) surrounded by a monolayer of phospholipids and cholesterol, and associated proteins. These proteins are involved in many different biological processes including lipid metabolic pathways, membrane trafficking, protein folding, signaling pathways, and translation, which suggest their involvement in roles apart from lipid metabolism alone.

(92–94) The most abundant proteins on lipid droplets are perilipins (PLINs). As structural proteins they bind to the droplet surface and regulate lipid storage and hydrolysis. (95) PLIN2 (previously adipophilin) and PLIN3 (previously TIP47) are the most ubiquitous members of the multi-protein family, including in enterocytes where they have been shown to play certain roles in lipid droplet formation and metabolic compartmentalization. (96) PLIN2 coats LDs in response to chronic high-fat intake whereas PLIN3 binds to LDs following an acute lipid challenge. (91,96) It has been suggested that PLIN3 is preferentially associated to transient lipid storage while PLIN2 takes part in a more prolonged storage of fats. (90)

TAGs stored in cytosolic LDs eventually have to be mobilized by TAG hydrolases to make them available for the cell's needs, such as energy production or membrane biosynthesis. Together with its co-activator CGI-58, the adipose triglyceride lipase (ATGL) is located on lipid droplets to mediate the hydrolysis of TAG into DAG and FAs. (97) In the following step another enzyme associated with lipid droplets, the hormone-sensitive lipase (HSL), then hydrolyzes DAG into MAG and FAs. The last step of hydrolysis of MAG into glycerol and FAs is completed by the monoacylglycerol lipase (MGL). (98)

1.1.7 Intestinal Lipoprotein Biogenesis and Secretion

The main kind of lipoproteins secreted by the intestine are chylomicrons (CM). They are produced to transport dietary fats and fat-soluble vitamins into the blood. Chylomicrons are very large, spherical particles with a core consisting of mostly TAGs, and cholesteryl esters, encased by a phospholipid monolayer (mainly phosphatidylcholine), free cholesterol, and proteins. (99,100) Key proteins that are associated with CM are apolipoproteins ApoB48, ApoA-I, and ApoA-IV.

The nascent ApoB protein begins translocating into the lumen of the rough ER while still in complex with the polysome and before the translation is completed. (101) The dominant form of ApoB expressed in the small intestine is ApoB48. Due to apobec-1 mediating a C-to-U RNA editing of the ApoB100 mRNA, a translational stop codon is introduced into the nuclear script and leads to production of a protein only 48% the size

of the underlying ApoB100, which is mainly expressed in the liver. (102,103) The microsomal triglyceride transfer protein (MTP) together with its chaperone disulfide isomerase (PDI) ensure the correct optimal folding of ApoB48 and facilitate the formation of lipoproteins in the ER by helping to shuttle the newly synthesized TAG from within the ER membrane bilayer to the acceptor ApoB48 peptide. (104) This lipidation results in a primordial particle within the rough ER which is then further modified through a second-step "fusion" with luminal lipid droplets through the activity of MTP. (105) In case of a deficient MTP or insufficient lipidation, ApoB is subjected to degradation either through ER-associated degradation (ERAD), ubiquitination for the proteasomal pathway or autophagy. (101,106,107)

The lipoprotein particles are enriched and expand according to the availability of lipids and the size of lipid droplets present in the smooth ER. (105) This creates the prechylomicron (preCM), which acquires another apolipoprotein, ApoA-IV. (108) To travel from the ER to the cis-Golgi for further maturation, the preCM is exported in a prechylomicron transport vesicle (PCTV). (109) Due to the very large size of the preCM it requires this special transport system which differs from the general transport vesicles for newly synthesized proteins. PCTVs can reach a size of 250 nm or more in diameter. (110)

Studies in rat intestinal ER showed that multiple proteins associated with the budding complex for PCTV are involved in the maturation process including vesicle-associated membrane protein 7 (VAMP7), ApoB48, FABP1, CD36, and cytosolic coat protein II (COPII) complex. (25) FABP1 and CD36 play a role in promoting the budding from the ER. (25,42) FABP1 is part of a cytosolic protein complex (SAR1B, Sec13, SVIP) that prevents it from binding to the ER. Upon phosphorylation of SAR1B by protein kinase C-zeta (PKCζ), FABP1 can now bind to the ER and enable the generation and budding of the PCTV. (111,112) The SNARE complex interaction between VAMP7, acting as the v-SNARE, and Golgi membrane proteins synthaxin 5, Bet1, and vti1a, the t-SNAREs, helps fuse the PCTV with the cis-Golgi membrane. (113,114) COPII proteins (SAR1B, Sec23/24, Sec13/31) are incorporated into the vesicular complex that buds from the ER and are required for the fusion with the Golgi membrane together with the SNARE proteins. (115)

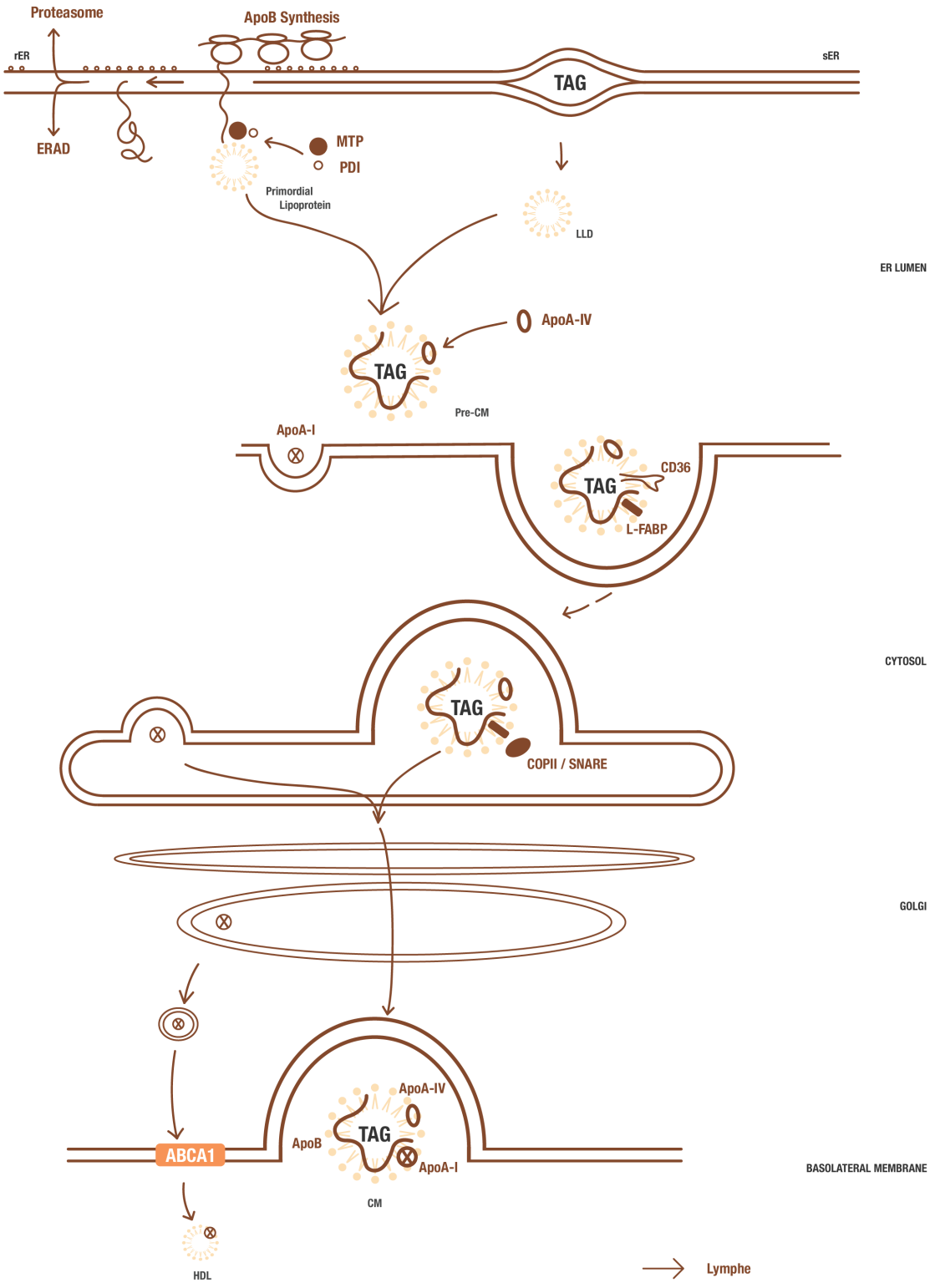

Figure 1.4. Model of intestinal chylomicron synthesis. The nascent ApoB polypeptide is co-translationally translocated across the ER membrane of the rough ER (rER). The direct interaction between the NH_2-terminal domain of ApoB and MTP leads to optimal folding of ApoB and the formation of a primordial lipoprotein particle, when TAG is available. The protein disulfide isomerase (PDI) is bound to MTP and acts as a chaperone. If MTP function is impaired or the availability of lipid limited, the nascent ApoB ends up being misfolded and is degraded by either the luminal ER-associated degradation pathway (ERAD) or the proteasomal pathway after ubiquitination. After the primordial lipoprotein particle fuses with luminal LDs (LLDs) and acquires ApoA-IV it results in a prechylomicron (preCM). Auxiliary proteins in the maturation and budding process of the prechylomicron transport vesicle (PCTV) are CD36 and FABP1. Subsequently it fuses with the Golgi membrane through the help of COPII proteins and a SNARE complex, including

SAR1B and VAMP7. After further maturation through addition of ApoA-I the chylomicrons are eventually secreted on the basolateral side of the cell. ApoA-I is also involved in the formation of cholesterol-rich HDL particles through the ABCA1 transporter. (adapted from (17,60,116))

SAR1B has been shown to stabilize the positive curvature of the membrane to help bud the vesicle. (117)

Apolipoprotein A-I (ApoA-I) arrives at the Golgi in a different transport vesicle than the PCTV. In the Golgi lumen it attaches to the prechylomicron in addition to the already bound ApoB48 and ApoA-IV resulting in a mature chylomicron. (60) ApoB48 undergoes glycosylation. (118) Then the chylomicrons leave the trans-Golgi in vesicles and travel to the basolateral membrane of the enterocyte where they are secreted into the lymphatic circulation. (119) From there they reach the blood circulation where lipoprotein lipase starts metabolizing the lipids. This releases FAs as an energy source for the body's cells or to be stored in the adipocytes of the fat tissue. The chylomicron remnants, now depleted from lipids, are taken up by the liver where they are degraded. (90)

1.1.8 Autophagy and Its Role in Lipid Metabolism

It has been shown in the past that autophagy is involved in cytosolic LD clearance in hepatocytes. (120–122) A major difference between the lipid metabolism in hepatocytes and enterocytes is the load of lipids these cells are confronted with. Hepatocytes take up lipids from the bloodstream through regulated receptor-mediated endocytosis while enterocytes are faced with an immediate and massive volume of dietary lipids in the lumen of the small intestine. Upon uptake of lipids the ER starts partitioning the newly synthesized TAGs into cytosolic lipid droplets or prepares them for lipoprotein biogenesis. Additionally, the ER plays a role in other pathways such as ER-stress-mediated signaling, membrane dynamics and trafficking, and autophagosome formation. (123) Studies in mouse enterocytes and differentiated Caco-2 cells showed that an immediate autophagic response is caused by the delivery of dietary lipid micelles to enterocytes, presumably to avoid TAG accumulation in the ER bilayer. (123)

There are three main forms of autophagy in a cell: macroautophagy, microautophagy, and chaperone-mediated autophagy (CMA) (see Figure 1.5). (124) The macroautophagy process begins with the formation of a phagophore, that together with autophagy-related actors including ATG proteins, phosphatidylinositol-3-phosphate (PI3P), beclin1, and LC3, starts maturing into an autophagosome. (125) After fusion with lysosomes or late endosomes the cargo is degraded by hydrolases. (126) Microautophagy is just the invagination on the surface of lysosomes trapping proteins from the cytosol for degradation while CMA is a specific process of targeting cytosolic proteins with CMA-targeting motifs that are biochemically related to the amino acid sequence "KFERQ[1]". (127,128) These proteins are bound by the heat shock cognate 70 (HSC70) chaperone complex and transferred to the lysosome-associated membrane protein type 2A (LAMP-2A) where they are unfolded and translocated into the lysosomal lumen for degradation. (129,130) In contrast to macroautophagy which is first activated in the event of starvation and reaches its peak for protein degradation in the first couple of hours, CMA is gradually activated after about 10 hours of starvation and can persist for up to three days. (131,132)

Recent studies by Kaushik and Cuervo, 2015 showed that CMA plays a role in regulating lipid homeostasis. (133) PLIN2 and PLIN3 are co-localized and directly interact with HSC70 on the surface of LDs; this interaction activates CMA. The removal and degradation of PLIN2 and PLIN3 enables ATGL and other lipases or autophagy-related proteins (ATGs) to bind to LDs. (133) ATGL is then able to mobilize the stored TAGs and generates fatty acids, which are subsequently used as building blocks for membrane synthesis, energy substrates, or mediators in cell signaling processes. (134) In the case that ATG proteins bind to cytosolic LDs they enable autophagosome membranes to be built and macrolipophagy of fractions or the complete LD to take place. (135) The stored TAGs are then broken down by lysosomal lipases. (120)

[1] CMA-targeting motif for HSC70 recognition; this motif consists of a glutamine (Q) residue at one end, one positively charged amino acid (lysine (K) or arginine (R)), one hydrophobic (either phenylalanine (F), valine (V), leucine (L) or isoleucine (I)), and one negatively charged amino acid (glutamic acid (E) or aspartic acid (D)) with the fifth being an amino acid with a positive or hydrophobic residue. (128)

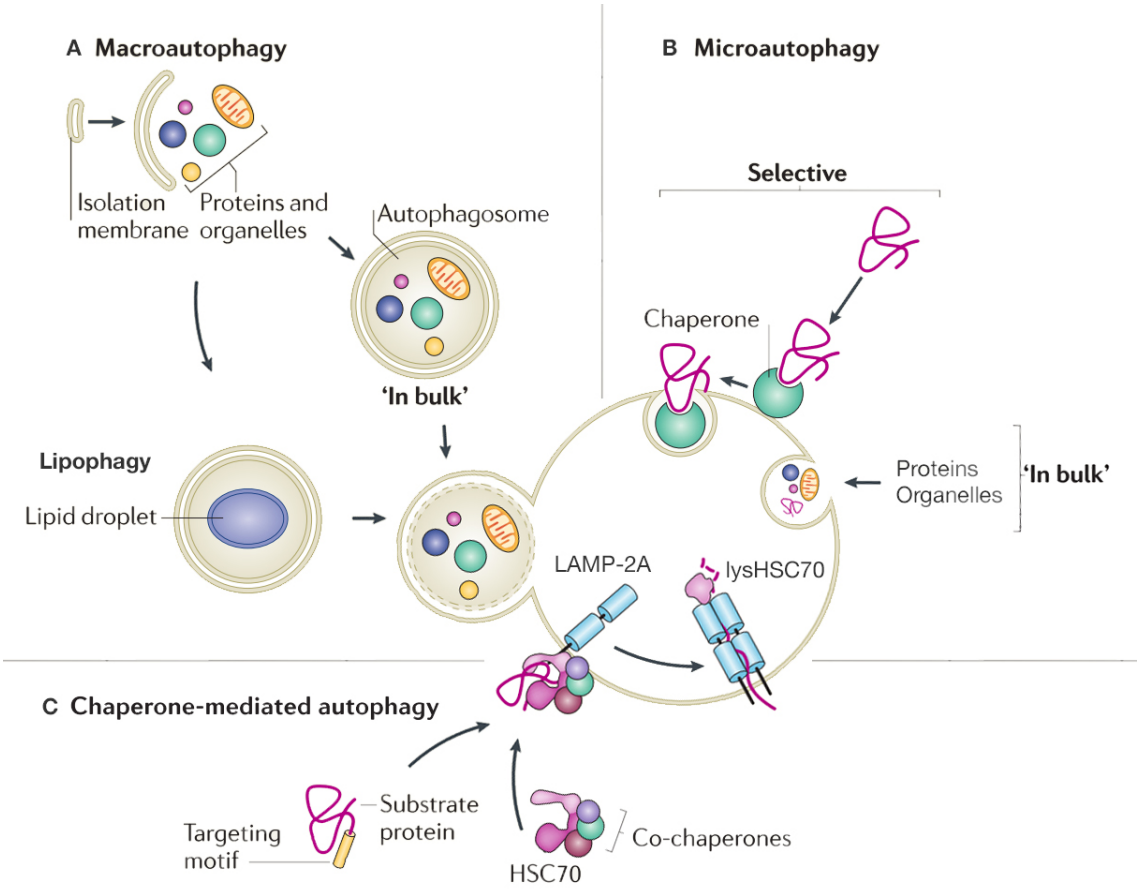

Figure 1.5. Different types of autophagy. There are three main ways cytosolic proteins can enter lysosomes for degradation. (A) Macroautophagy: Cytosolic proteins among other cytosolic components and organelles are encapsulated by a piece of ER-derived membrane forming a double-membrane vesicle, the autophagosome, which then fuses with lysosomes. Lipophagy describes the autophagic digestion of lipid droplets. (B) Microautophagy: Cytosolic components are sequestered 'in bulk' or selectively targeted by chaperones and are subjected to degradation through invagination and internalization into the lysosome. (C) CMA: The heat shock cognate 70 (HSC70) chaperone complex targets proteins containing a specific targeting motif and delivers them to the lysosomal membrane receptor LAMP-2A. After unfolding the protein is translocated into the lumen for degradation. lysHSC70, lysosomal HSC70. (adapted from (43))

2 METHODS

2.1 Protein Analysis of Mouse Tissue Samples

2.1.1 Protein Extraction from Small Intestine Tissue Samples

The tissue samples used in this study were harvested from *Lpin2*$^{-/-}$/*Lpin3*$^{-/-}$ double knockout (Lipin-2/3KO) mice which had been generated by breeding previously created mice carrying either one of the Lipin-2KO or Lipin-3KO alleles. (66)
The animals had been sacrificed after a 5 hour fasting period by cervical dislocation under anesthesia. Organs were dissected, immediately frozen in liquid nitrogen, and stored in -80°C. Protein was isolated from frozen samples of the duodenum part of the small intestine with the following protocol.

The buffer used for the extraction contained 10 mM Tris pH7.5, 10 mM NaCl, 1 mM EDTA and 1% Triton X-100. To prevent digestion of proteins, Phosphatase Inhibitor Cocktail 2 and 3 (Sigma-Aldrich Corp. St. Louis, MO, USA) in a 1:20 ratio each were added as well as 5x cOmplete Mini EDTA-free Protease Inhibitor Cocktail tablets (Roche Diagnostics, Indianapolis, IN, USA).

A small piece of tissue was cut on dry ice and transferred into 500 µL of ice cold buffer mix in a glass homogenizer. The samples were homogenized for 20 times and then transferred into microcentrifuge tubes. After a centrifugation of 6000 rpm at 4°C for 5 min the supernatant was transferred into new tubes. Protein concentrations were measured with the Pierce BCA Protein Assay Kit (Thermo Fisher Scientific, Waltham, MA, USA) with a 50:1 ratio of reagent A to reagent B and BSA as the standard. Samples were stored in a -80°C freezer until further use.

2.1.2 Western Blot

Polyacrylamide gel electrophoresis was performed using pre-poured gels (Thermo Fisher Scientific, Waltham, MA, USA). Gel selection was based on the size of proteins to be analyzed:

- The Novex NuPAGE 4-12% Bis-Tris Protein Gel, 1.0 mm thick with 15-wells, for proteins sized 15 kDa to 260 kDa, was run in 1x Novex NuPAGE MOPS SDS Running Buffer.
- The Novex NuPAGE 3-8% Tris-Acetate Protein Gel, 1.5 mm thick with 15-wells, for proteins sized 40 kDa to 500 kDa, was run in 1x Novex NuPAGE Tris-Acetate SDS Running Buffer.

As a molecular size reference, the Amersham ECL Full-Range Rainbow Marker (GE Healthcare, Chicago, IL, USA) or the Novex HiMark Pre-Stained Protein Standard (Thermo Fisher Scientific, Waltham, MA, USA) were used.

The protein samples were mixed with 1x Novex NuPAGE DS Sample Buffer (Thermo Fisher Scientific, Waltham, MA, USA) and 1:25 β-Mercaptoethanol, boiled in a water bath for 10 min, then cooled on ice and spun down at high speed for about 10 sec. 15 µg protein was generally loaded in each lane. The gels were pre-run for 15 min at 60 V. After loading the samples, the proteins were separated at 150 V for about 85 min.

A wet transfer was done in chilled 1x Novex NuPAGE Transfer Buffer (Thermo Fisher Scientific, Waltham, MA, USA) onto a 0.2 µm nitrocellulose membrane (Bio-Rad Laboratories, Hercules, CA, USA) at 100 V for 60 min. The membrane was then rinsed in 1x TBST (20 mM Tris-HCl, pH 7.6, 137 mM NaCl, 0.1% Tween-20) and stained with Ponceau S solution to check correct transfer as well as comparable protein amounts in all samples. Membrane was then rinsed in dH_2O and 1x TBST to remove Ponceau S staining. This was followed by blocking the membrane in 1x TBST supplemented with 5% non-fat dry milk powder on a shaker at room temperature (RT) for 60 min. After a rinse in 1x TBST the membrane was incubated with the primary antibody in a sealed plastic bag in 4°C on a rotating plate overnight. The antibody solution consists of 1% milk (or 5% BSA for certain antibodies) in 1x TBST and 0.1% NaN_3 for conservation purposes. The solutions were stored at 4°C and reused. The membrane was then washed three times in 1x TBST for 5 min each on a shaker at RT. Incubation with the secondary HRP-

conjugated antibody in 1% milk in 1x TBST was done at RT on a shaker for 60 min. After this the membrane was washed again. To detect the protein bands, the membrane was developed with the Amersham ECL Prime Western Blotting Detection Reagent (GE Healthcare, Chicago, IL, USA). Solution A and B were heated up to 37°C for 5 min and were then mixed in a 1:1 ratio. The membrane was shortly incubated in the solution, the excess liquid removed with a Kimwipe and the picture was taken with the ChemiDoc XRS+ imaging system together with the Image Lab software (both from Bio-Rad Laboratories, Hercules, CA, USA).

If necessary, the membrane was rinsed in 1x TBST and stripped with the Multi-Western Stripping Buffer (Bioland Scientific LLC, Paramount, CA, USA) to prepare it for the incubation with another primary antibody. The stripping was done on a shaker at RT for 15 min. Subsequently the membrane was thoroughly rinsed with dH_2O for about three times for 3 min each, blocked with 5% milk, and followed by the steps as described above.

The primary antibodies that were used are listed in Table 2.1:

Table 2.1. List of primary antibodies used for Western blots with information about dilution factor, animal species, conditions for working solution (1x TBST with either 1% milk or 5% BSA), and the company antibodies were obtained from.

primary antibody	dilution	species	1% milk / 5% BSA	company
alpha-Tubulin 4a	1:10000	rabbit	milk	GeneTex, Irvine, CA, USA
ApoA-I	1:1000	rabbit	milk	Karen Reue's Lab
ApoA-IV	1:1000	rabbit	milk	Karen Reue's Lab
ApoB	1:10000	mouse	milk	Stephen G Young's Lab
ATGL	1:200	rabbit	BSA	Cell Signaling Technology (CST), Danvers, MA, USA #2138
Calnexin	1:1000	rabbit	milk	Abcam, Cambridge, MA, USA
Hsp70/Hsc70 (13D3)	1:1000	mouse	milk	Novus Biologicals LLC, Littleton, CO, USA
LC3-I/-II (APG8)	1:1000	mouse	milk	Abgent, San Diego, CA, USA

Lipin-2	1:5000	rabbit	BSA	Brian N Finck's Lab
Lipin-3	1:1000	goat	BSA	LifeSpan BioScience, Seattle, WA, USA
p62	1:1000	rabbit	milk	Sigma-Aldrich, St. Louis, MO, USA
phospho-(Ser/Thr) PKA-substrate	1:1000	rabbit	BSA	CST, Danvers, MA, USA #9621
Phospho-HSL (Ser563)	1:1000	rabbit	BSA	CST, Danvers, MA, USA #4139

The secondary antibodies (see Table 2.2) that were used were all conjugated with the enzyme horseradish peroxidase (HRP), which has the ability to amplify weak signals through catalyzing the oxidation of luminol generating detectable chemiluminescence. All secondary antibodies were used in a working solution of 1x TBST with 1% milk.

Table 2.2. List of HRP-conjugated secondary antibodies with their dilution factors that were used for Western blots and the company they were obtained from.

secondary antibody	dilution	company
donkey anti-goat IgG-HRP	1:10000	Santa Cruz Biotechnology, Dallas, TX, USA
goat anti-rabbit IgG-HRP	1:10000	
rabbit anti-mouse IgG-HRP	1:20000	Karen Reue's Lab

2.1.3 Total Cholesterol in Mouse Small Intestine

The amount of total cholesterol in the protein extraction samples from the mouse small intestine was measured by using the Cholesterol E Kit (Wako Diagnostics, Mountain View, CA, USA). Following the manufacturer's instructions, a standard curve was established and samples were measured with 150 µL per well in triplicates in a 96-well plate on the Model 680 Microplate Reader (Bio-Rad Laboratories, Hercules, CA, USA) at 595 nm. Data was normalized to the protein concentration present in the samples and presented as ng cholesterol/µg protein. Statistical analysis with two-way ANOVA was done using GraphPad Prism version 6.0 (GraphPad Software, La Jolla, CA, USA, www.graphpad.com).

2.2 RNA Analysis of Mouse Tissue Samples

2.2.1 RNA Isolation from Small Intestine Tissue Samples

I. Homogenization

A 50-100 mg piece of tissue was cut on dry ice and transferred into 1 mL of TRIzol (Ambion by Thermo Fisher Scientific, Waltham, MA, USA) in a glass homogenizer on ice. It was homogenized for about 20 times and then transferred to a microcentrifuge tube.

II. Phase Separation

Samples were incubated at RT for 5 min. 0.2 mL chloroform per 1 mL of TRIzol was added and the tubes were vortexed for 15 sec. After another incubation at RT for 3 min the samples were centrifuged at 4°C at 12,000 rpm for 15 min to separate the aqueous phase containing the RNA from the phenol-chloroform phase.

III. RNA Precipitation

The aqueous phase (about 0.5 mL) was transferred into a fresh tube. 0.5 mL isopropanol per 1 mL TRIzol was added to precipitate the RNA. After mixing the samples they were incubated at RT for 10 min. This was followed by centrifugation at 4°C at 12,000 rpm for 10 min.

IV. RNA Wash

The supernatant was removed and the pellet washed with 1 mL of 75% ethanol per 1 mL TRIzol. Samples were vortexed and centrifuged at 4°C at 12,000 rpm for 5 min. The supernatant was removed and the tube was kept open for the pellet to dry.

V. Dissolution

The dried pellet was dissolved in 100 µL nuclease-free H_2O and the samples were stored at -80°C. RNA concentrations were measured with the NanoDrop Lite Spectrophotometer (Thermo Fisher Scientific, Waltham, MA, USA).

2.2.2 Reverse Transcription

The RNA isolated from the duodenum tissue samples of the small intestine was transcribed into cDNA with this reverse transcription reaction:

X µL	RNA [2µg]
X µL	nuclease-free H_2O
2 µL	5x all-in-one cDNA Synthesis Supermix (Biotool, Houston, TX, USA)
10 µL	total

The following temperature settings (see Table 2.3) for the thermocycler were chosen:

Table 2.3. Thermocycler temperature conditions for reverse transcription.

25°C	10 min
42°C	30 min
85°C	5 min
4°C	∞

2.2.3 Quantitative PCR

The cDNA samples were diluted with nuclease-free H_2O in a 1:8 ratio, which equals 70 µL of H_2O.
To obtain a standard curve an aliquot of all cDNA samples was mixed together in these dilutions: 1:1, 1:5, 1:25, 1:125.

The following reagents were combined together for the quantitative polymerase chain reaction (qPCR). There had to be a mixture for every gene of interest with its corresponding primer pair (see Table 2.4).

6.00 µL	2x SYBR Green qPCR MasterMix (Biotool, Houston, TX, USA)
0.45 µL	forward Primer [10 µM]
0.45 µL	reverse Primer [10 µM]
5.10 µL	nuclease-free H_2O
12.0 µL	total

The total volume of 12 µL was transferred into the wells of a Multiplate Low-Profile 96-Well Unskirted PCR Plate (Bio-Rad Laboratories, Hercules, CA, USA). To reach a final volume of 15 µL per well 3 µL of either the standard or the cDNA sample was added.

To prevent evaporation of the samples during the reaction the plate was covered with a Microseal 'B' Adhesive Seal (Bio-Rad Laboratories, Hercules, CA, USA). A centrifuge spin at 3500 rpm for 5 min was done to remove air bubbles in the samples which could otherwise interfere with the fluorescence detection.

The plate was read in the CFX Connect Real-Time PCR System and the data was analyzed with the CFX Manager Software (both Bio-Rad Laboratories, Hercules, CA, USA). Statistical data analysis was done with two-way ANOVA with a Sidak correction. In case of significance in genotype/diet comparison this was followed up with an unpaired parametric t-test with Welch's correction. Results are presented as the mean ± the standard deviation. Probability values (p) of less than 0.05 were considered statistically significant and are indicated with a single asterisk (*). Likewise, probability values less than 0.01 are indicated with two asterisks (**) and those less than 0.001 are indicated with three asterisks (***). Analyses were performed using GraphPad Prism version 6.0 (GraphPad Software, La Jolla, CA, USA, www.graphpad.com). The genes *36B4* (acidic ribosomal phosphoprotein P0, RPLP0) and *TBP* (TATA-box binding protein) were used for normalization. (136,137)

Table 2.4. List of primer sequences for all genes analyzed with qPCR.

gene	forward primer 5' – 3'	reverse primer 5' – 3'
36B4	AGTACACCTTCCCACTTACTG	ACCAAGTCAAGAGACTGTCTC
ABCG5	CTGCTCAGCATCTCTGGGCTG	AGGTGTTGGATCCACCACAAG
ACAD8	CTGCAAAGTCAAAGGCCACT	CTCAAGTCCCTGGCTCAGAC
ACOT8	CTGGATCACGAGGCCCTCATT	GGTGGGTTCACCACCTTGATC
ANGPTL4	GTTTGCAGACTCAGCTCAAGG	CCAAGAGGTCTATCTGGCTCTG
AOX/ACOX1	CAGGAAGAGCAAGGAAGTGG	CCTTTCTGGCTGATCCCATA
ApoB	CAGTATTCTGCCACTGCAACC	AGGACTTCACTAGATAAGGTCC
CD36	GAGACTGGGACCATTGGTGA	TATATGTAGGCTCATCCACTAC
CPT1A	AAACCCACCAGGCTACAGTG	TCCTTGTAATGTGCGAGCTG
FABP1	GTCAAGGCAGTCGTCAAGCT	TCTTGTAGACAATGTCGCCCA
FABP2	TAGACCGGAACGAGAACTATG	AATGGTCCAGGCCCCAGTGA

FABP4/AP2	GAACCTGGAAGCTTGTCTTCG	ACCAGCTTGTCACCATCTCG
FST	TTATACAGGACCTGGCAGCG	CCTCCTGCTGCTGCTACTCT
GRP78	CGGTGCAGCAGGACATCAAGTT	CTTGTCGCTGGGCATCATTGAA
HMGCL	AGCGCTTTGCTGGAGTCATGC	CCCATCGAGTACAACTTCTTG
HMGCS1	GACACACATCACTTAGCCAACT	CGAGGTTGCAGGGAGTCTTG
HMGCS2	ACTTGGTACCTTGAACGAGTG	GATGCTGTTTGGGTAGCAGCT
HSL	GGAACTAAGTGGACGCAAGC	CCAGGGCTGCCTCAGACAC
LPCAT3	TCACGGGCCTCTCAATTGCTT	GCCCATGAGTCGCAGGATGA
MGAT2	TGGTGGTACCTGGACTGGGACA	GTGGAAGCCCGCGATGTAGTTC
MTP	AGCTGCAATCTGGACTAAAGG	ACTGTGACGTCGCTGGTTATC
PPARα	CAGTGGGGAGAGAGGACA	AGTTCGGGAACAAGACGT
SAR1B	CAGCACGTCCCAACGCTACATC	ACGTGCCCACCCAGATCAAAA
TBP	ACCCTTCACCAATGACTCCTATG	ATGATGACTGCAGCAAATCGC
VAMP7	TTTGGCTGCACAACTGAAGCA	TCAGCAATTCCAACCTTTCTCCA

2.3 Immunofluorescence Staining of Mouse Small Intestine

After Lipin-2/3KO and wild-type mice were treated with oil gavage with added BODIPY 493/503 and were sacrificed two hours later, sections of the duodenum were frozen in Tissue-Tec O.C.T Compound Embedding Medium for Frozen Tissue Specimens (Sakura Finetek, Torrance, CA, USA) and cut with the Leica CM1900 cryostat at -20°C at a thickness of 20 µm. The slices were mounted onto Superfrost Plus Microscope Slides (Thermo Fisher Scientific, Waltham, MA, USA) for immunofluorescence staining.

The cryosections were air dried for 15 min and fixed in 10% formalin for 60 min. After drying they were washed with 1x PBS three times for 5 min. To prevent nonspecific binding of the antibodies a blocking buffer of 1x PBS with 5% donkey serum and 0.04% Triton X-100 was used for 30 min. Incubation with the primary antibody (see Table 2.5) in blocking buffer took place overnight at 4°C. The slides were rinsed with 1x PBS twice for 5 min. This was followed by incubation in secondary fluorescence-conjugated (cyanine 2 or 3) antibody in blocking buffer for 120 min in the dark at room temperature. Another washing step of three times 1x PBS for 5 min removing the excess antibody was done. A coverslip was placed on top of the tissue section with the ProLong Diamond Antifade Mountant with DAPI (Thermo Fisher Scientific, Waltham, MA, USA).

Table 2.5. List of primary and secondary antibodies (conjugated with cyanine 2 or 3) used for immunofluorescence staining of tissue samples from the mouse small intestine. Dilution, species, and company the antibodies were obtained from are listed.

primary antibodies	**dilution**	**species**	**company**
ApoB	1:500	mouse	Stephen G Young's Lab
Calnexin	1:300	rabbit	Abcam, Cambridge, MA, USA
Hsp70/Hsc70 (13D3)	1:300	mouse	Novus Biologicals LLC, Littleton, CO, USA
Lipin-2	1:500	rabbit	Brian N Finck's Lab
Lipin-3	1:300	goat	LifeSpan BioScience, Seattle, WA, USA
Perilipin2	1:200	guinea pig	Fitzgerald Industries International, Acton, MA, USA
secondary antibodies	**dilution**		**company**
Cy2 AffiniPure Donkey Anti-Guinea Pig IgG	1:500		Jackson Immuno Research Labs, West Grove, PA, USA
Cy2 AffiniPure Donkey Anti-Rabbit IgG	1:500		
Cy3 AffiniPure Donkey Anti-Goat IgG	1:500		
Cy3 AffiniPure Donkey Anti-Mouse IgG	1:500		

2.4 Engineering Human HT-29 Cell Line with CRISPR/Cas9

The target genes for this experiment were *LPIN2* and *LPIN3* with the region of interest of the first ~250 bp of the coding DNA sequence (CDS). The design of the guide RNAs (gRNAs) was done using the online CRISPR design tool developed by the Zhang Lab, MIT 2015 (http://crispr.mit.edu). This tool scans the input DNA sequence (in FASTA format), discovers possible off-targets genome wide, and selects guide sequences with high target specificity. The guide sequence is 20 nucleotides long followed by a protospacer adjacent motif (PAM) sequence of 5'-NGG-3' with "N" being any nucleobase. The job output is the resulting guide RNAs listed with their off-targets found in the genome and organized in order of their quality score indicating the faithful on-target activity ranging

from zero to 100%. The threshold was chosen as a quality score of >85. It has to be ensured that the guide sequence does not contain a *BbsI* cut site (GAAGAC or GTCTTC), which is used for cloning. Additionally, the four nucleotides CACC were added to the 5-prime end (5') and the following first nucleotide of the guide sequence was changed to a G (as depicted below). The reverse complement sequence was taken and the nucleotides AAAC were added to the 5' end to generate the other half of the guide RNA pair.

The following guide RNA pairs in Table 2.6 – three for each gene – were selected and ordered from Sigma-Aldrich, St. Louis, MO, USA (0.025 µM, desalted).

Table 2.6. Guide RNA oligos for CRISPR/Cas9 editing of *LPIN2* and *LPIN3* in HT-29 cells.

guide RNA	sequence 5' – 3'
Lip2-1F	CACC**G**GCACCTTTTCACGTTCGGTT
Lip2-1R	AAACAACCGAACGTGAAAAGGTGC**C**
Lip2-2F	CACC**G**GGGGTGCATTGATGTCATCG
Lip2-2R	AAACCGATGACATCAATGCACCCC**C**
Lip2-3F	CACC**G**GCTCTACAAGGGCATTAACC
Lip2-3R	AAACGGTTAATGCCCTTGTAGAGC**C**
Lip3-1F	CACC**G**GAGCGGCGGCATTGACGTGC
Lip3-1R	AAACGCACGTCAATGCCGCCGCTC**C**
Lip3-2F	CACC**G**GCAGCTTGCCAAAACGCACG
Lip3-2R	AAACCGTGCGTTTTGGCAAGCTGC**C**
Lip3-3F	CACC**G**GCACCCTTCCACGTGCGTTT
Lip3-3R	AAACAAACGCACGTGGAAGGGTGC**C**

For the PCR amplification of the region of interest later on genotype primers were designed. The region amplified by these primers has to envelope the chosen guide sequence and the minimal distance between either end of the PCR amplicon has to be >50 bp away from the guide. The overall length of the PCR amplicons should be between 200-500 bp. As well as the gRNA oligos above, the primers (see Table 2.7) were ordered from Sigma-Aldrich, St. Louis, MO, USA.

Table 2.7. List of forward and reverse primers for PCR amplification and sequencing of regions in the *LPIN2* and *LPIN3* gene where the guide RNAs bind and Cas9 endonuclease introduces a cut.

primer	sequence 5' – 3'
Lip2 fwd	GGCCTAGAAAACTCACAATAGC
Lip2 rev	TTGTTACGACTGTTATTTCTTTGTCA
Lip3 fwd	AGACCTTTGTGCAAGCCACT
Lip3 rev	CAAATGAAGGGAAGCCTGTC

The guide oligos were cloned into the backbone vector pSpCas9(BB)-2A-Puro (pX459) V2.0 plasmid (#62988 Addgene, Cambridge, MA, USA). (138) The 9175 bp large vector has an Ampicillin resistance gene for bacterial transformation. Puromycin was used as a selection marker in mammalian cells.

The following steps explain the overall process of how we successfully generated a HT-29 cell clone deficient in both *LPIN2* and *LPIN3* through CRISPR/Cas9 engineering.

I. Phosphorylation and annealing of each pair of oligos from Table 2.6 was done in the reaction below:

1.0 µL	Oligo 1 [100 µM]
1.0 µL	Oligo 2 [100 µM]
1.0 µL	10x T4 DNA Ligase Reaction Buffer (New England Biolabs (NEB), Ipswich, MA, USA)
0.5 µL	T4 Polynucleotide Kinase [10 U/µL] (NEB, Ipswich, MA, USA)
6.5 µL	ddH_2O
10 µL	total

The temperature profile for this reaction was set to the program in Table 2.8.

Table 2.8. Thermocycler program for phosphorylation and annealing of guide oligos.

37°C	30 min
95°C	5 min
ramp down to	
25°C	at 5°C/min

The annealed oligos were diluted 1:250 with ddH_2O.

II. Digestion of the vector and ligation of the oligo duplex was done combined in a single step.

X µL	pX459 [100 ng]
2 µL	diluted annealed oligo duplex (from step I.)
2 µL	10x Tango Buffer (Thermo Fisher Scientific, Waltham, MA, USA)
1 µL	DTT [10 mM] (Thermo Fisher Scientific, Waltham, MA, USA)
1 µL	ATP [10 mM] (NEB, Ipswich, MA, USA)
1 µL	FastDigest *BbsI* [10 U/µL] (Thermo Fisher Scientific, Waltham, MA, USA)
0.5 µL	T7 DNA Ligase [3000 U/µL] (NEB, Ipswich, MA, USA)
Y µL	ddH_2O
20 µL	total

The ligation reaction is incubated in a thermocycler using the following parameters (see Table 2.9).

Table 2.9. Thermocycler conditions for digestion and ligation reaction.

37°C	5 min	repeat 6x
23°C	5 min	
4°C	∞	

III. To prevent unwanted recombination products, the ligation reaction is treated with PlasmidSafe exonuclease.

11 µL	Ligation reaction
1.5 µL	10x PlasmidSafe Buffer (Epicentre, Madison, WI, USA)
1.5 µL	ATP [10 mM] (NEB, Ipswich, MA, USA)
1.0 µL	PlasmidSafe ATP-Dependent DNase [10 U/µL] (Epicentre, Madison, WI, USA)
15 µL	total

Samples were incubated in a thermocycler at 37°C for 30 min.

IV. Transformation

For the transformation, 1 µL of the final product was added into DH5α competent cells (Thermo Fisher Scientific, Waltham, MA, USA). After an incubation on ice for 30 min the cells underwent a heat shock at 42°C for 30 secs and were placed back on ice immediately. 250 µL LB broth were added. To ensure proper regeneration of the cells

they were placed in a shaker at 37°C for 35 min. Cells were plated onto pre-warmed LB-Ampicillin agar plates and incubated at 37°C overnight.

V. Miniprep

A few colonies were picked to each inoculate 2 mL LB broth with 100 µg/mL Ampicillin and were incubated in a shaker at 37°C overnight. The EasyPrep Plasmid Miniprep Kit (Bioland Scientific LLC, Paramount, CA, USA) was used according to the manufacturer's instructions.

VI. Sequencing

The DNA samples from the Miniprep were sequenced to confirm successful cloning. The U6 sequencing primer with the sequence 5'-ACTATCATATGCTTACCGTAAC-3' was used. It anneals to the U6 promoter located on the pX459 plasmid.

2 µL	BigDye Terminator v3.1 Ready Reaction Mix (Thermo Fisher Scientific, Waltham, MA, USA)
2 µL	5x Sequencing Buffer
1 µL	U6 primer [10 µM]
X µL	DNA [400 ng]
X µL	ddH_2O
10 µL	total

The following temperature protocol (see Table 2.10) was set for the sequencing reaction.

Table 2.10. Thermocycler temperature program for sequencing reaction.

96°C	10 sec	25 cycles
50°C	5 sec	
60°C	4 min	
4°C	∞	

The samples were then submitted to the UCLA Genotyping and Sequencing Core at CHS 36-125 (http://genoseq.ucla.edu/) for analysis. Sequencing was performed on the 3730 Capillary DNA Analyzer (Applied Biosystems, Foster City, CA, USA). Data was analyzed with 4Peaks v1.7.2 software (http://nucleobytes.com/index.php/4peaks) and

CRISPR/Cas9 mutations were investigated with the multiple sequence alignment tool Clustal Omega (http://www.ebi.ac.uk/Tools/msa/clustalo).

The clones with a successful cloning of the guide oligos into the plasmid were chosen for another transformation into DH5α competent cells (see protocol above under IV. Transformation).

VII. Midiprep

From these transformation colonies were picked for an all-day culture in 2 mL LB-Ampicillin medium which was transferred into a 100 mL culture overnight in a shaker at 37°C. To isolate the plasmid, the EasyPrep Plasmid Midiprep Kit (Bioland Scientific LLC, Paramount, CA, USA) was used according to the manufacturer's instructions.

VIII. Transfection and Selection

The goal was to generate double knockout cells with both a disrupted *LPIN2* as well as *LPIN3* gene. HT-29 cells, a human colorectal adenocarcinoma cell line, were chosen for the transfection. Cells were grown in 6-well plates to a density of about $60x10^5$ cells/mL. For the transfection with the BioT Cell Transfection Reagent (Bioland Scientific LLC, Paramount, CA, USA) 100 µL serum-free DMEM and 6 µL BioT were mixed with 2 µg DNA plasmid. For the double knockout co-transfections, a total of 4 µg DNA (2 µg each) was used. Different combinations of guide RNAs were used to generate double knockout cells (see Figure 2.1). Since the protein expression usually reaches a high level at around 48 hours post-transfection the selection treatment with 1 µg/mL Puromycin dihydrochloride (Santa Cruz Biotechnology, Dallas, TX, USA) was started and maintained for 5 days.

A week after the transfection and selection with Puromycin single clones were picked and transferred to a 96-well plate. From there the cells were split into larger wells when reaching about 60% confluency. At the point where enough cells had been obtained a part of them were frozen, the other part was used to isolate the genomic DNA. The protocol for extracting genomic DNA from cells is explained under 2.4.2.

SKO

Lip2-1	Lip2-1	Lip2-3
Lip3-1	Lip3-2	Lip3-3

DKO

Lip2-1	Lip2-2	Lip2-3
Lip3-1	Lip3-2	Lip3-3
Lip2-1	Lip2-2	Lip2-3
Lip3-2	Lip3-3	Lip3-1

Figure 2.1. Schematic picture of different guide RNA transfection combinations for CRISPR/Cas9 engineering of HT-29 cells. Three different guide RNAs for both *LPIN2* and *LPIN3* were used in different combinations to achieve single (SKO) and double knockouts (DKO) in HT-29 cells after transfection. For the sequences of guide oligos see Table 2.6. SKO were generated to investigate the efficiency and success of the different guide RNAs but were not further used for experiments presented in this thesis.

IX. PCR Amplification

To confirm a successful cut and deletion in the region of interest in the *LPIN2* and *LPIN3* gene a PCR amplification reaction was conducted using the DNA isolated from the selected cell clones and the primers designed to envelope this region (Table 2.7).

5.2 µL	ddH_2O
10 µL	FailSafe PCR 2x PreMix Buffer H (Epicentre, Madison, WI, USA)
1 µL	forward Primer [10 µM]
1 µL	reverse Primer [10 µM]
0.3 µL	Biolase DNA Polymerase [5U] (Bioline, Taunton, MA, USA)
2.5 µL	template [20 ng/µL]
20 µL	total

The temperature conditions for the thermocycler were set to the following touchdown PCR program (see Table 2.11).

Table 2.11. Thermocycler temperature settings for touchdown PCR reaction.

94°C	3 min	
92°C	40 sec	19 cycles
63°C	40 sec	
-0.5°C each cycle		
72°C	1 min	
92°C	40 sec	9 cycles
53°C	40 sec	
72°C	1 min	
+5 sec each cycle		
72°C	5 min	
4°C	∞	

To see if the PCR had worked a 1.5% agarose control gel with SYBR Safe DNA gel stain was run at 110 V for 30 min. Samples were loaded with the DNA Loading Buffer Blue and the 1kb ladder (both from Bioland Scientific LLC, Paramount, CA, USA) served as a size reference.

X. Cleaning

To rid the PCR reaction of remaining dNTPs and primers, which might interfere with the Sanger sequencing, a cleaning step with alkaline phosphatase and exonuclease I was performed.

5.2 µL	ddH_2O
1 µL	Exonuclease I [10 U/µL] (Affymetrix, Santa Clara, CA, USA)
1 µL	rShrimp Alkaline Phosphatase [1 U/µL] (Affymetrix, Santa Clara, CA, USA)
5 µL	PCR Amplification Mix
7 µL	total

The reaction was incubated in a thermocycler for 15 min at 37°C followed by 15 min at 80°C.

XI. Sequencing

The samples were mixed with the listed reagents. The forward primer is the same one as the one used for the IX. PCR amplification reaction.

5.2 µL	ddH_2O
2 µL	BigDye Terminator v3.1 Ready Reaction Mix (Thermo Fisher Scientific, Waltham, MA, USA)
2 µL	5x Sequencing Buffer
1 µL	forward Primer
5 µL	DNA sample from cleaning step
10 µL	total

The thermocycler program for the sequencing reaction as well as the fluorescence detection and data analysis were executed as previously described under VI. Sequencing on page 31.

2.4.1 General Cell Culture Conditions

Human colon adenocarcinoma HT-29 cells originally had been purchased from American Type Culture Collection (Manassas, VA, USA). The cell culture medium that was used for all experiments was 1x Dulbecco's Modified Eagle Medium (DMEM) containing 4.5 g/L glucose, sodium pyruvate, glutamine, 10% fetal bovine serum (FBS), and 1% Penicillin-Streptomycin (all from Gibco by Thermo Fisher Scientific, Waltham, MA, USA). All plates and the cryogenic vials used were from Corning Inc. (Corning, NY, USA). Cells were grown in a 37°C incubator with CO_2 levels of 5% and were passaged every 2-3 days.

2.4.1.1 Freezing Cells

When a p100 plate reached about 100% confluency, the medium was removed and the cells were rinsed with 1x PBS. 3 mL Trypsin were added and the plate was incubated at 37°C for 5 min. Cells were collected, mixed with 7 mL of medium, and centrifuged at 1000 rpm for 5 min. After discarding the supernatant, 1 mL of freezing medium (DMEM + 20% FBS +10% DMSO) was added. The suspension was transferred to a 2 mL cryogenic tube and slowly frozen in an isopropanol filled Mr. Frosty Freezing Container (Thermo Fisher Scientific, Waltham, MA, USA) at -80°C. For long-term storage the vials were transferred into a liquid nitrogen tank.

2.4.1.2 Thawing Cells

The cryogenic vial was thawed in a 37°C water bath for 2 min/1 mL. The cell suspension was then transferred into 5 mL pre-warmed complete medium in a centrifugation tube and centrifuged at 1000 rpm for 5 min. After discarding the supernatant, the cells were replenished with 5 mL of fresh pre-warmed medium to dissolve the pellet. The cells were then plated on a p100 plate.

2.4.2 Genomic DNA Extraction from Cells

To extract the genomic DNA from cells a digestion buffer with the following composition was prepared:

10 mM	Tris-HCl, pH 8
100 mM	NaCl
25 mM	EDTA, pH 8
0.5 %	SDS
0.1 mg/mL	Proteinase K (Invitrogen Carlsbad, CA, USA)

I. Collection and digestion of cells from 6-well plate

The medium was aspirated and 1 mL 1x PBS was added to scrape the adherent cells off the plate. The cell suspension was collected in a microcentrifuge tube and centrifuged at 6000 rpm for 5 min at 4°C. The supernatant was discarded and the pellet resuspended in 500 µL digestion buffer. The samples were incubated at 50°C shaking overnight.

II. Extraction and purification of nucleic acids

250 µL chloroform and then 250 µL phenol were added to each sample. Tubes were vortexed and centrifuged at 8000 rpm for 10 min to achieve phase separation. The aqueous top layer of about 400 µL was transferred to a new tube and 200 µL of 7.5 M ammonium acetate and 1 mL of 100% ethanol were added to precipitate the DNA. Samples were centrifuged at 12,000 rpm for 10 min. The pellet was rinsed with 1 mL of 70% ethanol and centrifuged at 7,500 g for 5 min. The supernatant was removed and the pellet air-dried. The DNA was dissolved in 70 µL TE buffer, pH 8 under shaking for 40 min at 40°C. DNA concentration was measured with the NanoDrop Lite Spectrophotometer (Thermo Fisher Scientific, Waltham, MA, USA).

2.4.3 Protein Extraction from Cells

The cultured cells in 6-well plates were rinsed with cold 1x PBS, then 1 mL of PBS was added and the cells were scratched off while keeping the plate on ice. The cell suspension was centrifuged in a cooled centrifuge at 1500 rpm for 10 min. After

discarding the supernatant, 100 µL of the Triton X-100 lysis buffer were added to the pellet. It consists of 10 mM Tris, 10 mM NaCl, 1 mM EDTA, and 0.5% Triton X-100, set to a pH of 7.5. Before use, a 1x Protease Inhibitor Cocktail (Biotool LLC, Houston, TX, USA) (100x) was added to the buffer to prevent the degradation of proteins through proteases.

The protein concentration was measured with the Pierce BCA Protein Assay (Thermo Fisher Scientific, Waltham, MA, USA). Samples were then stored at -80°C. The samples were used for Western blots (for description of procedure see 2.1.2 Western Blot on page 20).

2.5 Cell Culture Experiments

Cell culture experiments with the CRISPR/Cas9 modified HT-29 cells were conducted in 6-well plates to harvest cell culture medium and cell lysates for protein analysis via Western blot and in 24-well plates for microscopic analysis with different staining methods. Glass coverslips were sterilized in a flame in the tissue culture hood and placed into 24-well plates. To achieve better cell attachment, the wells with the coverslips were covered with 3 mg/mL rat tail Collagen I (Gibco by Thermo Fisher Scientific, Waltham, MA, USA). Plates were dried for at least 2 hours before plating the cells. Cells were seeded at a density of about $60x10^4$ cells/well for 6-well plates and $6x10^4$ cell/well for 24-well plates.

Cells were treated with 0.4 mM BSA-conjugated oleic acid in DMEM for 2, 4, and 8 hours in a short-time experiment and for 24, 48, and 72 hours experiment (with an additional group that was fasted for 24 hours) to study the long-term effects. To induce chylomicron secretion cells were treated with a micelle mixture to mimic the natural way of lipids being transported to intestinal cells for uptake. The protocol was adapted from Xie et al., 2003 with a mixture of 0.3 mM phosphatidylcholine (Avanti Polar Lipids, Alabaster, AL, USA), 0.54 mM sodium taurodeoxycholate, 0.4 mM sodium taurocholate, 0.45 mM oleic acid, and 0.26 mM monoolein (all from Sigma-Aldrich, St. Louis, MO, USA) in DMEM without FBS. (139) Cells were treated for 0.5, 1, and 2 hours.

2.5.1 Oil Red O and BODIPY Staining in HT-29 Cells

The lysochrome diazo dye Oil Red O (Sigma-Aldrich, St. Louis, MO, USA) was used to stain neutral lipids, which include triglycerides and cholesteryl esters in the cells. It is a colorimetric staining for bright field microscopy. For the stock solution 0.14 g Oil Red O (ORO) was dissolved in 40 mL isopropanol, stirred overnight and filtered with a Millex-GS Syringe Filter Unit, 0.22 µm (EMD Millipore, Billerica, MA, USA). The working solution was mixed by adding 6 parts from the ORO stock and 4 parts of dH_2O. After mixing and a resting time of 20 min the solution was filtered with a 0.22 µm syringe filter again.
The cells were rinsed with 1x PBS after removing the medium, followed by a 30 min incubation with 10% formalin. After cells were rinsed with PBS again, they were washed with 60% isopropanol and left to dry. The ORO working solution was added for 10 min. The solution was removed and dH_2O was immediately added. Four more washing cycles with dH_2O followed before the coverslips were mounted onto microscope slides with ProLong Diamond Antifade Mountant with DAPI (Thermo Fisher Scientific, Waltham, MA, USA). Pictures were taken with the Zeiss Axio Observer D1 microscope and the AxioVision Software version 4.8.2.

BODIPY 493/503 (Invitrogen, Carlsbad, CA, USA) is a cell permeable dye, which permits green fluorescence. To stain lipid droplets in the cells it was added to the cell culture medium at a concentration of 1 mg/mL. Pictures were taken with the Leica TCS SP5 confocal microscope and the Leica LAS AF Imaging Software version 2.6.

2.5.2 Immunoprecipitation

Wild-type and Lipin-2/3KO HT-29 cells were grown in 6-well plates. The culture medium from cells treated with oleate or a micelle mixture (as described under 2.5 Cell Culture Experiments) was collected and used for immunoprecipitation of ApoB with two different protocols.

The culture medium from the oleate treated cells was incubated with 1 µL anti-ApoB antibody [3 mg/mL] overnight at 4°C while rotating. An aliquot of the culture medium

was saved as fraction 0. After about 2 hours of incubation 20 µL of 100x cOmplete Mini EDTA-free Protease Inhibitor Cocktail tablets (Roche Diagnostics, Indianapolis, IN, USA) in lysis buffer were added. The lysis buffer contains 1x PBS with 0.1% NP-40, 1 tablet/10 mL of cOmplete Mini EDTA-free Protease Inhibitor Cocktail tablets (Roche Diagnostics, Indianapolis, IN, USA), and 1% Phosphatase Inhibitor Cocktail 2 and 3 each (Sigma-Aldrich Corp. St. Louis, MO, USA). For the pulldown 30 µL of Protein A/G PLUS-Agarose beads (Santa Cruz Biotechnology, Dallas, TX, USA) were added and tubes were rotated at 4°C for 2 hours. After centrifugation at 3,500 rpm for 1 min at 4°C the supernatant was collected as the fraction 1 flow through. 1 mL ice cold 1x PBS with 0.1% NP-40 was mixed with the beads and centrifuged at 3,500 rpm for 1 min at 4°C. This washing step was repeated twice. 15 µL 1x SDS loading buffer and 1:25 β-Mercaptoethanol were used to resuspend the pellet. Aliquots of fraction 0 and 1 were prepared with the loading buffer mixture as well. Samples were boiled for 5 min, spun for 1 min to pellet the beads and then loaded onto a Western blot SDS-PAGE gel as described in chapter 2.1.2 Western Blot.

The cell culture medium from the micelle treated cells was mixed with 1x NET Buffer (150 mM NaCl, 5 mM EDTA, 50 mM Tris-HCl, pH 7.4, 0.5% Triton X-100, 0.1% SDS) as described in Wu et al., 1994. (140) 1x cOmplete Mini EDTA-free Protease Inhibitor Cocktail tablets (Roche Diagnostics, Indianapolis, IN, USA), 1x Phosphatase Inhibitor Cocktail 2 and 3 (Sigma-Aldrich Corp. St. Louis, MO, USA), and 0.5 µL anti-ApoB antibody [3 mg/mL] were added. After an overnight incubation at 4°C while rotating the same protocol was followed as described above.

2.5.2.1 Overexpression of Lipin-2-V5 in HT-29 Cells

To test for interactions between ApoB and Lipin-2 HT-29 wild-type cells were transfected with a plasmid coding for Lipin-2-V5 using the Amaxa Cell Line Nucleofector Kit R for HT-29 cells (Lonza, Cologne, Germany). The V5 tag adds about 25 kDa to the total protein size and can be detected with a specific antibody. Cells were grown on p100 plates, then trypsinized and counted. $1x10^6$ cells per transfection reaction were centrifuged at 1000 rpm for 5 min and the pellet was mixed with 82 µL Nucleofector Solution R as well as 18 µL Supplement 1. This cell suspension was combined with either

3 µg Lipin-2-V5 plasmid or 2 µg pmax GFP Vector as a control. The mixture was transferred into a cuvette and cells were transfected with the program W-017 on the Nucleofector Device (Lonza, Cologne, Germany). Cells were cultured in 6-well plates until the next day. After aspirating the culture medium and a washing step with 1 mL of cold 1x PBS per well on ice, 1mL cold PBS was added and cells were scraped and transferred into centrifuge tubes. Samples were centrifuged at 1000 rpm for 5 min at 4°C to pellet the cells. 100 µL of the lysis buffer were added to the pellet and vortexed for 2 min. Tubes with the lysates were snap frozen in liquid nitrogen for 30 sec. Lysates were slowly thawed at 25°C for 2 min and subsequently placed on ice. A centrifugation step at 14,000 rpm for 10 min at 4°C followed and the supernatant was transferred to fresh pre-chilled microcentrifuge tubes. 20 µL of the lysate supernatant was saved as fraction 0. The rest of the protocol was done as described above but with 0.4 µL of anti-V5 antibody [1 mg/mL] (Invitrogen, Carlsbad, CA, USA) for the pulldown.

3 RESULTS

3.1 Lipin-2 and Lipin-3 in Small Intestine

The small intestine is the part of the gastrointestinal tract where most of the digestion and absorption of food takes place. It consists of three distinct regions – the duodenum, jejunum, and the ileum. As it was shown in Csaki et al., 2013 the dominant isoforms expressed in the small intestine are Lipin-2 and Lipin-3. (141) This was confirmed via Western blot with protein samples from all three small intestinal regions from WT mice (Figure 3.1).

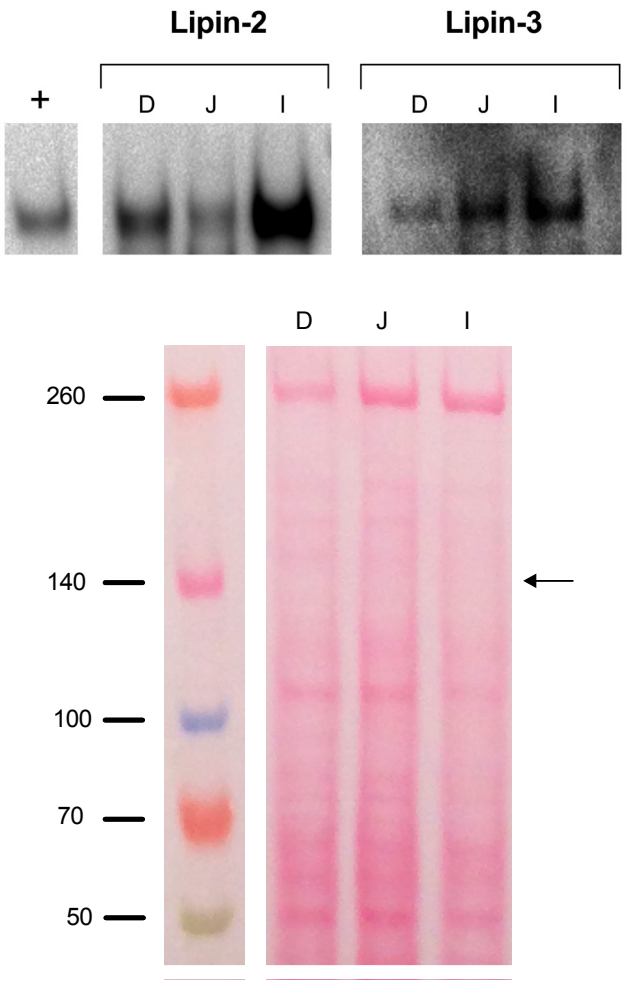

Figure 3.1. Western blot to confirm Lipin-2 and Lipin-3 proteins in the small intestine. Top: Western Blot with antibodies against Lipin-2 and Lipin-3. D, duodenum; J, jejunum; I, ileum; (+) positive control Lipin-2-V5 purified protein as a size reference. Bottom: Ponceau S staining of membrane as a loading control. Arrow indicates size of bands detected with antibodies against Lipin-2/3.

3.2 Protein Levels in WT and DKO Mice

As described in the Introduction, the Reue lab has demonstrated that Lipin-2/3 DKO mice exhibit impaired post-prandial chylomicronemia, which appears to be a result of reduced chylomicron production. To begin to assess how chylomicron production in the small intestine is impacted by the loss of Lipin-2/3, we characterized the apolipoprotein of chylomicrons. Protein extracts from duodenum tissue were used for Western blots using antibodies against the apolipoproteins A-I, A-IV, and ApoB to investigate whether diet or the genotype might influence the intracellular levels of proteins.

Compared to WT mice, the levels of apolipoproteins A-I and A-IV are elevated in the DKO when both are fed a chow diet. Feeding a high-fat diet leads to increased ApoA-IV levels in WT mice, and even higher levels in DKO mice (Figure 3.2). It has been shown that ApoA-IV is able to sense the nutritional status. (108) Our data coincides with results from several studies showing that dietary fat absorption after fat feeding leads to increased ApoA-IV and ApoA-I synthesis and secretion in a dose-dependent way. (142–145) On the contrary, blocking the secretion of chylomicrons can inhibit this diet-induced rise in ApoA-IV synthesis. (146)

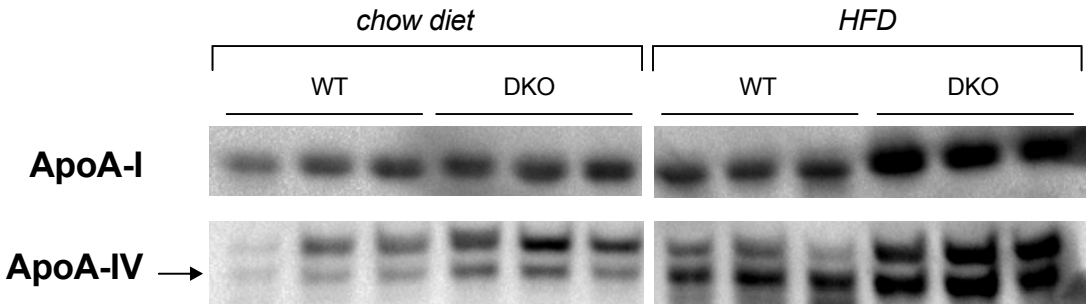

Figure 3.2. Western blot of ApoA-I and ApoA-IV in small intestine tissue samples from WT and Lipin-2/3KO mice. Protein isolated from the duodenum of WT and DKO mice fed either a chow standard diet or a high fat diet (HFD) were used. Higher amounts of apolipoproteins A-I and A-IV are present in the DKO mice when fed a HFD.

ApoB protein levels show a very interesting pattern depending on the feeding state of the mouse, the genotype, and the diet. ApoB protein in the WT mice in the fed state appears as a major species corresponding to the known size of ApoB48 (Figure 3.3 lanes 1-2). Under fasting conditions, ApoB48 does not become fully incorporated into

chylomicrons and undergoes regulated degradation, leading to the appearance of specific degradation products and appears as multiple defined bands (Figure 3.3 lane 3-6, 9-10). Under fasting conditions, DKO mice exhibit impaired degradation of ApoB48 irrespective of diet (Figure 3.3 lane 7-8, 11-12). This led us to believe that ApoB accumulates in the enterocytes, which we were able to show with the immunofluorescence staining as well (Figure 3.9).

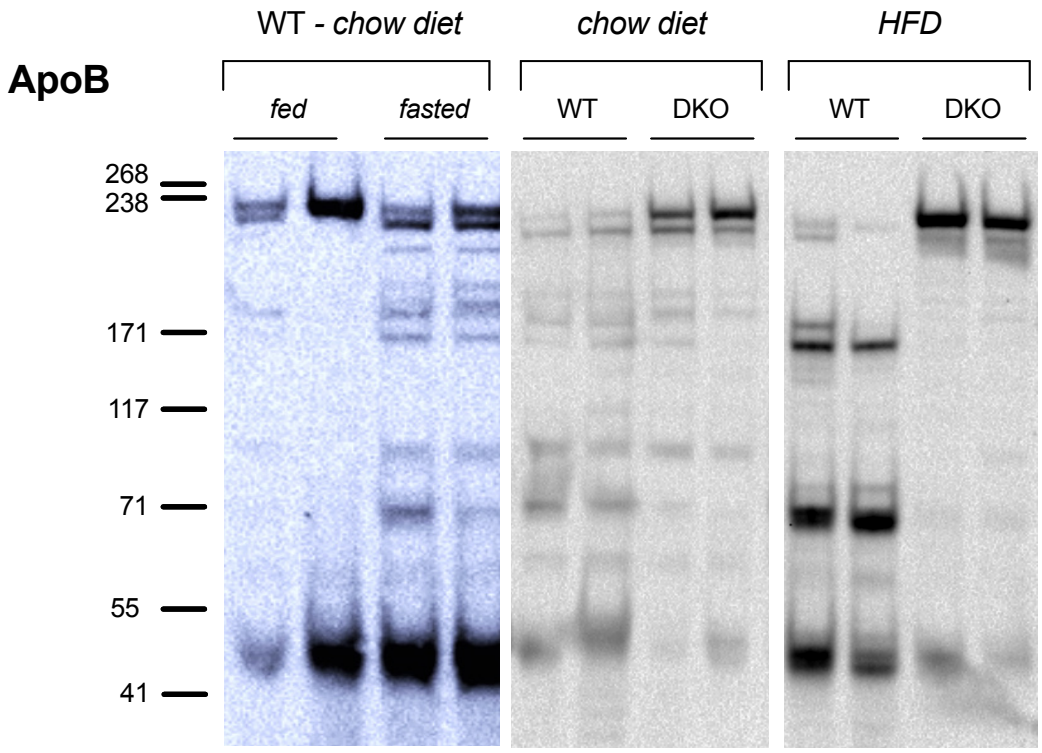

Figure 3.3. Western blot of ApoB in small intestine tissue samples from WT and Lipin-2/3KO mice shows difference in fed vs. fasted state and degradation pattern in the DKO. Protein isolated from the duodenum mice fed either a chow standard diet or a high fat diet (HFD) were used. Apart from the first two lanes (*fed*) animals were fasted ~5 hours before being sacrificed.

In enterocytes, ApoB degradation has been shown to occur via autophagy, which is also activated in response to the delivery of excess dietary lipids. (123) The Reue group previously showed that Lipin-1 protein is required for normal autophagy in muscle, raising the possibility that Lipin-2/3 are involved in autophagy in enterocytes. (147) To test this, we assessed markers of autophagy induction and autophagy clearance I intestinal protein extracts. Microtubule-associated protein light chain 3 (LC3) is a widely used marker of autophagy induction. Its cytosolic form LC3-I is linked to phosphatidylethanolamine to form LC3-II during autophagosome formation. LC3-II is

then recruited to autophagosomal membranes and gets degraded by lysosomal hydrolases after autophagosomes fuse with lysosomes. (148) We detected increased levels of both LC3 forms in the DKO tissue (Figure 3.4). This might be associated with increased autophagosome synthesis or reduced autophagosome turnover, possibly caused by a delay in trafficking to the lysosomes, reduction of fusion between compartments or impairment of the lysosomal proteolytic activity. (149)

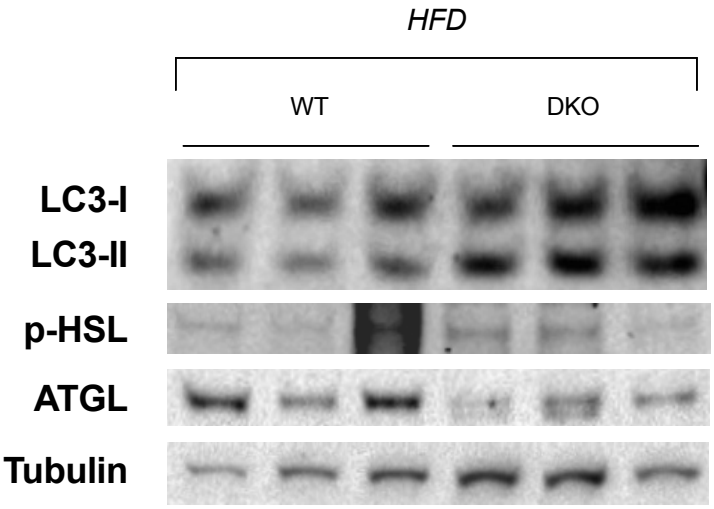

Figure 3.4. Western blot of LC3, p-HSL, and ATGL in small intestine tissue samples from WT and Lipin-2/3KO mice shows elevated autophagy in the DKO but no difference in lipolysis. Protein was isolated from the duodenum of WT and DKO mice, that had been fasted for 5 hours. Data only from mice fed a high fat diet. Housekeeping control protein as a reference is α-Tubulin.

A marker of autophagy clearance is the p62 protein, which binds to ubiquitinated proteins and directly interacts with LC3-I and LC3-II. It is required for the formation and the degradation of cytoplasmic inclusion bodies containing ubiquitinated proteins by autophagy. (150) Notably, p62 itself is degraded exclusively by autophagy so that p62 levels are a barometer of autophagic completion. We did not observe changes in the protein levels of p62 (Figure 3.5). Together, our results suggest that there is increased induction of autophagy in DKO intestine (perhaps due to the necessity of degrading excess lipids that accumulate due to impaired chylomicron secretion), but normal capability to degrade lipids via autophagy. These results also indicate that ApoB48 accumulation in DKO intestine is not due to impaired autophagy.

HSL and ATGL protein levels are not significantly altered from WT mice, which implies that the rate of lipolysis is comparable in both genotypes (Figure 3.4). Generally, both proteins are expressed at very low levels in the small intestine compared to other tissues. (151) HSL levels in adipose tissue are downregulated during acute fasting. (152)

The p-PKA substrate antibody was used to investigate the regulation of phosphorylation by the cAMP-dependent protein kinase (PKA). It detects proteins containing a phospho-serine/threonine residue with arginine at the -3 position. (153) It has been shown in adipocytes that PKA phosphorylates perilipin located on lipid droplets. This leads to the release of the ATGL co-activator CGI-58 and results in stimulated lipolysis because perilipin moves away from the lipid droplet extending the surface area accessible for lipolysis. (154) CGI-58 increases the activity of ATGL, which in turn provides more DAG as a substrate for HSL. HSL itself is activated through phosphorylation by PKA, which results in its translocation from the cytosol to the lipid droplet surface. (155,156) In our small intestine tissue samples there is clear difference in the pattern of phosphorylated PKA-substrates between the WT and the Lipin-2/3KO mice, especially under HFD conditions (Figure 3.5). PKA activity seems to be elevated in the DKO regardless of diet, perhaps to induce lipolysis of the accumulated lipid droplets.

Another mechanism for lipid droplet degradation is chaperone-mediated autophagy. Studies have shown that HSC70 colocalizes and interacts with both perilipins, PLIN2 and PLIN3, on the surface of lipid droplets to induce their degradation via chaperone-mediated autophagy. This facilitates the access of cytosolic lipases to the lipid core and allows ATG proteins, that are involved in autophagosome formation, to bind to the LD. They then initiate the sequestration of parts of the LD into autophagosomes for fusion with lysosomes and degradation through macrolipophagy. (133) HSC70 protein levels were slightly elevated in the DKO mice when fed a HFD, which might be connected with the cells trying to rid themselves of the many lipid droplets that have accumulated using multiple pathways including macroautophagy, chaperone-mediated autophagy, as well as lipolysis (Figure 3.5).

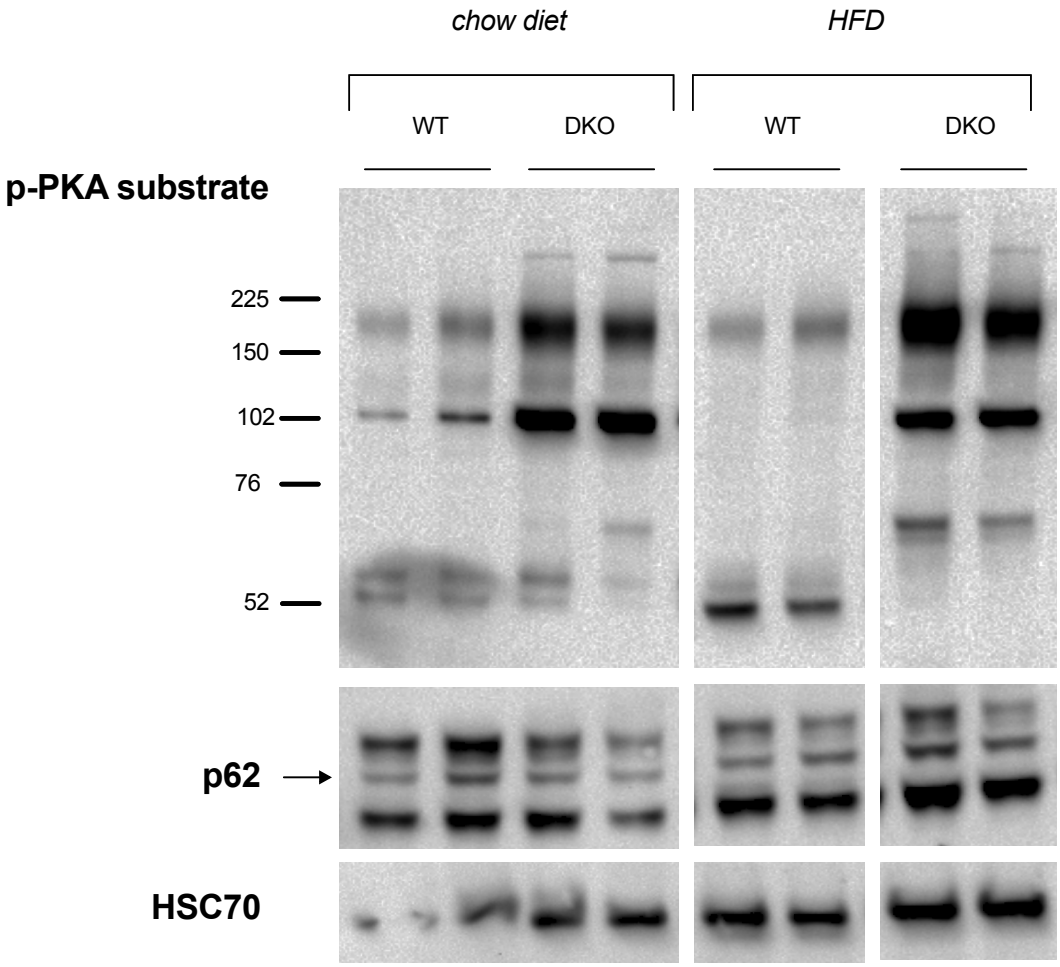

Figure 3.5. Western blot of p-PKA substrate, p62, and HSC70 in small intestine tissue samples from WT and Lipin-2/3KO mice shows differences in PKA activity and slightly elevated HSC70 levels in the DKO. Protein was isolated from the duodenum of WT and DKO mice, that had been fasted for 5 hours after feeding on a standard chow diet or a high fat diet (HFD). Transfer problem in first lane of HSC70.

3.3 Gene Expression Changes with Genotype and Diet in WT and DKO Mice

To get a better understanding of the changes that happen in a cell when two important proteins – Lipin-2 and Lipin-3 – are disrupted, the expression of different genes involved in lipid metabolism in enterocytes were investigated. The DKO genotype was compared to the wild-type mouse tissue samples and the differences caused by the influence of the high fat diet (HFD) and the standard chow diet were measured.

On the apical cell border of the enterocyte CD36 and ABCG5 are two of many proteins, which play an important role in the transport into and out of the cell as they deal with the dietary contents passing by through the intestinal lumen. They are responsible for the uptake of fatty acids and secretion of cholesterol, respectively. (36,157) CD36 mRNA levels are not changed while ABCG5 shows significantly higher expression levels in the DKO when mice were on a HFD (see Figure 3.6 A). This might be due to a higher amount of cholesterol in the cells (see Figure 3.7). To protect cells from sterol accumulation the efflux of cholesterol can be elevated. (158)

MGAT2 is involved in the TAG synthesis as an acylglycerol acyltransferase mediating the synthesis of DAG in the ER membrane. (54) A statistical difference between the genotypes with lower mRNA levels in the DKO under both diet regiments was measured (Figure 3.6 B). The impairment of the G3P pathway due to the lack of Lipin-2 and Lipin-3 might suggest the opposite, which would be a compensatory upregulation of the MGAT pathway to sustain efficient TAG synthesis activity. Global and intestine-specific *MGAT2*$^{-/-}$ mice have an impaired TAG synthesis. When fed a HFD they are protected against diet-induced obesity, possibly due to increased energy expenditure. Absorption of fats takes place at a normal rate but secretion into the circulation is delayed and cytosolic LDs accumulate in the cells. (50,159,160)

Out of the proteins responsible for transporting FAs through the cytosol – FABP1, FABP2, and adipocyte protein 2 (AP2 or FABP4) – only FABP1 mRNA expression is elevated when mice are fed a HFD (Figure 3.6 C). (161) A HFD leads to a much higher lipid load that enterocytes have to deal with resulting in a higher uptake of FA. Elevated levels for FABP1 in WT and DKO under the HFD are in line with FABP1 having to transport more FA through the cytosol. Due to its ability of binding two FAs or other lipids it helps with transporting more lipids more efficiently and targets them towards oxidative pathways (and MAGs towards anabolic pathways) for dietary fats to be metabolized more quickly. (41) FABP1 also mediates the budding of PCTVs from the ER. (42) Related to this, FABP1 subcellular localization seems to be dependent on the feeding status. During times of FA availability, it is found throughout the cytosol of the enterocyte, while fasting leads to a more apical localization of FABP1. (162)

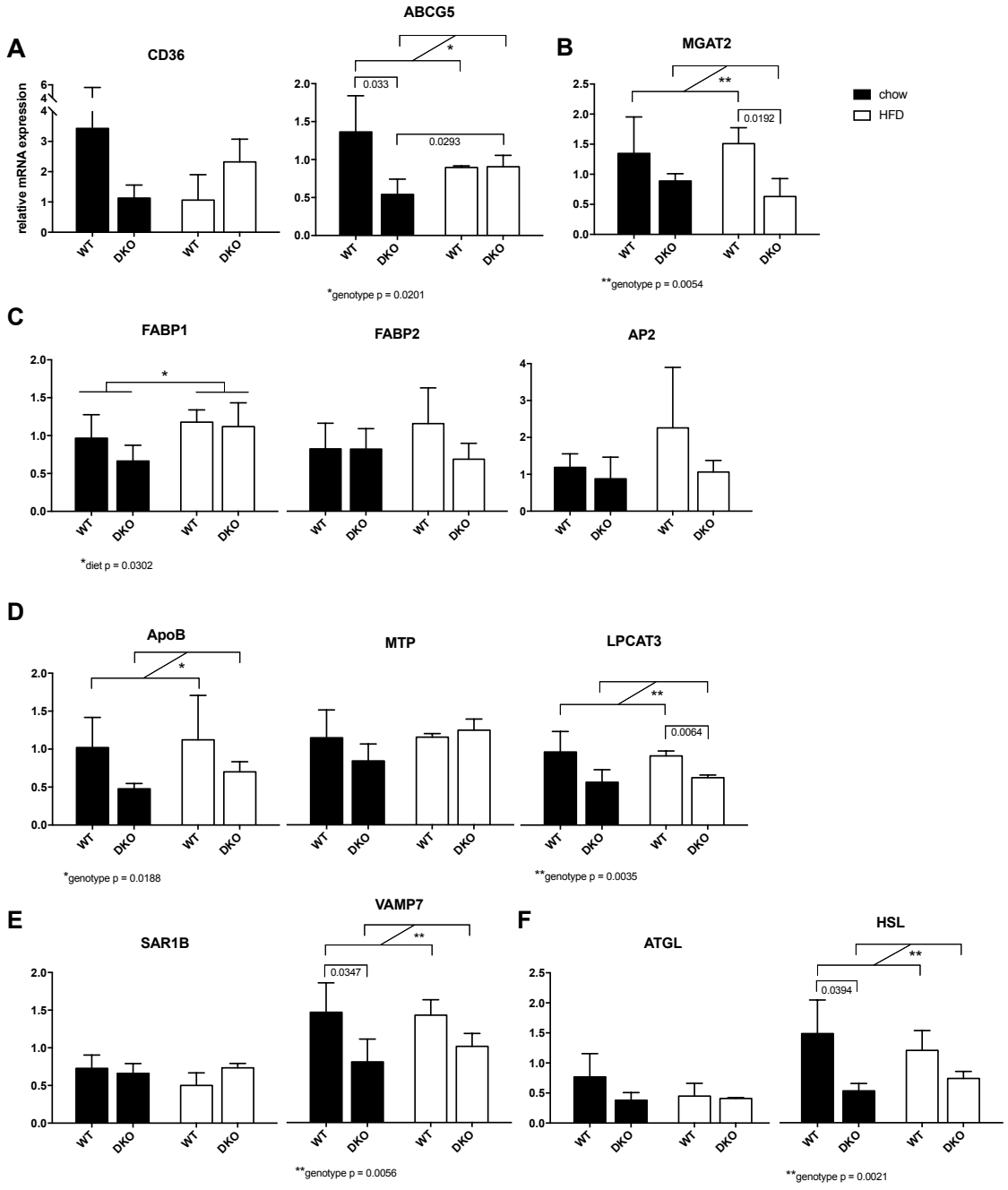

Figure 3.6. Relative gene expression in small intestine from wild-type and Lipin-2/3KO mice. (A) CD36 and ABCG5 are involved in influx and efflux of FAs and cholesterol, respectively. (B) MGAT2 is an important enzyme in the TAG synthesis of dietary FAs. (C) FABP1, FABP2, and AP2 transport FA through the cytosol. (D) ApoB, MTP, and LPCAT3 are involved in the biogenesis of lipoproteins in the ER. (E) SAR1B and VAMP7 are needed for the budding of the PCTV from the ER and the subsequent fusion with the Golgi. (F) TAG lipolysis in the cytosol is catalyzed by ATGL and HSL. All values represent the mean ± standard deviation. Significant comparisons for genotype and diet differences are depicted as brackets. * p≤0.05, ** p≤0.01, *** p≤0.001. WT, wild-type; DKO, double-knockout. Black bars represent data for chow diet, unfilled bars the data for high-fat diet.

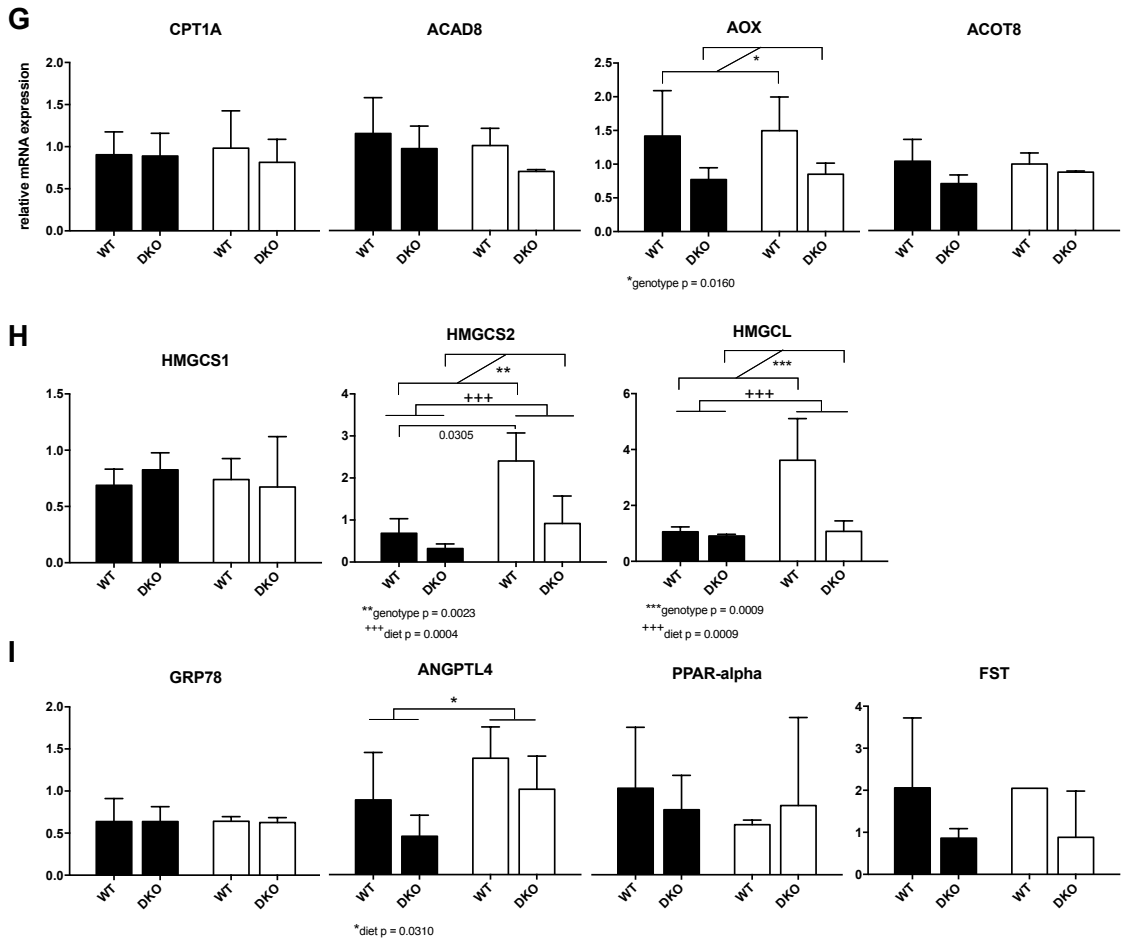

Figure 3.6 *continued*. Relative gene expression in small intestine from wild-type and Lipin-2/3KO mice. (G) CPT1A, ACAD8, AOX, and ACOT8 are involved in mitochondrial or peroxisomal fatty acid oxidation. (H) HMGCS1 plays a role in cholesterol synthesis, while HMGCS2 and HMGCL are important for ketogenesis. (I) GRP78 is a chaperone in the ER. ANGPTL4 regulates lipid metabolism as a secreted signaling hormone. PPARα is a nuclear receptor involved in regulating the expression of genes important for FA oxidation and metabolism. FST is an autocrine glycoprotein acting as a safeguard against uncontrolled cellular proliferation. All values represent the mean ± standard deviation. Significant comparisons for genotype and diet differences are depicted as brackets. * p≤0.05, ** p≤0.01, *** p≤0.001. WT, wild-type; DKO, double-knockout. Black bars represent data for chow diet, unfilled bars the data for high-fat diet.

ApoB and MTP are very important proteins for the biogenesis of lipoproteins. ApoB gene expression levels are significantly lower in the DKO mice regardless of diet (see Figure 3.6 D). This could be caused by a regulatory feedback loop because, as is shown in Figure 3.3, and Figure 3.9, ApoB proteins accumulate in Lipin-2/3KO mice and supposedly do not undergo the normal degradation process as they do in the WT.

The enzyme lysophospholipid acyltransferase 3 (LPCAT3) remodels the ER membrane by concentrating arachidonate-containing phospholipids around itself generating a local membrane area rich in polyunsaturated fatty acids (PUFAs). This PUFA-enriched domain favors a better formation of the TAG lens structure with a high capacity and high surface

curvature, when TAG synthesis occurs in proximity enabling a more efficient TAG transfer. (62,59,63) LPCAT3 shows the same expression pattern as ApoB with generally lower levels in DKO mice (Figure 3.6 D). This could mean that the PUFA enrichment in the ER membrane might not be as efficient leading to a lower curvature of the TAG lens in the ER bilayer (Figure 1.2). Therefore, slower flip-flop movement of the TAGs to either side of the membrane take place, which could lead to an excess of lipid droplets. (59) This would be in line with the observation of accumulation of lipid droplets in the enterocytes of DKO mice.

SAR1B and VAMP7 proteins are both involved in the budding of the PCTV from the ER, its transport, and fusion with the Golgi membrane. The gene expression of VAMP7 shows significant differences between the genotypes with DKO mice expressing less mRNA (Figure 3.6 E). This reduced expression of VAMP7 in DKO mice might lead to a less efficient delivery of TAG-rich pre-chylomicrons to the Golgi. Studies have shown that VAMP7 is required for the successful export of chylomicrons from enterocytes. CaCo-2 cells synthesize TAG and form the lipoprotein particles for chylomicrons but they are unable to deliver them to the basal side of the cell for export. (163,164) This seems to be due to the fact that Vamp7 is expressed in CaCo-2 cells but not present in their ER, which suggest that its absence reduces CM secretion. (113,165)

From the two lipases – ATGL and HSL – only HSL shows a difference in gene expression levels. It is significantly reduced in the DKO under both dietary settings (Figure 3.6 F). However, it is unclear why HSL gene expression is reduced while lipid droplets accumulate in the Lipin-2/3KO mice. HSL is a substrate of the protein kinase A (PKA) and needs to be phosphorylated in order to actively hydrolyze diacylglycerol, and other lipids such as cholesteryl esters. This activation causes HSL to translocate from the cytosol to the LD, which might be hindered by perilipins located on the LD surface. (166,167)

Out of the next four genes (Figure 3.6 G), only the peroxisomal acyl-CoA oxidase (AOX or ACOX1), the first enzyme of the LCFA β-oxidation pathway, shows a significant difference in gene expression with reduced levels in the DKO mice, regardless of diet. (168) This might result in higher levels of LCFA, because deficiency of AOX in mice can lead to the accumulation of very long chain saturated and unsaturated fatty acids. (169)

The carnitine palmitoyltransferase I (CPT1A) as well as the mitochondrial acyl-CoA dehydrogenase ACAD8 play a role in the β-oxidation of fatty acids in mitochondria. (170,171) Acyl-coA thioesterase 8 (ACOT8) is a peroxisomal thioesterase that appears to be involved in the oxidation of fatty acids. (172) No changes in their level of expression were observed.

Hydroxymethylglutaryl-CoA synthase (HMGCS) catalyzes the reaction of acetoacetyl-CoA to 3-hydroxy-3-methylglutaryl-CoA (HMG-CoA). The soluble cytosolic form HMGCS1 is involved in cholesterol synthesis while the mitochondrial HMGCS2 plays a role in ketogenesis. (173) 3-hydroxy-3-methylglutaryl-CoA lyase (HMGCL) catalyzes the next step in the synthesis of ketone bodies. (174) Ketogenesis in enterocytes is induced when animals are fed a HFD. This was shown in a study where HMGCS2 was present in suckling rat intestine and disappeared after weaning onto regular chow diet, but expression of the gene could be reintroduced by only 1 week of HFD feeding. (175) This is in line with the results in our WT and DKO mice, both showing elevated expression levels when fed the HFD (Figure 3.6 H). HMGCS1 mRNA levels were not affected.

The gene expression levels of 78 kDa glucose-regulated protein (GRP78 or HSPA5), a molecular chaperone located in the ER, where it binds newly synthesized proteins as they are translocated into the lumen, showed no changes (Figure 3.6 I). GRP78 plays a role in facilitating the correct folding and oligomerization into protein complexes and is involved in the degradation of misfolded proteins. (176)

The mRNA levels of angiopoietin-like 4 (ANGPTL4) show differences influenced by diet with higher levels in the mice fed the HFD (Figure 3.6 I). As a secreted signaling hormone it is involved in regulating lipid metabolism. (177) Similar results of elevated ANGPTL4 expression levels in the small intestine during HFD have been shown in a study in mice before. (175)

The gene expression of both PPARα, a nuclear receptor mediating the gene expression of FA oxidation, and follistatin (FST), which is involved in cellular proliferation and differentiation, were unaffected by genotype and diet (Figure 3.6 I).

PPARα regulates the gene expression of many of the above-mentioned genes by forming a heterodimer with the retinoid X receptor and by binding to peroxisome proliferator response elements (PPRE) located in the regulatory domain of said genes. (178) Genome-wide analyses identified more than 1000 genes that were PPARα-dependently regulated in the murine small intestine, whereas about half of them were activated or repressed. (179) It was also shown that a high-fat diet leads to activation of PPARα in the small intestine. (175) This means that the diet alone is capable of effecting the regulation of many genes let alone the impact a deficiency in both Lipin-2 and 3 might have on PPARα expression as well.

3.4 Total Cholesterol in Small Intestine

The total amount of cholesterol in samples from the duodenum of WT and Lipin-2/3KO mice was measured and shows significantly higher levels in both genotypes when fed a HFD. This might be explainable due to the elevated lipid load and higher uptake into the enterocytes. However, the caveat with this experiment is that a part of the whole small intestine was used which includes multiple cell types such as other intestine-specific cells and muscle cells.

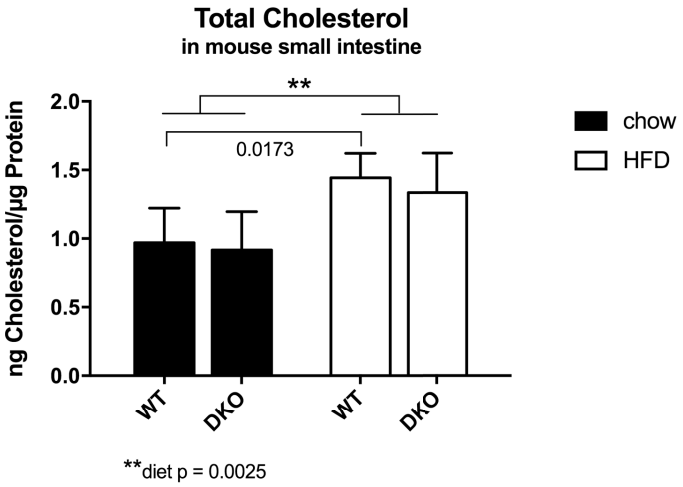

Figure 3.7. Total cholesterol assay in small intestine from wild-type and Lipin-2/3KO mice. Cholesterol was measured in protein extractions from the duodenum of WT and DKO mice fed both a chow and high-fat diet. Values are represented as the mean ± standard deviation. Significant comparisons for genotype and diet differences are depicted as brackets. * p≤0.05, ** p≤0.01. WT, wild-type; DKO, double-knockout. Black bars represent data for chow diet, unfilled bars the data for high-fat diet.

The high-fat diet that was used contains virtually no cholesterol and is therefore very different from the so-called Western diet. Gene expression differences might be due to different cholesterol levels in the diet. Desmarchelier et al., 2012 showed that cholesterol levels in the intestine of C57Bl/6 N mice were significantly reduced, despite the higher dietary cholesterol supply from the Western diet. The expression of several genes related to cholesterol or lipid metabolism also differ from our results. (180)

3.5 Immunofluorescence Staining in Small Intestine

Mice were treated with oil gavage containing BODIPY 493/503-labeled fatty acids and sacrificed after 2 hours to investigate the uptake of lipids into enterocytes as lipid droplets and and the storage of lipids as TAG in the cell. The size, amount, and shape of lipid droplets in the WT differed significantly from LDs in the Lipin-2/3KO mice. The intensity of lipid droplets resulting from acute dietary fatty acids was dramatically lower in the DKO and lipid droplets look fuzzy with very undefined borders (Figure 3.8 B). The distribution and localization of ApoB in the cell seems to differ between genotypes as well. In the wild-type mice it interacts with some of the lipid droplets encasing them (Figure 3.8 A), which suggests a colocalization of ApoB with the ER. ApoB in DKO cells seems to accumulate in the ER, when additionally stained with Calnexin as an ER marker (Figure 3.9 B). Calnexin is an integral protein found in endoplasmic reticulum membranes. As a chaperone it binds to newly synthesized proteins to help with their folding and plays a role in protein retention or degradation of misfolded proteins in the ER, including safeguarding ApoB by promoting its folding and completing the translocation into the lumen. (181) This might be representative for the differences in ApoB protein levels investigated by Western blot (Figure 3.3), which shows an impaired degradation pattern suggesting accumulation of ApoB in the DKO. Lipin-2 and ApoB show colocalization in WT mice (Figure 3.10). The reduced intensity of the BODIPY signal could be due to reduced uptake, but could also result from reduced incorporation of the labeled fatty acids into TAG. Free fatty acids or fatty acids incorporated into phospholipids would not show a fluorescence signal as intense as TAG.

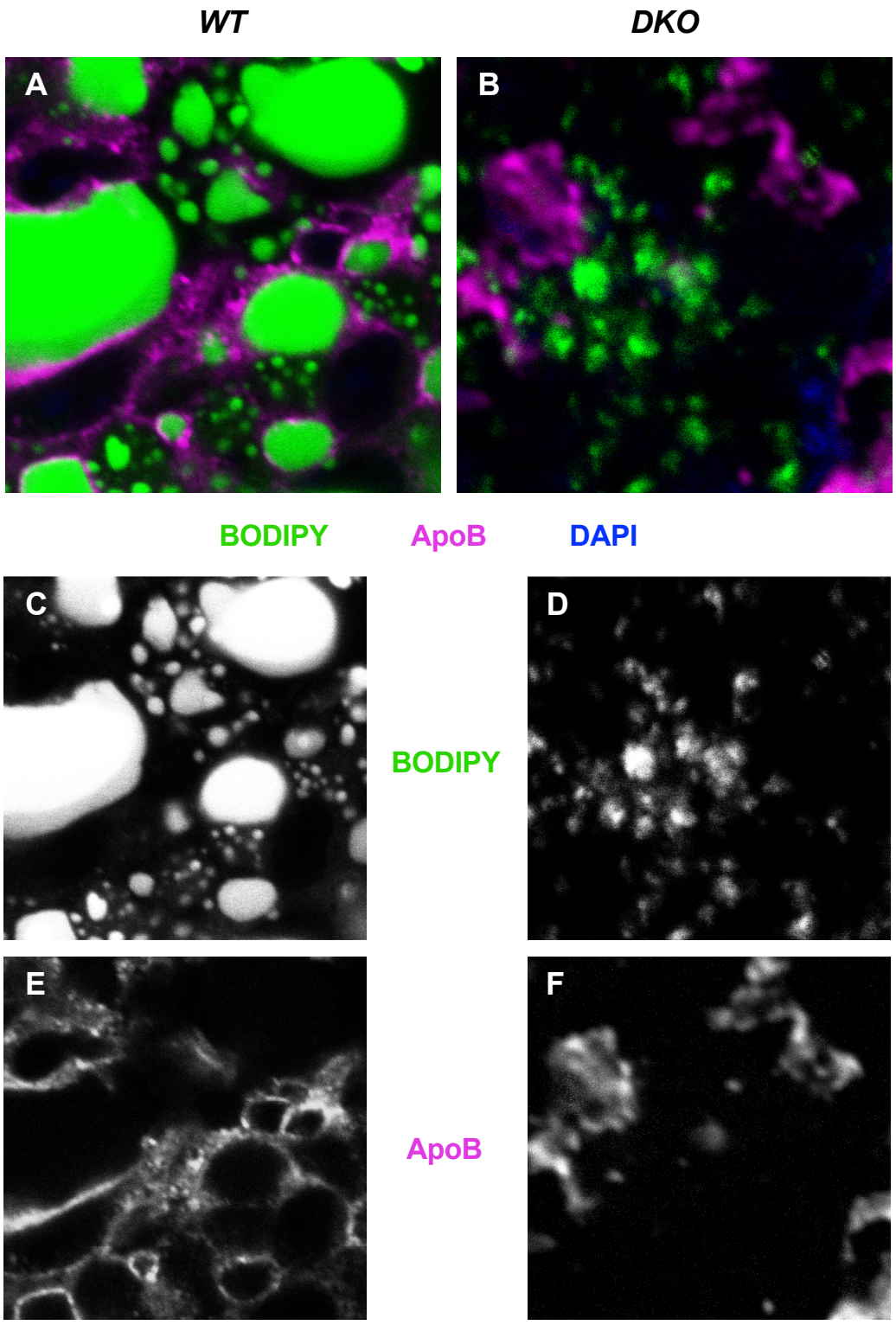

Figure 3.8. Immunofluorescence staining of lipid droplets in small intestine enterocytes in WT and Lipin-2/3KO mice shows a significant difference. Mice were treated with oil gavage containing BODIPY to stain lipid droplets. (A, C, E) WT mice show significant lipid droplets (green) with ApoB (magenta) being associated with them possibly through localization in the ER. (B, D, F) Both lipid droplets and the ApoB structures are different in appearance in the DKO enterocytes. The amount and size of LDs is drastically reduced with unclear borders defining their shape. Cell nuclei are stained with DAPI (blue). Images were taken at 1000x magnification.

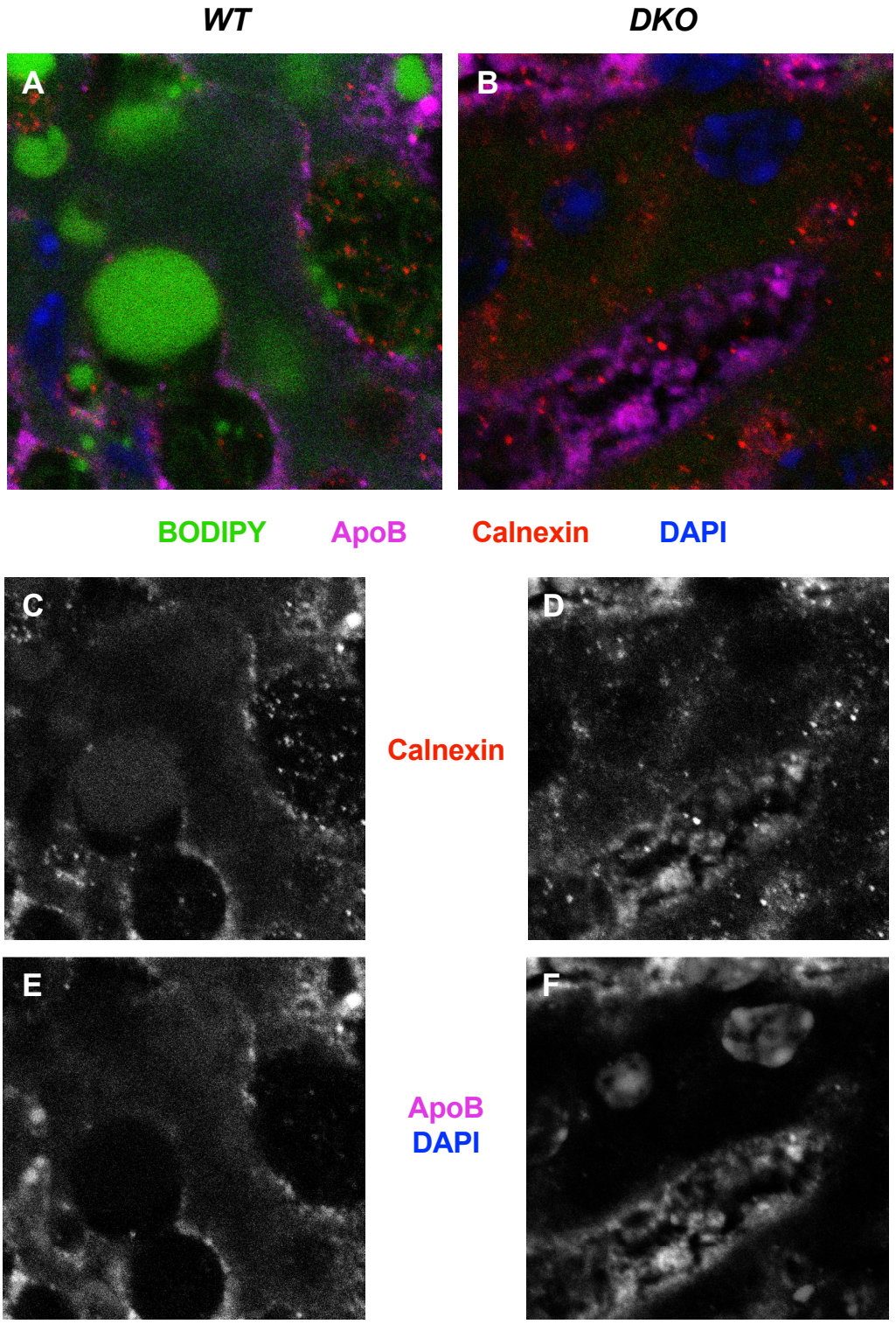

Figure 3.9. Immunofluorescence staining of lipid droplets and the ER in small intestine enterocytes in Lipin-2/3KO mice reveals ApoB accumulation in the ER. Mice were treated with oil gavage containing BODIPY to stain lipid droplets (green). (A, C, E) WT mice show only a few areas of colocalization between Calnexin (red) and ApoB (magenta). (B, D, F) In the DKO mice ApoB seems to be accumulated in the ER. Cell nuclei are stained with DAPI (blue). Images were taken at 1000x magnification.

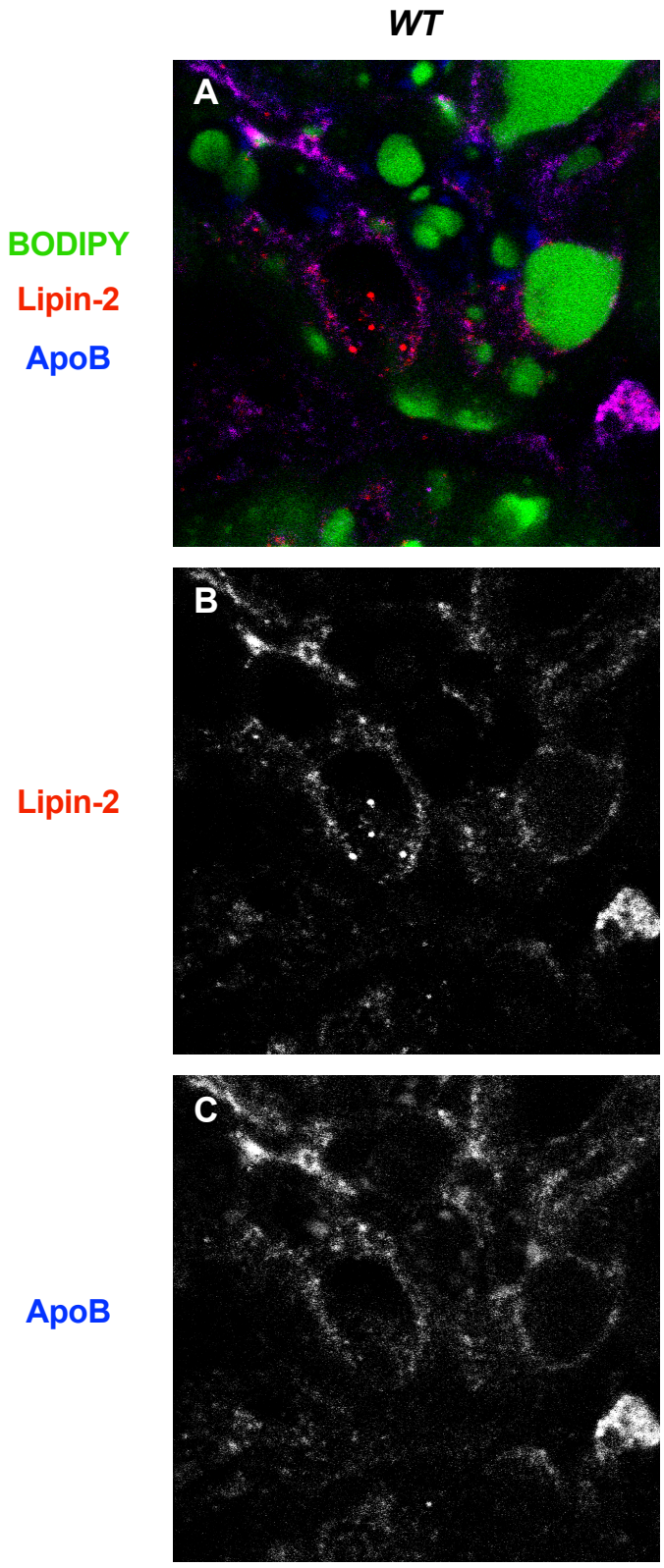

Figure 3.10. Immunofluorescence staining of Lipin-2 and ApoB in small intestine enterocytes in WT mice shows colocalization of the two proteins. Mice were treated with oil gavage containing BODIPY to stain lipid droplets. (A) The colocalization of Lipin-2 (red) and ApoB (blue) is clearly visible as the magenta-colored structures. Lipid droplets are stained with BODIPY (green). Images were taken at 1000x magnification.

3.6 CRISPR/Cas9 Engineering of HT-29 Cells

The studies performed in intestinal tissues of Lipin-2/3 DKO mice revealed disruption of many aspects of lipid homeostasis. To develop a model system that will allow more in-depth mechanistic studies, we used CRISPR/Cas9 genome modification to inactivate the LPIN2 and LPIN3 genes in a human intestinal cell line (HT-29). After sequencing and analyzing about 100 HT-29 clones that had been transfected with appropriate guide RNAs to target the lipin genes, we isolated a single clone that had a mutation in both alleles of the *LPIN2* and the *LPIN3* genes.

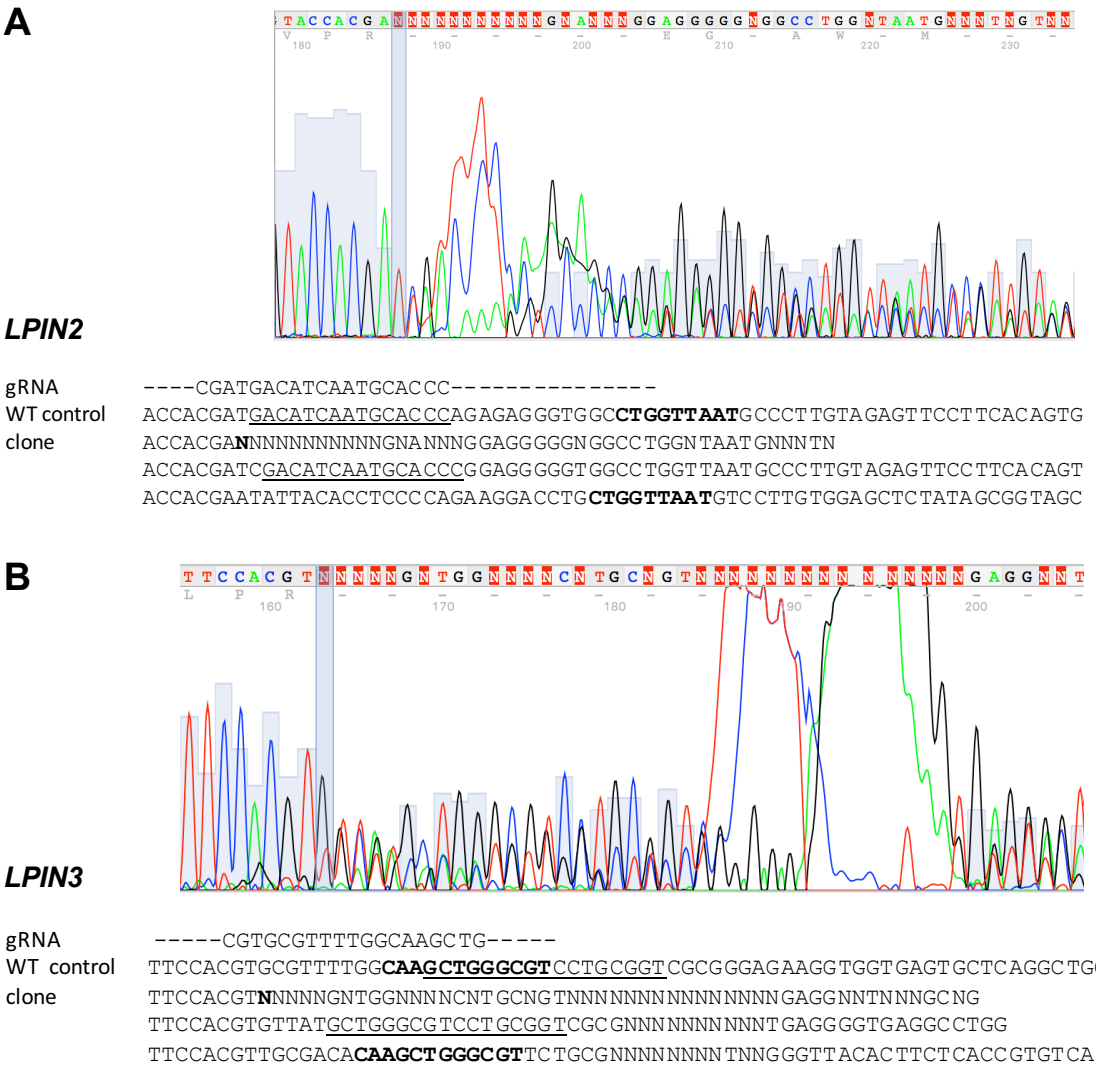

Figure 3.11. Confirmation of double knockout of *LPIN2* and *LPIN3* on the genetic level. Sequencing results of the regions of interest in the *LPIN2* and *LPIN3* gene, where the guide RNA sequence aligned. Comparison in a multiple sequence alignment with the wild-type sequence as a control. Peaks were read out (as far as possible) to distinguish different mutations in the different alleles. (A) *LPIN2* shows a 1 bp insertion as well as a 2 bp deletion. (B) *LPIN3* is disrupted by a 7 bp and a 2 bp deletion. Changes are highlighted as underlined or in bold, respectively.

The detected sequences and alignments with the guide RNA and the wild-type sequence are presented in Figure 3.11. The non-specific peaks around bp-position 190 are artifacts from the 3730 Capillary DNA Analyzer that was used to read the samples. The first nucleotide position that shows two different peaks is highlighted in the sequence. The cut by the Cas9 DNA endonuclease enzyme was introduced right before this first double peak and led to a 1 bp insertion in one allele and a 2 bp deletion in the other in the *LPIN2* gene. The *LPIN3* gene was interrupted by a 7 bp and a 2 bp deletion in the two alleles. Each of these mutations leads to a frame-shift and premature termination of the corresponding coding sequences, resulting in non-functional genes.

A Western blot with HT-29 cell lysates confirmed a successful mutation in both genes resulting in a knockout of the proteins they code for (see Figure 3.12).

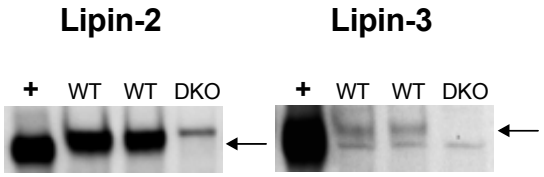

Figure 3.12. Confirmation of successful knockdown of Lipin-2 and Lipin-3 by CRISPR/Cas9. Western blot with HT-29 cell lysate samples shows double knockout (DKO) compared to wild-type (WT) samples, indicated by an arrow. Positive control of purified Lipin-2 and Lipin-3 protein (+).

3.7 Cell Culture Experiments

To investigate the status of ApoB, Western blots were conducted with cell lysates from both wild-type and Lipin-2/3KO HT-29 cells that were loaded with the fatty acid oleate to stimulate feeding. After a 0.4 mM oleate treatment for 2, 4, and 8 hours, ApoB was detectable in cell lysates without significant differences in protein levels. (see Figure 3.13).

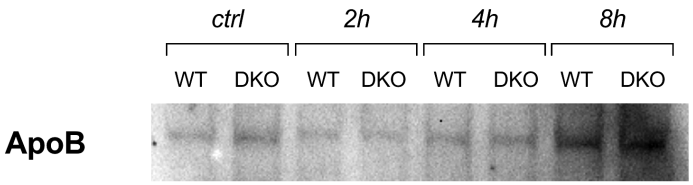

Figure 3.13. Detection of ApoB via Western blot in cell lysates from HT-29 cells. Cells were treated with 0.4 mM oleate-BSA for 2, 4, or 8 hours. WT, wild-type; DKO, double-knockout.

We were not able to detect ApoB in the cell culture medium from HT-29 cells after treatment with oleate nor after treatment with micelles as an alternate method to introduced lipids (data not shown). It is unclear whether HT-29 cells did not secrete any ApoB-containing lipoproteins or the amount was below the detection limit. Radioactive labeling and detection as a more sensitive method could clarify this. It may also be that the lipid concentrations or treatment times did not allow for ApoB secretion to occur. Indeed, studies in the CaCo-2 human intestinal cell line have shown that the exposure to oleic acid requires titration of the concentration and time to obtain ApoB secretion, as long exposure could cause ER stress leading to inhibition of lipoprotein secretion. (182–184)

Western blot analysis of a few proteins in the WT and DKO cells after long-term exposure to oleate did not show any significant differences (Figure 3.14). Levels of ApoB as well as Calnexin, an ER marker protein, were unchanged. Successful knockout of Lipin-2 and 3 was again confirmed. The housekeeping protein α-tubulin was used as a control protein. It should be kept in mind, that the cell culture system may be best used to examine events that occur rapidly, whereas some of the findings from intestinal samples are likely the result of direct and indirect (*i.e.,* compensatory) changes that occur throughout the lifetime of the mouse.

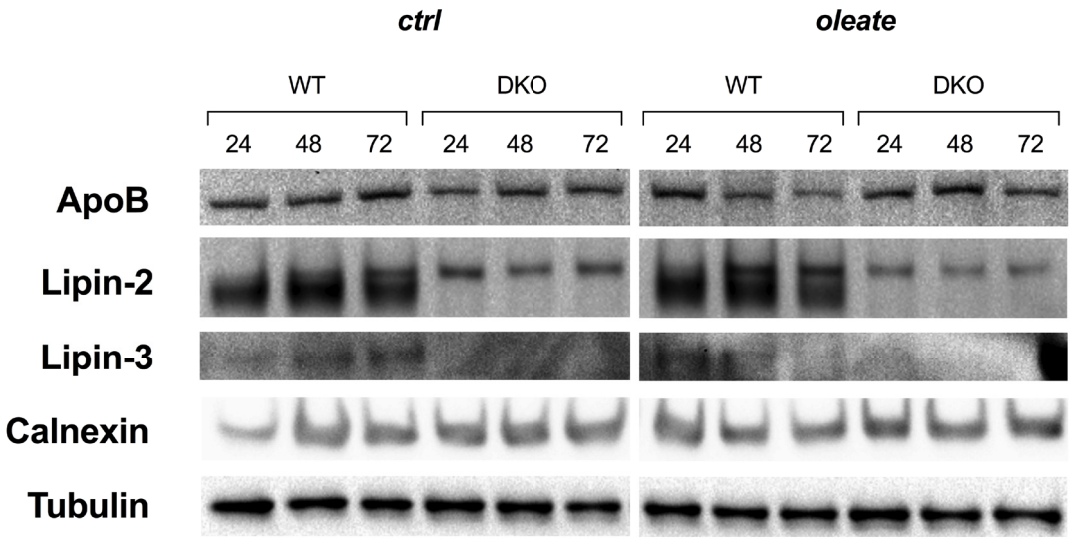

Figure 3.14. Western blot with HT-29 cell lysates after long-term oleate treatment. WT and DKO cells were treated with 0.4 mM oleate-BSA for 24, 48, and 72 hours and compared to the control group (no oleate). Antibodies against ApoB, Lipin-2, Lipin-3, calnexin were used; α-tubulin served as the housekeeping control protein.

3.7.1 Immunoprecipitation

Immunofluorescence staining in the small intestine showed that Lipin-2 and ApoB colocalize in the enterocytes (Figure 3.10). This potential protein-protein interaction was investigated further via immunoprecipitation. Using the anti-ApoB antibody to pull down endogenous ApoB from the cell culture medium after oleate or micelle treatment was not successful. ApoB was not detectable in any of the fractions, therefore the data from those experiments is not shown.

Immunoprecipitation was also performed in cell lysates after the overexpression of Lipin-2-V5 using anti-V5 antibody. ApoB was detected in fraction 0 and 1 as expected but was not pulled down by binding to Lipin-2 (Figure 3.15). Lipin-2 itself was detected in all three fractions, which means that the immunoprecipitation worked, if only a small amount of protein was present in the pulldown fraction. This could be due to the fact that the transfection efficiency in the HT-29 cells was rather low at around 20%. This would mean that the majority of Lipin-2 detected in fraction 0 and 1 is constitutive Lipin-2 or the pulldown with the V5 antibody was not very efficient. Detection of Lipin-2-V5 shows no band, which could be due to inefficient antibody binding or insufficient amounts of protein. Overall we could not detect a direct interaction between ApoB and

Lipin-2 with this experiment, although the co-localization of these proteins was shown with immunofluorescence staining in the enterocytes of the small intestine in mice (Figure 3.10). It may be that Lipin-2 and ApoB interact through a larger complex, and that Lipin-2 does not directly bind ApoB.

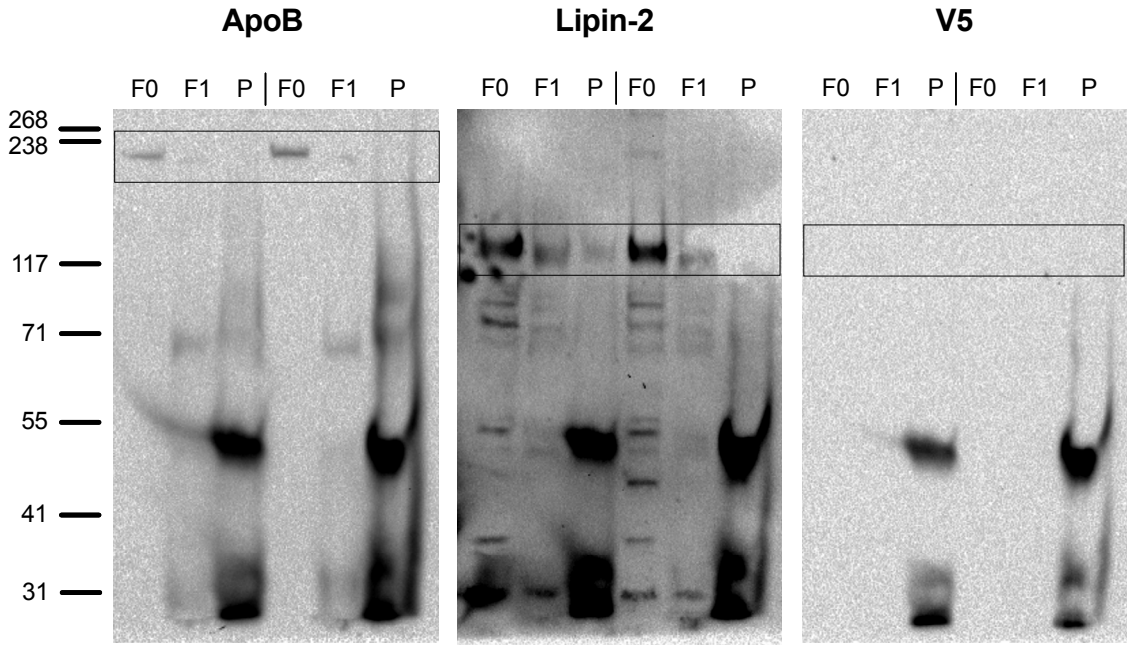

Figure 3.15. Immunoprecipitation of Lipin-2 with anti-V5 antibody in HT-29 cell lysates after Lipin-2-V5 overexpression. Western blot detection with antibodies against ApoB, Lipin-2 and V5. Unspecific bands at a size of about 50 and 25 kDa are the IgG heavy and light chain, respectively. F0, fraction 0; F1, fraction 1; P, pulldown.

3.7.2 Microscopy – Staining of Lipid Droplets After Short- and Long-Term Oleate Treatment in HT-29 Cells

Oil Red O and BODIPY 493/503 both stain neutral triglycerides and lipids in cells for bright field and fluorescence microscopy, respectively. Wild type and Lipin-2/3KO HT-29 cells were first treated with a short-term oleate treatment (2, 4, and 8 hours) to study the possible effects of the lipid load on the lipid droplet phenotype in the cells. We did not see a significant difference in the amount or shape of LDs after a 2h treatment with either staining. With the ORO staining, more large lipid droplets are present in the WT cells after 4 and especially 8 hours of treatment (Figure 3.16 E and G). The BODIPY staining shows very small lipid droplets slowly growing in size after 4 and 8 hours and

being slightly more abundant in the WT cells (Figure 3.17 E and G). This seems to be due to a slower lipid uptake or reduced synthesis of TAG in the DKO.

The short-term treatment was definitely not intense or long enough to see clear effects. Instead of raising the concentration of oleate to not cause cell stress, the treatment regimen was extended to 24, 48, and 72 hours. The cells were healthy and proliferating even after 72 hours. As another reference group for the long-term treatment cells were fasted for 24 hours. This caused many of them to die or at least stop proliferating, which led to single cells instead of the typical groups they tend to grow in. Because there were only so very few LDs present in the fasted cells, BODIPY also stained the cell membrane. There is no visible difference between the WT and the DKO cells, which also applies to the control group of untreated cells (Figure 3.18 A-F).

The 24h treatment resulted in a significant difference in the phenotype of the lipid droplets. More than 90% of DKO cells have small LDs while more than 90% of WT cells contain LDs that are a lot bigger (Figure 3.18 G-L). These effects remained consistent for the 48h and 72h time points (48h images are not shown). After 72 hours the lipid droplets in the DKO cells are slightly bigger when compared to the images taken at the 24h time point (Figure 3.18 N, P, R). In the WT cells the LDs are still very large in size but there are also small ones present, which might be newly formed lipid droplets after excess lipids had already been secreted. (Figure 3.18 M, O, Q). The results show reduced accumulation of neutral lipid droplets in DKO cells which could be caused by reduced fatty acid uptake, reduced incorporation of fatty acids into TAG, or both. These results are important because they demonstrate that our cell culture system mirrors that same phenotype observed in the DKO mice, which accumulate only small lipid droplets in intestinal enterocytes after an acute meal.

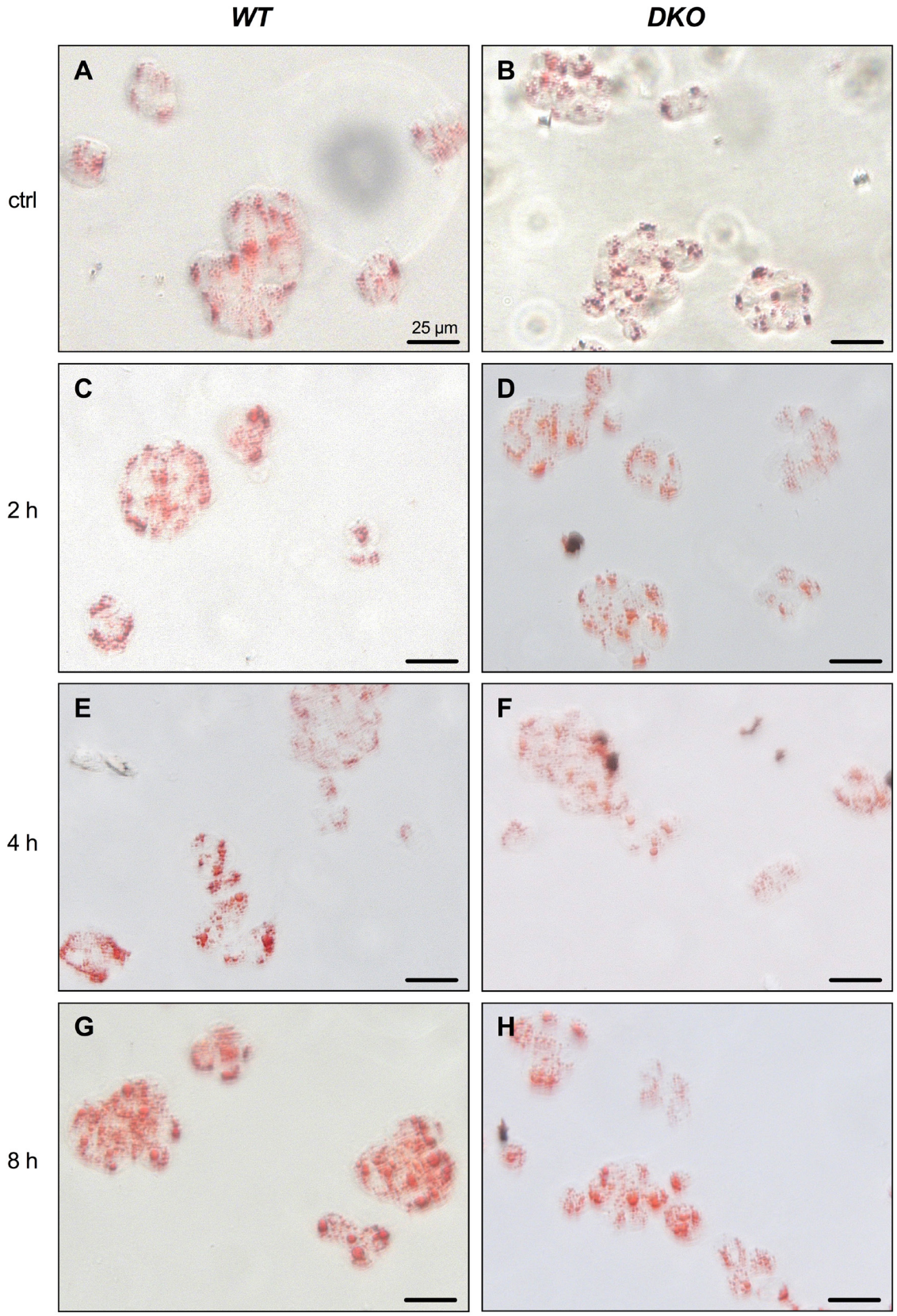

Figure 3.16. Oil Red O staining of HT-29 WT and Lipin-2/3KO cells after short-term oleate treatment. WT (A, C, E, G) and DKO (B, D, F, H) cells were treated with 0.4 mM oleate-BSA for 2, 4, or 8 hours. No oleate was added to the control group (ctrl). Images were taken with a bright field microscope at 400x magnification. Lipid droplets are stained in red by ORO. Scale bar is 25 µm.

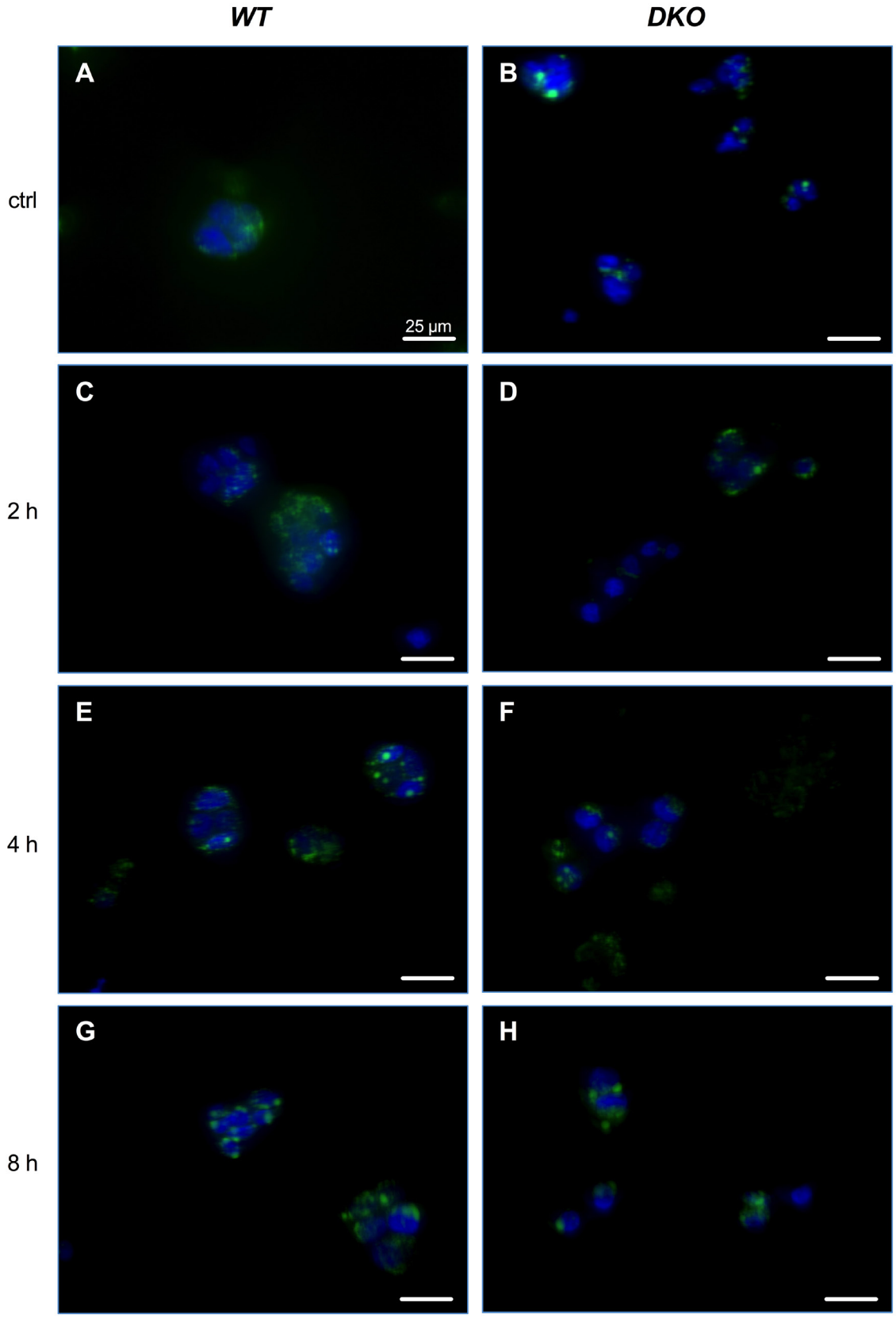

Figure 3.17. BODIPY/DAPI staining of HT-29 WT and Lipin-2/3KO cells after short-term oleate treatment. WT (A, C, E, G) and DKO (B, D, F, H) cells were treated with 0.4 mM oleate-BSA for 2, 4, or 8 hours. No oleate was added to the control group (ctrl). Images were taken at 400x magnification. Lipid droplets are stained by BODIPY (green), cell nuclei are stained by DAPI (blue). Scale bar is 25 µm.

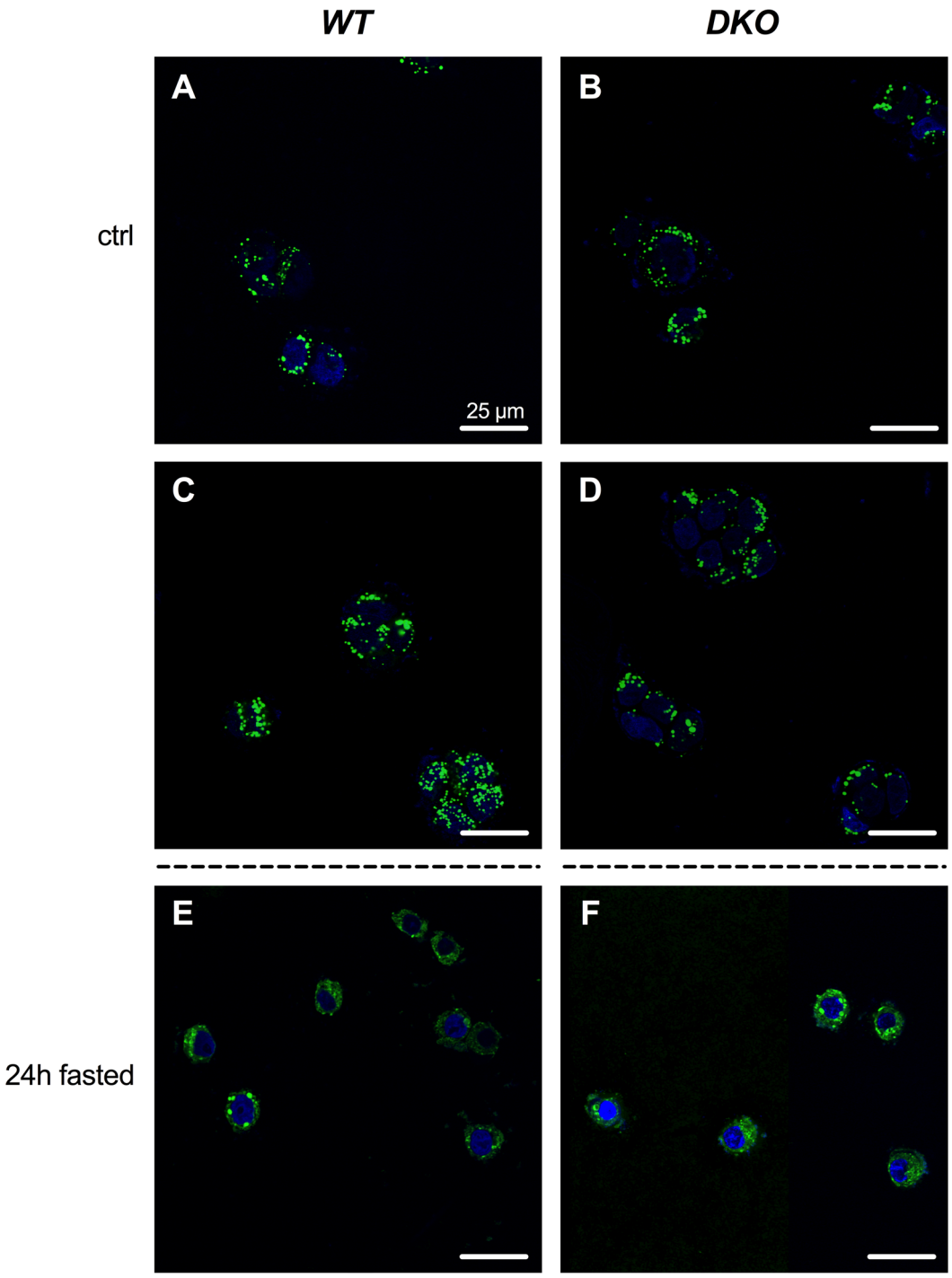

Figure 3.18. BODIPY/DAPI staining of HT-29 WT and Lipin-2/3KO cells after long-term oleate treatment. A concentration of 0.4 mM oleate-BSA was used for a 24h, 48h (images not shown), and 72h treatment. (A-D) The control group (ctrl) was incubated with DMEM alone. (E, F) HBSS was used for a 24h long starvation. Images were taken at 1000x magnification. Lipid droplets are stained with BODIPY (green), cell nuclei are stained by DAPI (blue). Scale bar is 25 µm.

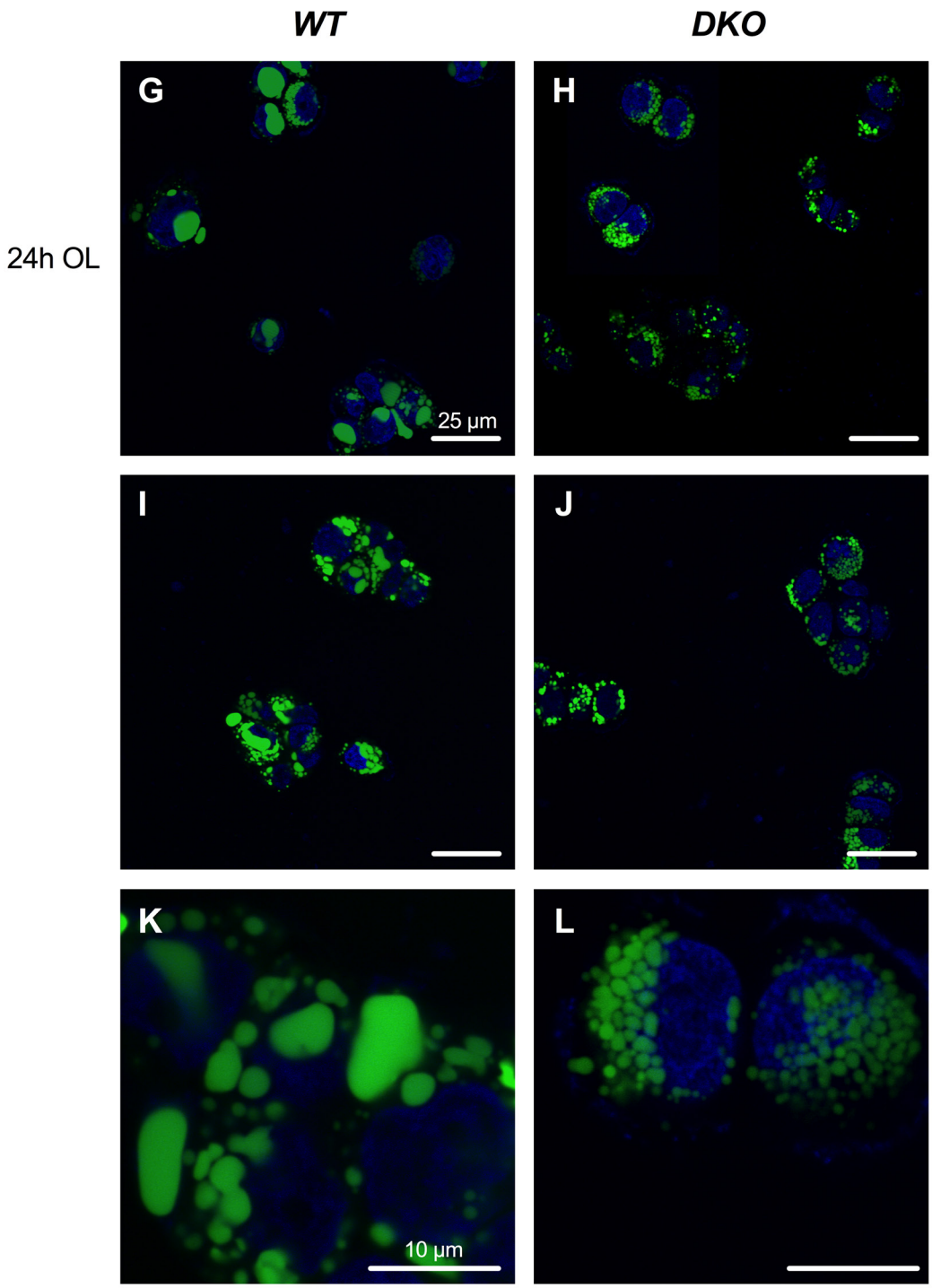

Figure 3.18 *continued*. BODIPY/DAPI staining of HT-29 WT and Lipin-2/3KO cells after long-term oleate treatment (OL). A concentration of 0.4 mM oleate-BSA was used for a 24h treatment. (G-J) Images were taken at 1000x magnification. (K, L) Images were taken at 8000x magnification. Corresponding scale bars are 25 µm and 10 µm. BODIPY stains lipid droplets (green), DAPI stains cell nuclei (blue).

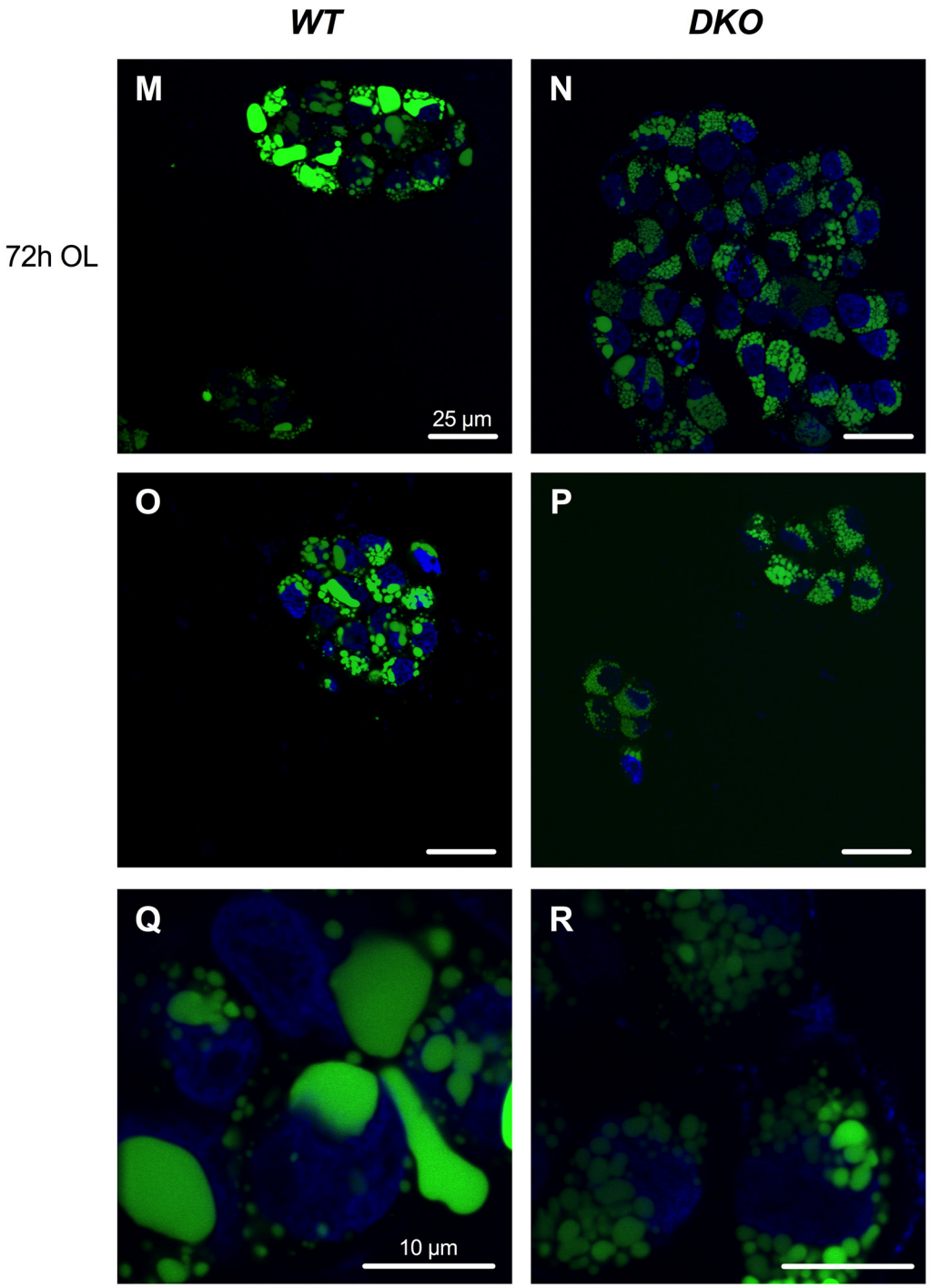

Figure 3.18 *continued II*. BODIPY/DAPI staining of HT-29 WT and Lipin-2/3KO cells after long-term oleate treatment (OL). A concentration of 0.4 mM oleate-BSA was used for a 72h treatment. (M-P) Images were taken at 1000x magnification. (Q, R) Images were taken at 8000x magnification. Corresponding scale bars are 25 µm and 10 µm. BODIPY stains lipid droplets (green), DAPI stains cell nuclei (blue).

4 DISCUSSION

The general belief is, that TAG synthesis in intestinal enterocytes is mainly mediated by the monoacylglycerol pathway. (51–53,185) In contrast to this, studies with mice and HT-29 cell that lack Lipin-2 and Lipin-3 PAP enzymes have revealed a more critical and important role of the glycerol phosphate pathway in lipid metabolism in the gut than anticipated. We were able to show that this deficiency results in a striking phenotype and has a far-reaching impact on lipid metabolism especially on pathways and processes in enterocytes. The generation of Lipin-2/3KO HT-29 cells now provides us with another model organism to further investigate the effects.

Interestingly, Lipin-2/3KO mice share many phenotypic similarities regarding their phenotypic features with mice lacking ApoB expression in the intestine. (186) That mouse was established as the first genetic model of defective absorption of fats and fat-soluble vitamins. Thereby it serves as a useful animal model for studying lipoprotein metabolism to give more insight into human hypobetalipoproteinemia disorders, which include abetalipoproteinemia, familial hypobetalipoproteinemia, and chylomicron retention disease. The causes of these related disorders are often mutations in genes such as *APOB*, *MTP*, *SAR1B*, *ANGPTL3*, and others, whose protein products are involved in chylomicron synthesis and secretion in enterocytes. (187–190)

In studies performed earlier in the Reue laboratory, Lipin-2/3KO mice also exhibited severely increased fecal cholesterol content, while plasma levels of high-density lipoproteins (HDL) and fat-soluble Vitamin D were reduced, providing further evidence to an impairment of fat and cholesterol absorption. Interestingly, mRNA expression levels of the transporter protein ABCG5, which is responsible for limiting absorption and promoting the excretion of sterols back into the intestinal lumen, were reduced in the DKO on a chow diet but compared to that upregulated in the DKO on HFD (Figure 3.6). (191) A higher load of dietary fats seems to induce expression of ABCG5 to manage the efficient efflux of excess sterols. This is in line with the results from the total cholesterol assay in the small intestine showing increased levels in mice fed the high-fat diet (Figure 3.7). Fat and cholesterol absorption were nearly completely lacking in the intestine-

specific ApoB-deficient mice, while compensatory cholesterol synthesis, and reduced plasma levels of HDL and Vitamin A were observed. (186) Probably as a compensation for the low lipid absorption rates, these mice consumed more food together with a higher production of feces. The opposite – lower food intake and fecal output – were true for mice deficient in Lipin-3 alone. Therefore, the drastic changes in intestinal lipid metabolism in Lipin-2/3KO mice are due to a combination of phenotypes originating from the loss of either Lipin-2 or Lipin-3. The amount of obvious similarities between

the Lipin-2/3KO and the intestine-specific ApoB-deficient mice suggests related underlying mechanisms. In regard to human hypobetalipoproteinemia cases with unidentified genetic causes this suggests the possibility of mutations in *LPIN2* and *LPIN3* being involved.

How do Lipin-2 and 3 influence the formation and secretion of chylomicrons? It is possible that Lipins are involved in the formation of the small ER luminal LDs that fuse with the lipidated ApoB (preCM), which are particles too small to be visualized by electron microscopy because a lack of Lipin-2/3 might result in reduced amounts of newly synthesized TAGs, which are needed for proper lipidation. Another effect of Lipin-2/3 deficiency are the reduced amounts of several different phospholipids, which are necessary for the formation of membrane "buds" to generate the needed transport vesicles for lipoprotein secretion. A study in HeLa cells has shown that DAG is required for the membrane budding in the Golgi. (192)

ApoB is an important factor in the regulation of chylomicron secretion. Together with ApoA-IV and MTP it affects lipoprotein biogenesis. (193) Diurnal variations in MTP expression levels can influence the rate of lipid absorption and might be responsible for changes in the total ApoB-containing lipoprotein levels. (194) Abnormal accumulation of ApoB in the ER of Lipin-2/3KO mice might be connected to improper formation of pre-chylomicrons. In addition, we showed that ApoB in the DKO is not properly degraded. When ApoB is not sufficiently lipidated in wild-type cells it binds to cytosolic lipid droplets and proteasomal or autophagic degradation is induced. It has been suggested that proteasomal degradation of ApoB might be promoted by HSC70 together with other chaperones. (195) Our data suggest that macroautophagy and chaperone-mediated autophagy are not reduced in the DKO cells, however, some other mechanism

must be responsible for the accumulation of ApoB. All these defects combined result in a drastically reduced secretion of chylomicrons.

What role do Lipin-2 and 3 play in the accumulation of lipid droplets in the cells while uptake of dietary lipids is decreased? We show that acute lipid uptake and/or incorporation of fatty acids into TAG in Lipin-2/3KO cells is reduced. Over the long term, DKO cells are unable to process the absorbed fats and start accumulating them as cytosolic lipid droplets. Because the delivery of dietary lipids to enterocytes has been shown to induce an autophagic response to break down the newly stored LDs, we expected autophagy to be increased in the Lipin-2/3KO cells trying to deal with the overload of lipids. (123) The LC3 autophagy marker we looked at was increased in DKO intestine, consistent with increased flux through the autophagic pathway, suggesting that a defect in this pathway was not responsible for accumulation of lipid droplets.

Another important aspect is the regulatory influence fatty acids can have on effectors in cellular signaling pathways, including PPARα.

PPARα is activated by different natural ligands including eicosanoids, unsaturated as well as long-chain fatty acids, and their activated derivatives (acyl-CoA esters). Because the average Western diet (equivalent to HFD in mouse studies) contains high amounts of TAG, supplying the enterocytes with fatty acids and MAG, the small intestine is frequently exposed to high levels of PPARα ligands. Together with the range of genes, that are regulated by it, PPARα plays a functionally important role in the small intestine. Activation of PPARα leads to the specific induction of genes involved in fatty acid uptake, binding, transport, and catabolism, as well as genes involved in triacylglycerol and glycerolipid metabolism. This basically means, that PPARα serves as a FA sensor that itself is part of a feed-forward mechanism in which FAs stimulate their own catabolism, storage, transfer through the enterocyte, and secretion as TAGs. (178,179) Additionally to the impact on PPARα activity of feeding mice a HFD, the deficiency of Lipin-2 and 3 is another important factor. A mouse model with PGC-1α deficiency led to the discovery of the role of Lipin-1 in transcriptional activation, because the expression of Lipin-1, PPARα and its target genes was not induced in the liver during fasting. (78) It has been described that CREB-regulated transcriptional coactivator 2 (TORC2) mediates the induction of Lipin-1 and PGC-1α in liver and adipose tissue, which leads to an increase

in the synthesis of DAG and TAG. Sirtuin 2 ortholog 1 (SIRT1) seems to be the centerpiece in this regulatory loop of PPARα, PGC-1α, Lipin-1, and TORC2 controlling the response of lipid metabolism in the liver. It has been suggested that this system might also play a role in other tissues, induced and regulated by different nutrient and physiological signals. (196) This might mean that PPARα activation in DKO mice or cells is not only influenced by the lipid load and impaired processing of fats but also directly by the deficiency of Lipins as transcriptional activators of PPARα.

The results indicate that a lack of Lipin-2 and Lipin-3 does not interfere with the formation of lipid droplets but may affect how they are further used and processed in cell. Since the secretion of chylomicrons is impaired there is reason to believe that Lipin-2/3 may interfere with this process. They may also affect phospholipid synthesis and the downstream processes PLs are used for and involved in. Their basic function in TAG synthesis is definitely affected by a lack of Lipin-2/3. It is possible that each one of the two TAG synthesis pathways has a specific role with the MGAT pathway being predominantly involved in formation of cytosolic LDs while the G3P pathway plays an important role in the formation of TAG destined for secretion. An interesting study would be to design intestine-specific knockout mice deficient in Lipin-2/3 and MGAT2 to see the effects when both pathways of TAG synthesis are impaired. These mice might completely lack cytosolic lipid droplets and be even more depleted of TAG droplets for secretion.

It is still difficult to understand the full relationship between Lipin-2 and 3 and their roles in lipid homeostasis in small intestine. Generating a mouse model with an enterocyte-specific knockout would possibly lead to new insights into the separate local functions of each Lipin instead of the full body knockout where effects are global and hard to distinguish from one another. Further studying and implementing the CRISPR/Cas9 engineered HT-29 cells as a model cell line will increase the knowledge about the effects of a lack of Lipin-2/3 specifically in enterocytes and might facilitate a wide range of experiments. The elucidation of the molecular and physiological roles of the different Lipins will greatly improve our understanding of the regulation of fatty acid and glycerolipid metabolism and could lead to novel approaches to treating cellular lipid storage and metabolic disease.

BIBLIOGRAPHY

1. Clandinin MT, Cheema S, Field CJ, Garg ML, Venkatraman J, Clandinin TR. Dietary fat: exogenous determination of membrane structure and cell function. FASEB J. 1991 Oct;5(13):2761–9.
2. Carey MC, Small DM, Bliss CM. Lipid digestion and absorption. Annu Rev Physiol. 1983;45:651–77.
3. Tso P, Balint JA. Formation and transport of chylomicrons by enterocytes to the lymphatics. Am J Physiol. 1986 Jun;250(6 Pt 1):G715–26.
4. Pan X, Hussain MM. Gut triglyceride production. Biochim Biophys Acta. 2012 May;1821(5):727–35.
5. Coleman RA, Mashek GD. Mammalian Triacylglycerol Metabolism: Synthesis, Lipolysis and Signaling. Chem Rev. 2011;111(10):6359–86.
6. Péterfy M, Phan J, Xu P, Reue K. Lipodystrophy in the fld mouse results from mutation of a new gene encoding a nuclear protein, lipin. Nat Genet. 2001 Jan;27(1):121–4.
7. Reue K, Zhang P. The lipin protein family: Dual roles in lipid biosynthesis and gene expression. FEBS Lett. 2008;582(1):90–6.
8. Hamosh M, Scow RO. Lingual lipase and its role in the digestion of dietary lipid. J Clin Invest. 1973;52(1):88–95.
9. Bodmer MW, Angal S, Yarranton GT, Harris TJ, Lyons A, King DJ, et al. Molecular cloning of a human gastric lipase and expression of the enzyme in yeast. Biochim Biophys Acta. 1987 Aug 25;909(3):237–44.
10. Verger R. Enzyme kinetics of lipolysis. Methods Enzymol. 1980;64:340–92.
11. Van Tilbeurgh H, Bezzine S, Cambillau C, Verger R, Carrière F. Colipase: Structure and interaction with pancreatic lipase. Biochim Biophys Acta - Mol Cell Biol Lipids. 1999;1441(2-3):173–84.
12. Hofmann AF, Borgstroem B. The intraluminal phase of fat digestion in man: The lipid content of the micellar and oil phases of intestinal content obtained during fat digestion and absorption. J Clin Invest. 1964 Feb;43:247–57.
13. Carriere F, Barrowman JA, Verger R, Laugier R. Secretion and contribution to lipolysis of gastric and pancreatic lipases during a test meal in humans.

Gastroenterology. 1993 Sep;105(3):876–88.

14. Akesson B, Gronowitz S, Herslof B, Ohlson R. Absorption of synthetic, stereochemically defined acylglycerols in the rat. Lipids. 1978 May;13(5):338–43.
15. Borgstrom B. Influence of bile salt, pH, and time on the action of pancreatic lipase; physiological implications. J Lipid Res. 1964 Oct 1;5(4):522–31.
16. Stahl A, Hirsch DJ, Gimeno RE, Punreddy S, Pei G, Watson N, et al. Identification of the major intestinal fatty acid transport protein. Mol Cell. 1999;4(3):299–308.
17. Abumrad N a, Davidson NO. Role of the gut in lipid homeostasis. Physiol Rev. 2012;92(3):1061–85.
18. Kamp F, Guo W, Souto R, Pilch PF, Corkey BE, Hamilton JA. Rapid flip-flop of oleic acid across the plasma membrane of adipocytes. J Biol Chem. 2003;278(10):7988–95.
19. Stahl A, Gimeno RE, Tartaglia LA, Lodish HF. Fatty acid transport proteins: a current view of a growing family. Trends Endocrinol Metab. 2001;12(6):266–73.
20. Abumrad NA, El-Maghrabi MR, Amri EZ, Lopez E, Grimaldi PA. Cloning of a rat adipocyte membrane protein implicated in binding or transport of long-chain fatty acids that is induced during preadipocyte differentiation. Homology with human CD36. J Biol Chem. 1993;268(24):17665–8.
21. Lobo M V, Huerta L, Ruiz-Velasco N, Teixeiro E, de la Cueva P, Celdrán A, et al. Localization of the lipid receptors CD36 and CLA-1/SR-BI in the human gastrointestinal tract: towards the identification of receptors mediating the intestinal absorption of dietary lipids. J Histochem Cytochem. 2001 Oct;49(10):1253–60.
22. Pepino MY, Kuda O, Samovski D, Abumrad NA. Structure-Function of CD36 and Importance of Fatty Acid Signal Transduction in Fat Metabolism. Annu Rev Nutr. 2014 Jul 17;34(1):281–303.
23. Sundaresan S, Shahid R, Riehl TE, Chandra R, Nassir F, Stenson WF, et al. CD36-dependent signaling mediates fatty acid-induced gut release of secretin and cholecystokinin. FASEB J. 2013 Mar;27(3):1191–202.
24. Tran TTT, Poirier H, Clément L, Nassir F, Pelsers MMAL, Petit V, et al. Luminal lipid regulates CD36 levels and downstream signaling to stimulate chylomicron synthesis. J Biol Chem. 2011;286(28):25201–10.

25. Siddiqi S, Saleem U, Abumrad N a, Davidson NO, Storch J, Siddiqi S a, et al. A novel multiprotein complex is required to generate the prechylomicron transport vesicle from intestinal ER. J Lipid Res. 2010;51(7):1918–28.
26. Smith J, Su X, El-Maghrabi R, Stahl PD, Abumrad NA. Opposite regulation of CD36 ubiquitination by fatty acids and insulin: effects on fatty acid uptake. J Biol Chem. 2008 May 16;283(20):13578–85.
27. Siddiqi S, Sheth A, Patel F, Barnes M, Mansbach CM. Intestinal caveolin-1 is important for dietary fatty acid absorption. Biochim Biophys Acta. 2013 Aug;1831(8):1311–21.
28. Milger K, Herrmann T, Becker C, Gotthardt D, Zickwolf J, Ehehalt R, et al. Cellular uptake of fatty acids driven by the ER-localized acyl-CoA synthetase FATP4. J Cell Sci. 2006;119(Pt 22):4678–88.
29. Moulson CL, Martin DR, Lugus JJ, Schaffer JE, Lind AC, Miner JH. Cloning of wrinkle-free, a previously uncharacterized mouse mutation, reveals crucial roles for fatty acid transport protein 4 in skin and hair development. Proc Natl Acad Sci USA. 2003 Apr 29;100(9):5274–9.
30. Moulson CL, Lin M-H, White JM, Newberry EP, Davidson NO, Miner JH. Keratinocyte-specific expression of fatty acid transport protein 4 rescues the wrinkle-free phenotype in Slc27a4/Fatp4 mutant mice. J Biol Chem. 2007 May 25;282(21):15912–20.
31. Shim J, Moulson CL, Newberry EP, Lin M-H, Xie Y, Kennedy SM, et al. Fatty acid transport protein 4 is dispensable for intestinal lipid absorption in mice. J Lipid Res. 2009 Mar;50(3):491–500.
32. Schulthess G, Lipka G, Compassi S, Boffelli D, Weber FE, Paltauf F, et al. Absorption of monoacylglycerols by small intestinal brush border membrane. Biochemistry. 1994 Apr 19;33(15):4500–8.
33. Ho SY, Storch J. Common mechanisms of monoacylglycerol and fatty acid uptake by human intestinal Caco-2 cells. Am J Physiol Cell Physiol. 2001;281(4):C1106–17.
34. Murota K, Matsui N, Kawada T, Takahashi N, Fushuki T. Inhibitory effect of monoacylglycerol on fatty acid uptake into rat intestinal epithelial cells. Biosci Biotechnol Biochem. 2001 Jun;65(6):1441–3.
35. Altmann SW, Davis HR, Zhu L-J, Yao X, Hoos LM, Tetzloff G, et al. Niemann-Pick

C1 Like 1 protein is critical for intestinal cholesterol absorption. Science. 2004 Feb 20;303(5661):1201–4.

36. Lee MH, Lu K, Hazard S, Yu H, Shulenin S, Hidaka H, et al. Identification of a gene, ABCG5, important in the regulation of dietary cholesterol absorption. Nat Genet. 2001 Jan;27(1):79–83.
37. Lu K, Lee MH, Hazard S, Brooks-Wilson A, Hidaka H, Kojima H, et al. Two genes that map to the STSL locus cause sitosterolemia: genomic structure and spectrum of mutations involving sterolin-1 and sterolin-2, encoded by ABCG5 and ABCG8, respectively. Am J Hum Genet. 2001 Aug;69(2):278–90.
38. Iqbal J, Hussain MM. Evidence for multiple complementary pathways for efficient cholesterol absorption in mice. J Lipid Res. 2005;46(7):1491–501.
39. Bass NM. Function and regulation of hepatic and intestinal fatty acid binding proteins. Chem Phys Lipids. 1985 Aug 30;38(1-2):95–114.
40. Thumser AE, Storch J. Liver and intestinal fatty acid-binding proteins obtain fatty acids from phospholipid membranes by different mechanisms. J Lipid Res. 2000;41:647–56.
41. Storch J, Thumser AE. Tissue-specific functions in the fatty acid-binding protein family. J Biol Chem. 2010;285(43):32679–83.
42. Neeli I, Siddiqi SA, Siddiqi S, Mahan J, Lagakos WS, Binas B, et al. Liver fatty acid-binding protein initiates budding of pre-chylomicron transport vesicles from intestinal endoplasmic reticulum. J Biol Chem. 2007;282(25):17974–84.
43. Lagakos WS, Gajda AM, Agellon L, Binas B, Choi V, Mandap B, et al. Different functions of intestinal and liver-type fatty acid-binding proteins in intestine and in whole body energy homeostasis. Am J Physiol Gastrointest Liver Physiol. 2011 May;300(5):G803–14.
44. Ellis JM, Frahm JL, Li LO, Coleman RA. Acyl-coenzyme A synthetases in metabolic control. Curr Opin Lipidol. 2010 Jun;21(3):212–7.
45. Fujino T, Kang MJ, Suzuki H, Iijima H, Yamamoto T. Molecular characterization and expression of rat acyl-CoA synthetase 3. J Biol Chem. 1996 Jul 12;271(28):16748–52.
46. Oikawa E, Iijima H, Suzuki T, Sasano H, Sato H, Kamataki A, et al. A novel acyl-CoA synthetase, ACS5, expressed in intestinal epithelial cells and proliferating preadipocytes. J Biochem. 1998 Sep;124(3):679–85.

47. Langhans W, Leitner C, Arnold M. Dietary fat sensing via fatty acid oxidation in enterocytes: possible role in the control of eating. Am J Physiol Regul Integr Comp Physiol. 2011;300(3):R554–65.
48. Lehner R, Kuksis A. Biosynthesis of triacylglycerols. Prog Lipid Res. 1996;35(2):169–201.
49. Bell RM, Coleman RA. Enzymes of glycerolipid synthesis in eukaryotes. Annu Rev Biochem. 1980;49:459–87.
50. Yen CL, Nelson DW, Yen MI. Intestinal triacylglycerol synthesis in fat absorption and systemic energy metabolism. J Lipid Res. 2015;56(3):489–501.
51. Mattson FH, Volpenhein RA. The digestion and absorption of triglycerides. J Biol Chem. 1964 Sep;239:2772–7.
52. Fred K, Borgström B. Quantitative study of the pathways of triglyceride synthesis by hamster intestinal mucosa. Biochim Biophys Acta - Lipids Lipid Metab. 1965 Jun;98(3):520–31.
53. Kayden HJ, Senior JR, Mattson FH. The monoglyceride pathway of fat absorption in man. J Clin Invest. 1967 Nov;46(11):1695–703.
54. Yen C-LE, Farese R V. MGAT2, a monoacylglycerol acyltransferase expressed in the small intestine. J Biol Chem. 2003 May 16;278(20):18532–7.
55. Cao J, Cheng L, Shi Y. Catalytic properties of MGAT3, a putative triacylgycerol synthase. J Lipid Res. 2007 Mar;48(3):583–91.
56. Bell RM, Ballas LM, Coleman RA. Lipid topogenesis. 1981;22:391–403.
57. Csaki LS, Reue K. Lipins: Multifunctional Lipid Metabolism Proteins. Annu Rev Nutr. 2010;30(1):257–72.
58. Yen C-LE, Stone SJ, Koliwad S, Harris C, Farese R V. Thematic review series: glycerolipids. DGAT enzymes and triacylglycerol biosynthesis. J Lipid Res. 2008;49(11):2283–301.
59. Hashidate-Yoshida T, Harayama T, Hishikawa D, Morimoto R, Hamano F, Tokuoka SM, et al. Fatty acyl-chain remodeling by LPCAT3 enriches arachidonate in phospholipid membranes and regulates triglyceride transport. Elife. 2015;2015(4):1–75.
60. Mansbach CM, Gorelick F. Development and physiological regulation of intestinal lipid absorption. II. Dietary lipid absorption, complex lipid synthesis, and the intracellular packaging and secretion of chylomicrons. Am J Physiol

Gastrointest Liver Physiol. 2007;293(4):G645–50.

61. Phan CT, Tso P. Intestinal lipid absorption and transport. Front Biosci. 2001 Mar 1;6:D299–319.

62. Rong X, Wang B, Dunham MM, Hedde PN, Wong JS, Gratton E, et al. Lpcat3-dependent production of arachidonoyl phospholipids is a key determinant of triglyceride secretion. Elife. 2015;2015(4):1–23.

63. Kabir I, Li Z, Bui HH, Kuo M-S, Gao G, Jiang X-C. Small Intestine but Not Liver Lysophosphatidylcholine Acyltransferase 3 (Lpcat3) Deficiency Has a Dominant Effect on Plasma Lipid Metabolism. J Biol Chem. 2016 Apr 1;291(14):7651–60.

64. Phan J, Péterfy M, Reue K. Lipin expression preceding peroxisome proliferator-activated receptor-γ is critical for adipogenesis in vivo and in vitro. J Biol Chem. 2004;279(28):29558–64.

65. Phan J, Reue K. Lipin, a lipodystrophy and obesity gene. Cell Metab. 2005;1(1):73–83.

66. Dwyer JR, Donkor J, Zhang P, Csaki LS, Vergnes L, Lee JM, et al. Mouse lipin-1 and lipin-2 cooperate to maintain glycerolipid homeostasis in liver and aging cerebellum. Proc Natl Acad Sci. 2012;109(37):E2486–95.

67. Nadra K, Médard J-J, Mul JD, Han G-S, Grès S, Pende M, et al. Cell autonomous lipin 1 function is essential for development and maintenance of white and brown adipose tissue. Mol Cell Biol. 2012;32(23):4794–810.

68. Zhang P, Takeuchi K, Csaki LS, Reue K. Lipin-1 phosphatidic phosphatase activity modulates phosphatidate levels to promote peroxisome proliferator-activated receptor γ (PPARγ) gene expression during adipogenesis. J Biol Chem. 2012;287(5):3485–94.

69. Johnston JM. The Absorption of Fatty Acids by the Isolated Intestine. J Biol Chem. 1959;234:1065–7.

70. Johnston JM, Bearden JH. Phosphatidic acids as intermediates in fatty acid absorption. Arch Biochem Biophys. 1960 Sep;90(1):57–62.

71. Clark B, Hünscher G. Biosynthesis of glycerides in subcellular fractions of intestinal mucosa. Biochim Biophys Acta. 1961 Jan;46(3):479–94.

72. Coleman R, Hübscher G. Metabolism of phospholipids: Studies of Phosphatidic Acid Phosphatase. Biochim Biophys Acta. 1962 Jan;56:479–90.

73. Sarzala MG, Wlodawer P. Phosphatidate phosphohydrolase in frog intestinal

tissue. Comp Biochem Physiol. 1969 Mar;28(3):1029–44.

74. Short VJ, Dils R, Brindley DN. Enzymes of glycerolipid synthesis in small-intestinal mucosa of foetal and neonatal guinea pigs. Biochem J. 1975 Dec;152(3):675–9.

75. Johnston JM, Rao GA, Lowe PA. The separation of the α-glycerophosphate and monoglyceride pathways in the intestinal biosynthesis of triglycerides. Biochim Biophys Acta - Lipids Lipid Metab. 1967 Jun;137(3):578–80.

76. Langner CA, Birkenmeier EH, Ben-Zeev O, Schotz MC, Sweet HO, Davisson MT, et al. The fatty liver dystrophy (fld) mutation. A new mutant mouse with a developmental abnormality in triglyceride metabolism and associated tissue-specific defects in lipoprotein lipase and hepatic lipase activities. J Biol Chem. 1989;264(14):7994–8003.

77. Han G-S, Wu W-I, Carman GM. The Saccharomyces cerevisiae Lipin homolog is a Mg2+-dependent phosphatidate phosphatase enzyme. J Biol Chem. 2006;281(14):9210–8.

78. Finck BN, Gropler MC, Chen Z, Leone TC, Croce MA, Harris TE, et al. Lipin 1 is an inducible amplifier of the hepatic PGC-1alpha/PPARalpha regulatory pathway. Cell Metab. 2006;4(3):199–210.

79. Hübscher G, Brindley DN, Smith ME, Sedgwick B. Stimulation of Biosynthesis of Glyceride. Nature. 1967 Nov 4;216(5114):449–53.

80. Kok BPC, Brindley DN. Regulation of Lipins and Their Role in Lipid Metabolism - The Role of Phosphatidate Phosphatase in Glycerolipid Biosynthesis. AOCS Lipid Library. 2011.

81. Takeuchi K, Reue K. Biochemistry, physiology, and genetics of GPAT, AGPAT, and lipin enzymes in triglyceride synthesis. Am J Physiol Endocrinol Metab. 2009;296(6):E1195–209.

82. Bou Khalil M, Sundaram M, Zhang H-Y, Links PH, Raven JF, Manmontri B, et al. The level and compartmentalization of phosphatidate phosphatase-1 (lipin-1) control the assembly and secretion of hepatic VLDL. J Lipid Res. 2009;50:47–58.

83. Liu G-H, Gerace L. Sumoylation regulates nuclear localization of lipin-1alpha in neuronal cells. PLoS One. 2009;4(9):e7031.

84. Péterfy M, Phan J, Reue K. Alternatively spliced lipin isoforms exhibit distinct expression pattern, subcellular localization, and role in adipogenesis. J Biol Chem. 2005;280(38):32883–9.

85. Ren H, Federico L, Huang H, Sunkara M, Drennan T, Frohman MA, et al. A phosphatidic acid binding/nuclear localization motif determines lipin1 function in lipid metabolism and adipogenesis. Mol Biol Cell. 2010 Sep 15;21(18):3171–81.
86. Reue K, Brindley DN. Thematic Review Series: Glycerolipids. Multiple roles for lipins/phosphatidate phosphatase enzymes in lipid metabolism. J Lipid Res. 2008;49(12):2493–503.
87. Harris TE, Finck BN. Dual function lipin proteins and glycerolipid metabolism. Trends Endocrinol Metab. Elsevier Ltd; 2011;22(6):226–33.
88. Donkor J, Sariahmetoglu M, Dewald J, Brindley DN, Reue K. Three Mammalian Lipins Act as Phosphatidate Phosphatases with Distinct Tissue Expression Patterns. J Biol Chem. 2006;282(6):3450–7.
89. Nevin P, Koelsch D, Mansbach CM. Intestinal triacylglycerol storage pool size changes under differing physiological conditions. J Lipid Res. 1995 Nov;36(11):2405–12.
90. Beilstein F, Carrière V, Leturque A, Demignot S. Characteristics and functions of lipid droplets and associated proteins in enterocytes. Exp Cell Res. Elsevier; 2015 Sep;1–8.
91. Zhu J, Lee B, Buhman KK, Cheng J-X. A dynamic, cytoplasmic triacylglycerol pool in enterocytes revealed by ex vivo and in vivo coherent anti-Stokes Raman scattering imaging. J Lipid Res. 2009 Jun;50(6):1080–9.
92. Bouchoux J, Beilstein F, Pauquai T, Guerrera IC, Chateau D, Ly N, et al. The proteome of cytosolic lipid droplets isolated from differentiated Caco-2/TC7 enterocytes reveals cell-specific characteristics. Biol Cell. 2011;103(11):499–517.
93. Beilstein F, Bouchoux J, Rousset M, Demignot S. Proteomic Analysis of Lipid Droplets from Caco-2/TC7 Enterocytes Identifies Novel Modulators of Lipid Secretion. PLoS One. 2013;8(1):1–17.
94. D'Aquila T, Sirohi D, Grabowski JM, Hedrick VE, Paul LN, Greenberg AS, et al. Characterization of the proteome of cytoplasmic lipid droplets in mouse enterocytes after a dietary fat challenge. PLoS One. 2015;10(5):126823.
95. Sztalryd C, Kimmel AR. Perilipins: lipid droplet coat proteins adapted for tissue-specific energy storage and utilization, and lipid cytoprotection. Biochimie. 2014 Jan;96:96–101.

96. Lee B, Zhu J, Wolins NE, Cheng J-X, Buhman KK. Differential association of adipophilin and TIP47 proteins with cytoplasmic lipid droplets in mouse enterocytes during dietary fat absorption. Biochim Biophys Acta. 2009 Dec;1791(12):1173–80.
97. Obrowsky S, Chandak PG, Patankar J V, Povoden S, Schlager S, Kershaw EE, et al. Adipose triglyceride lipase is a TG hydrolase of the small intestine and regulates intestinal PPARα signaling. J Lipid Res. 2013;54:425–35.
98. Zechner R, Zimmermann R, Eichmann TO, Kohlwein SD, Haemmerle G, Lass A, et al. FAT SIGNALS - Lipases and Lipolysis in Lipid Metabolism and Signaling. Cell Metab. 2012 Mar;15(3):279–91.
99. Miller KW, Small DM. Surface-to-core and interparticle equilibrium distributions of triglyceride-rich lipoprotein lipids. J Biol Chem. 1983 Nov 25;258(22):13772–84.
100. Mahmood Hussain M. A proposed model for the assembly of chylomicrons. Atherosclerosis. 2000 Jan;148(1):1–15.
101. Fisher EA, Ginsberg HN. Complexity in the secretory pathway: the assembly and secretion of apolipoprotein B-containing lipoproteins. J Biol Chem. 2002;277(20):17377–80.
102. Greeve J, Altkemper I, Dieterich JH, Greten H, Windler E. Apolipoprotein B mRNA editing in 12 different mammalian species: hepatic expression is reflected in low concentrations of apoB-containing plasma lipoproteins. J Lipid Res. 1993 Aug;34(8):1367–83.
103. Blanc V, Davidson NO. C-to-U RNA editing: mechanisms leading to genetic diversity. J Biol Chem. 2003 Jan 17;278(3):1395–8.
104. Rava P, Hussain MM. Acquisition of triacylglycerol transfer activity by microsomal triglyceride transfer protein during evolution. Biochemistry. 2007 Oct 30;46(43):12263–74.
105. Cartwright IJ, Higgins JA. Direct evidence for a two-step assembly of ApoB48-containing lipoproteins in the lumen of the smooth endoplasmic reticulum of rabbit enterocytes. J Biol Chem. 2001 Dec 21;276(51):48048–57.
106. Fisher EA, Pan M, Chen X, Wu X, Wang H, Jamil H, et al. The triple threat to nascent apolipoprotein B. Evidence for multiple, distinct degradative pathways. J Biol Chem. 2001 Jul 27;276(30):27855–63.

107. Fisher EA, Williams KJ. Autophagy of an oxidized, aggregated protein beyond the ER: a pathway for remarkably late-stage quality control. Autophagy. 2008 Jul;4(5):721–3.
108. Kohan AB, Wang F, Lo C-M, Liu M, Tso P. ApoA-IV: current and emerging roles in intestinal lipid metabolism, glucose homeostasis, and satiety. Am J Physiol - Gastrointest Liver Physiol. 2015;308(6):G472–81.
109. Kumar NS, Mansbach CM. Prechylomicron transport vesicle: isolation and partial characterization. Am J Physiol. 1999 Feb;276(2 Pt 1):G378–86.
110. Siddiqi SA, Gorelick FS, Mahan JT, Mansbach CM. COPII proteins are required for Golgi fusion but not for endoplasmic reticulum budding of the pre-chylomicron transport vesicle. J Cell Sci. 2003 Jan 15;116(Pt 2):415–27.
111. Siddiqi S, Mansbach CM. Phosphorylation of Sar1b protein releases liver fatty acid-binding protein from multiprotein complex in intestinal cytosol enabling it to bind to endoplasmic reticulum (ER) and bud the pre-chylomicron transport vesicle. J Biol Chem. 2012;287(13):10178–88.
112. Siddiqi S a, Mansbach CM. PKC zeta-mediated phosphorylation controls budding of the pre-chylomicron transport vesicle. J Cell Sci. 2008;121(Pt 14):2327–38.
113. Siddiqi SA, Mahan J, Siddiqi S, Gorelick FS, Mansbach CM. Vesicle-associated membrane protein 7 is expressed in intestinal ER. J Cell Sci. 2006;119(Pt 5):943–50.
114. Siddiqi SA, Siddiqi S, Mahan J, Peggs K, Gorelick FS, Mansbach CM. The identification of a novel endoplasmic reticulum to Golgi SNARE complex used by the prechylomicron transport vesicle. J Biol Chem. 2006;281(30):20974–82.
115. Siddiqi S, Siddiqi SA, Mansbach CM. Sec24C is required for docking the prechylomicron transport vesicle with the Golgi. J Lipid Res. 2010 May;51(5):1093–100.
116. Black DD. Development and physiological regulation of intestinal lipid absorption. I. Development of intestinal lipid absorption: cellular events in chylomicron assembly and secretion. Am J Physiol Gastrointest Liver Physiol. 2007;293(3):G519–24.
117. Hanna MG, Mela I, Wang L, Henderson RM, Chapman ER, Edwardson JM, et al. Sar1 GTPase activity is regulated by membrane curvature. J Biol Chem. 2015;jbc.M115.672287.

118. Dash S, Xiao C, Morgantini C, Lewis GF. New Insights into the Regulation of Chylomicron Production. Annu Rev Nutr. 2015;35(1):265–94.
119. Mansbach CM, Siddiqi SA. The biogenesis of chylomicrons. Annu Rev Physiol. 2010;72:315–33.
120. Singh R, Kaushik S, Wang Y, Xiang Y, Novak I, Komatsu M, et al. Autophagy regulates lipid metabolism. Nature. 2009 Apr 30;458(7242):1131–5.
121. Singh R, Cuervo AM. Lipophagy: Connecting Autophagy and Lipid Metabolism. Int J Cell Biol. 2012;2012:1–12.
122. Weidberg H, Shvets E, Elazar Z. Lipophagy: Selective Catabolism Designed for Lipids. Dev Cell. 2009 May;16(5):628–30.
123. Khaldoun SA, Emond-Boisjoly M-A, Chateau D, Carriere V, Lacasa M, Rousset M, et al. Autophagosomes contribute to intracellular lipid distribution in enterocytes. Mol Biol Cell. 2014;25(1):118–32.
124. Cuervo AM. Chaperone-mediated autophagy: Dice's "wild" idea about lysosomal selectivity. Nat Rev Mol Cell Biol. Nature Publishing Group; 2011;12(8):535–41.
125. Klionsky DJ. Autophagy: from phenomenology to molecular understanding in less than a decade. Nat Rev Mol Cell Biol. 2007 Nov;8(11):931–7.
126. Feng Y, He D, Yao Z, Klionsky DJ. The machinery of macroautophagy. Cell Res. 2014 Jan 24;24(1):24–41.
127. Massey AC, Zhang C, Cuervo AM. Chaperone-mediated autophagy in aging and disease. Curr Top Dev Biol. 2006;73:205–35.
128. Dice JF. Peptide sequences that target cytosolic proteins for lysosomal proteolysis. Trends Biochem Sci. 1990 Aug;15(8):305–9.
129. Cuervo AM, Dice JF. A receptor for the selective uptake and degradation of proteins by lysosomes. Science. 1996 Jul 26;273(5274):501–3.
130. Agarraberes FA, Terlecky SR, Dice JF. An Intralysosomal hsp70 Is Required for a Selective Pathway of Lysosomal Protein Degradation. J Cell Biol. 1997 May 19;137(4):825–34.
131. Cuervo AM, Knecht E, Terlecky SR, Dice JF. Activation of a selective pathway of lysosomal proteolysis in rat liver by prolonged starvation. Am J Physiol. 1995 Nov;269(5 Pt 1):C1200–8.
132. Massey AC, Kaushik S, Sovak G, Kiffin R, Cuervo AM. Consequences of the selective blockage of chaperone-mediated autophagy. Proc Natl Acad Sci U S A.

2006 Apr 11;103(15):5805–10.

133. Kaushik S, Cuervo AM. Degradation of lipid droplet-associated proteins by chaperone-mediated autophagy facilitates lipolysis. Nat Cell Biol. 2015 Jun 20;17(6):759–70.

134. Lass A, Zimmermann R, Oberer M, Zechner R. Lipolysis – A highly regulated multi-enzyme complex mediates the catabolism of cellular fat stores. Prog Lipid Res. 2011 Jan;50(1):14–27.

135. Dupont N, Chauhan S, Arko-Mensah J, Castillo EF, Masedunskas A, Weigert R, et al. Neutral lipid stores and lipase PNPLA5 contribute to autophagosome biogenesis. Curr Biol. 2014 Mar 17;24(6):609–20.

136. Wang F, Wang J, Liu D, Su Y. Normalizing genes for real-time polymerase chain reaction in epithelial and nonepithelial cells of mouse small intestine. Anal Biochem. 2010 Apr 15;399(2):211–7.

137. Li B, Matter EK, Hoppert HT, Grayson BE, Seeley RJ, Sandoval DA. Identification of optimal reference genes for RT-qPCR in the rat hypothalamus and intestine for the study of obesity. Int J Obes. 2014 Feb 24;38(2):192–7.

138. Ran FA, Hsu PD, Wright J, Agarwala V, Scott DA, Zhang F. Genome engineering using the CRISPR-Cas9 system. Nat Protoc. 2013 Nov;8(11):2281–308.

139. Xie Y, Nassir F, Luo J, Buhman K, Davidson NO. Intestinal lipoprotein assembly in apobec-1-/- mice reveals subtle alterations in triglyceride secretion coupled with a shift to larger lipoproteins. Am J Physiol Gastrointest Liver Physiol. 2003;285(4):G735–46.

140. Wu X, Sakata N, Dixon J, Ginsberg HN. Exogenous VLDL stimulates apolipoprotein B secretion from HepG2 cells by both pre- and post-translational mechanisms. J Lipid Res. 1994;35(7):1200–10.

141. Csaki LS, Dwyer JR, Fong LG, Tontonoz P, Young SG, Reue K. Lipins, lipinopathies, and the modulation of cellular lipid storage and signaling. Prog Lipid Res. 2013 Jul;52(3):305–16.

142. Kalogeris TJ, Tsuchiya T, Fukagawa K, Wolf R, Tso P. Apolipoprotein A-IV synthesis in proximal jejunum is stimulated by ileal lipid infusion. Am J Physiol. 1996 Feb;270(2 Pt 1):G277–86.

143. Kalogeris TJ, Holden VR, Tso P. Stimulation of jejunal synthesis of apolipoprotein A-IV by ileal lipid infusion is blocked by vagotomy. Am J Physiol. 1999 Nov;277(5

Pt 1):G1081–7.

144. Kalogeris TJ, Painter RG. Adaptation of intestinal production of apolipoprotein A-IV during chronic feeding of lipid. Am J Physiol Regul Integr Comp Physiol. 2001 Apr;280(4):R1155–61.
145. Glickman RM, Green PH. The intestine as a source of apolipoprotein A1. Proc Natl Acad Sci U S A. 1977 Jun;74(6):2569–73.
146. Tso P, Balint JA, Bishop MB, Rodgers JB. Acute inhibition of intestinal lipid transport by Pluronic L-81 in the rat. Am J Physiol. 1981 Dec;241(6):G487–97.
147. Zhang P, Verity MA, Reue K. Lipin-1 regulates autophagy clearance and intersects with statin drug effects in skeletal muscle. Cell Metab. Elsevier Inc.; 2014;20(2):267–79.
148. Tanida I, Ueno T, Kominami E. LC3 and Autophagy. Methods Mol Biol. 2008;445:77–88.
149. Barth S, Glick D, Macleod KF. Autophagy: assays and artifacts. J Pathol. 2010 Jun;221(2):117–24.
150. Pankiv S, Clausen TH, Lamark T, Brech A, Bruun J-A, Outzen H, et al. p62/SQSTM1 Binds Directly to Atg8/LC3 to Facilitate Degradation of Ubiquitinated Protein Aggregates by Autophagy. J Biol Chem. 2007 Aug 17;282(33):24131–45.
151. Zechner R, Kienesberger PC, Haemmerle G, Zimmermann R, Lass A. Adipose triglyceride lipase and the lipolytic catabolism of cellular fat stores. J Lipid Res. 2008 Aug 18;50(1):3–21.
152. Sztalryd C, Kraemer FB. Regulation of hormone-sensitive lipase during fasting. Am J Physiol. 1994 Feb;266(2 Pt 1):E179–85.
153. Pearson RB, Kemp BE. Protein kinase phosphorylation site sequences and consensus specificity motifs: tabulations. Methods Enzymol. 1991;200:62–81.
154. Clifford GM, Londos C, Kraemer FB, Vernon RG, Yeaman SJ. Translocation of hormone-sensitive lipase and perilipin upon lipolytic stimulation of rat adipocytes. J Biol Chem. 2000 Feb 18;275(7):5011–5.
155. Duncan RE, Ahmadian M, Jaworski K, Sarkadi-Nagy E, Sul HS. Regulation of Lipolysis in Adipocytes. Annu Rev Nutr. 2007 Aug;27(1):79–101.
156. Krintel C, Mörgelin M, Logan DT, Holm C. Phosphorylation of hormone-sensitive lipase by protein kinase A in vitro promotes an increase in its hydrophobic

surface area. FEBS J. 2009 Sep;276(17):4752–62.

157. Nassir F, Wilson B, Han X, Gross RW, Abumrad NA. CD36 is important for fatty acid and cholesterol uptake by the proximal but not distal intestine. J Biol Chem. 2007;282(27):19493–501.

158. Wang J, Mitsche MA, Lütjohann D, Cohen JC, Xie X-S, Hobbs HH. Relative roles of ABCG5/ABCG8 in liver and intestine. J Lipid Res. 2015 Feb;56(2):319–30.

159. Nelson DW, Gao Y, Yen M-I, Yen C-LE. Intestine-specific Deletion of Acyl-CoA:Monoacylglycerol Acyltransferase (MGAT) 2 Protects Mice from Diet-induced Obesity and Glucose Intolerance. J Biol Chem. 2014 Jun 20;289(25):17338–49.

160. Yen C-LE, Cheong M-L, Grueter C, Zhou P, Moriwaki J, Wong JS, et al. Deficiency of the intestinal enzyme acyl CoA:monoacylglycerol acyltransferase-2 protects mice from metabolic disorders induced by high-fat feeding. Nat Med. 2009 Apr 15;15(4):442–6.

161. Furuhashi M, Tuncman G, Görgün CZ, Makowski L, Atsumi G, Vaillancourt E, et al. Treatment of diabetes and atherosclerosis by inhibiting fatty-acid-binding protein aP2. Nature. 2007 Jun 21;447(7147):959–65.

162. Gajda AM, Storch J. Enterocyte fatty acid-binding proteins (FABPs): different functions of liver and intestinal FABPs in the intestine. Prostaglandins Leukot Essent Fatty Acids. 2015 Feb;93:9–16.

163. Trotter PJ, Storch J. Fatty acid uptake and metabolism in a human intestinal cell line (Caco-2): comparison of apical and basolateral incubation. J Lipid Res. 1991 Feb;32(2):293–304.

164. Traber MG, Kayden HJ, Rindler MJ. Polarized secretion of newly synthesized lipoproteins by the Caco-2 human intestinal cell line. J Lipid Res. 1987 Nov;28(11):1350–63.

165. Galli T, Zahraoui A, Vaidyanathan V V, Raposo G, Tian JM, Karin M, et al. A novel tetanus neurotoxin-insensitive vesicle-associated membrane protein in SNARE complexes of the apical plasma membrane of epithelial cells. Mol Biol Cell. 1998 Jun;9(6):1437–48.

166. Holm C, Osterlund T, Laurell H, Contreras JA. Molecular mechanisms regulating hormone-sensitive lipase and lipolysis. Annu Rev Nutr. 2000;20:365–93.

167. Kraemer FB, Shen W-J. Hormone-sensitive lipase: control of intracellular tri-(di-

)acylglycerol and cholesteryl ester hydrolysis. J Lipid Res. 2002;43(10):1585–94.

168. Varanasi U, Chu R, Chu S, Espinosa R, LeBeau MM, Reddy JK. Isolation of the human peroxisomal acyl-CoA oxidase gene: organization, promoter analysis, and chromosomal localization. Proc Natl Acad Sci U S A. 1994 Apr 12;91(8):3107–11.
169. Infante JP, Tschanz CL, Shaw N, Michaud AL, Lawrence P, Brenna JT. Straight-chain acyl-CoA oxidase knockout mouse accumulates extremely long chain fatty acids from alpha-linolenic acid: evidence for runaway carousel-type enzyme kinetics in peroxisomal beta-oxidation diseases. Mol Genet Metab. 2002 Feb;75(2):108–19.
170. Jogl G, Tong L. Crystal structure of carnitine acetyltransferase and implications for the catalytic mechanism and fatty acid transport. Cell. 2003 Jan 10;112(1):113–22.
171. Nguyen T V, Andresen BS, Corydon TJ, Ghisla S, Abd-El Razik N, Mohsen A-WA, et al. Identification of isobutyryl-CoA dehydrogenase and its deficiency in humans. Mol Genet Metab. 77(1-2):68–79.
172. Hunt MC, Alexson SEH. The role Acyl-CoA thioesterases play in mediating intracellular lipid metabolism. Prog Lipid Res. 2002 Mar;41(2):99–130.
173. Hegardt FG. Mitochondrial 3-hydroxy-3-methylglutaryl-CoA synthase: a control enzyme in ketogenesis. Biochem J. 1999;338:569–82.
174. Ashmarina LI, Robert MF, Elsliger M a, Mitchell G a. Characterization of the hydroxymethylglutaryl-CoA lyase precursor, a protein targeted to peroxisomes and mitochondria. Biochem J. 1996;315 (Pt 1:71–5.
175. de Wit NJ, Bosch-Vermeulen H, de Groot PJ, Hooiveld GJ, Bromhaar MMG, Jansen J, et al. The role of the small intestine in the development of dietary fat-induced obesity and insulin resistance in C57BL/6J mice. BMC Med Genomics. 2008;1:14.
176. Mayer MP, Bukau B. Hsp70 chaperones: cellular functions and molecular mechanism. Cell Mol Life Sci. 2005 Mar;62(6):670–84.
177. Zhu P, Goh YY, Chin HFA, Kersten S, Tan NS. Angiopoietin-like 4: a decade of research. Biosci Rep. 2012 Jun;32(3):211–9.
178. Mandard S, Müller M, Kersten S. Peroxisome proliferator-activated receptor alpha target genes. Cell Mol Life Sci. 2004 Feb;61(4):393–416.
179. Bünger M, van den Bosch HM, van der Meijde J, Kersten S, Hooiveld GJEJ, Müller

M, et al. Genome-wide analysis of PPARalpha activation in murine small intestine. Physiol Genomics. 2007 Jul 18;30(2):192–204.

180. Desmarchelier C, Dahlhoff C, Keller S, Sailer M, Jahreis G, Daniel H. C57Bl/6 N mice on a western diet display reduced intestinal and hepatic cholesterol levels despite a plasma hypercholesterolemia. BMC Genomics. 2012;13:84.
181. Kleizen B, Braakman I. Protein folding and quality control in the endoplasmic reticulum. Curr Opin Cell Biol. 2004 Aug;16(4):343–9.
182. Luchoomun J, Hussain MM. Assembly and Secretion of Chylomicrons by Differentiated Caco-2 cells. J Biol Chem. 1999;274(28):19565–72.
183. Chateau D, Pauquai T, Delers F, Rousset M, Chambaz J, Demignot S. Lipid micelles stimulate the secretion of triglyceride-enriched apolipoprotein B48-containing lipoproteins by Caco-2 cells. J Cell Physiol. 2005;202(3):767–76.
184. Caviglia JM, Gayet C, Ota T, Hernandez-Ono A, Conlon DM, Jiang H, et al. Different fatty acids inhibit apoB100 secretion by different pathways: unique roles for ER stress, ceramide, and autophagy. J Lipid Res. 2011 Sep;52(9):1636–51.
185. Shi Y, Cheng D. Beyond triglyceride synthesis: the dynamic functional roles of MGAT and DGAT enzymes in energy metabolism. AJP Endocrinol Metab. 2009 Jul 1;297(1):E10–8.
186. Young SG, Cham CM, Pitas RE, Burri BJ, Connolly A, Flynn L, et al. A genetic model for absent chylomicron formation: mice producing apolipoprotein B in the liver, but not in the intestine. J Clin Invest. 1995 Dec;96(6):2932–46.
187. Peretti N, Sassolas A, Roy CC, Deslandres C, Charcosset M, Castagnetti J, et al. Guidelines for the diagnosis and management of chylomicron retention disease based on a review of the literature and the experience of two centers. Orphanet J Rare Dis. 2010;5:24.
188. Schonfeld G, Lin X, Yue P. Familial hypobetalipoproteinemia: Genetics and metabolism. Cell Mol Life Sci. 2005;62(12):1372–8.
189. Hooper AJ, van Bockxmeer FM, Burnett JR. Monogenic hypocholesterolaemic lipid disorders and apolipoprotein B metabolism. Crit Rev Clin Lab Sci. 2005;42(5-6):515–45.
190. Tarugi P, Averna M, Di Leo E, Cefalù AB, Noto D, Magnolo L, et al. Molecular diagnosis of hypobetalipoproteinemia: an ENID review. Atherosclerosis. 2007

Dec;195(2):e19–27.

191. Schmitz G, Langmann T, Heimerl S. Role of ABCG1 and other ABCG family members in lipid metabolism. J Lipid Res. 2001;42(10):1513–20.
192. Asp L, Kartberg F, Fernandez-Rodriguez J, Smedh M, Elsner M, Laporte F, et al. Early stages of Golgi vesicle and tubule formation require diacylglycerol. Mol Biol Cell. 2009 Feb;20(3):780–90.
193. Iqbal J, Hussain MM. Intestinal lipid absorption. AJP Endocrinol Metab. 2009;296(6):E1183–94.
194. Pan X, Hussain MM. Diurnal regulation of microsomal triglyceride transfer protein and plasma lipid levels. J Biol Chem. 2007 Aug 24;282(34):24707–19.
195. Gusarova V, Caplan AJ, Brodsky JL, Fisher EA. Apoprotein B Degradation is Promoted by the Molecular Chaperones hsp90 and hsp70. J Biol Chem. 2001;276(27):24891–900.
196. Sugden MC, Caton PW, Holness MJ. PPAR control: it's SIRTainly as easy as PGC. J Endocrinol. 2010 Feb 1;204(2):93–104.